UNIVERSITY OF CRETE
DEPARTMENT OF PHYSICS

Master Thesis

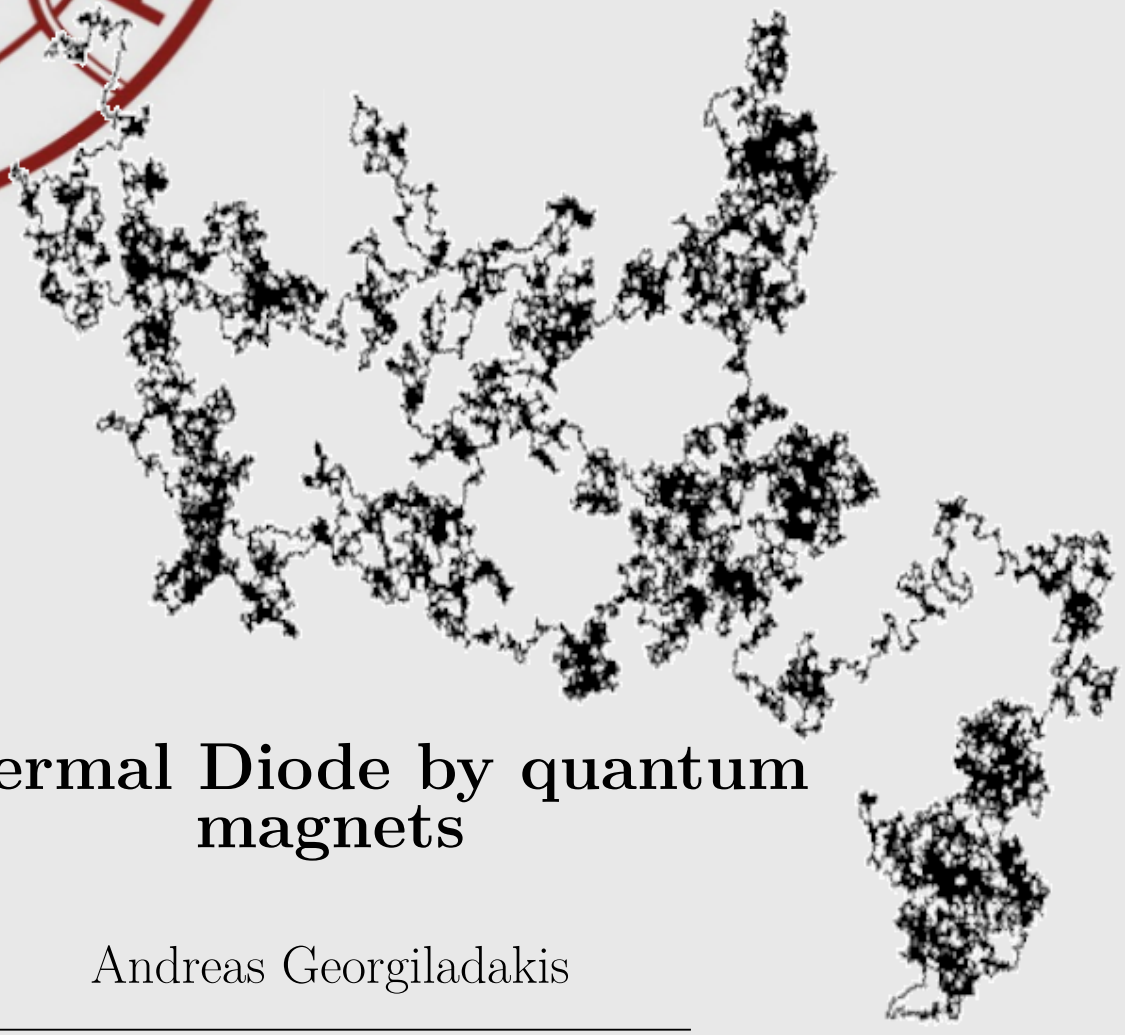

Thermal Diode by quantum magnets

Andreas Georgiladakis

Advisor: *Prof.* Xenophon Zotos - University of Crete

UNIVERSITY OF CRETE
DEPARTMENT OF PHYSICS

MSc THESIS

IN

- CONDENSED MATTER PHYSICS -

Defended by
ANDREAS GEORGILADAKIS

Thermal Diode by quantum magnets

COMMITTEE

Prof.	Xenophon Zotos	-	UNIVERSITY OF CRETE
Prof.	Giorgos Tsironis	-	UNIVERSITY OF CRETE
Prof.	Nikos Flytzanis	-	UNIVERSITY OF CRETE

Date of the defense:
23/07/2014

Περίληψη

Μελετάμε την διάδοση θερμότητας σε μαγνητικά υλικά, όπου έχουμε δύο φορείς θερμότητας που αντιδρούν μεταξύ τους, σε μία διάσταση. Παρουσιάσαμε τα υλικά εν ονόματι αλυσίδες και σκάλες spin, στα οποία παρατηρείται μία ασυνήθιστα μεγάλη συνεισφορά των μαγνονίων στην ολική θερμική αγωγιμότητα των υλικών αυτών. Έπειτα, αναφέραμε το φαινόμενο του θερμικού rectification, κατά το οποίο η διάδοση θερμότητας κατά μήκος ενός συγκεκριμένου άξονα εξαρτάται από το πρόσημο της βαθμίδας της θερμοκρασίας ή του ρεύματος θερμότητας, και μπορεί να βοηθήσει στην βελτιωμένη διαχείρηση της θερμότητας. Μελετήσαμε κάτω από ποιές συνθήκες παρατηρείται αυτό το φαινόμενο, καταλήγωντας στο ότι θα πρέπει στα υλικά που θα χρησιμοποιήσουμε, η θερμική αγωγιμότητα τους να εξαρτάται από τη θερμοκρασία, αλλιώς το φαινόμενο του θερμικού rectification δεν παρατηρείται. Έπειτα επικεντρωθήκαμε σε δύο περιπτώσεις, το στατικό θερμικό rectification και στο δυναμικό θερμικό rectification. Στην πρώτη περίπτωση, για να εξάγουμε τον παράγοντα του rectification χρησιμοποιήσαμε την εξίσωση του ρεύματος θερμότητας, ενώ στη δεύτερη λύσαμε αριθμητικά την εξίσωση Bloch-Boltzmann-Peierls για τα φωνόνια και τα μαγνόνια. Και στις δύο περιπτώσεις καταλήξαμε στο ότι ο μεγαλύτερος παράγοντας βρέθηκε στο υλικό που αποτελείται από την αλυσίδα spin Sr_2CuO_3 και την σκάλα spin $Ca_9La_5Cu_{24}O_{41}$, τα οποία είναι κολλημένα μεταξύ τους. Τέλος μελετήσαμε την περίπτωση όπου εφάπτουμε μία χρονοεξαρτημένη πηγή θερμότητας στην αριστερή επιφάνεια του μαγνητικού υλικού μας (ή της συστοιχίας μαγνητικών υλικών) και παρατηρούμε την απόκριση της θερμοκρασίας στην απέναντι επιφάνεια, προσπαθώντας να καταλήξουμε σε ποιές περιπτώσεις η θερμότητα διαδίδεται βαλλιστικά και πότε διαχέεται. Καταλήξαμε στο ότι όταν ο χρόνος διάχυσης των φωνονίων είναι ίσος ή μικρότερος από την περίοδο της πηγής, τότε η θερμότητα διαδίδεται βαλλιστικά, αλλιώς διαχέεται.

Abstract

The propagation of heat in magnetic materials, where we have two heat carriers that interact with each other, is studied in one-dimension. We introduced the spin chain and the spin ladder materials, that have an unusually large magnetic contribution to the total thermal conductivity. After that, we present the phenomenon of thermal rectification in which thermal transport along a specific axis is dependent upon the sign of the temperature gradient or heat current and can offer improved thermal management. We examined under which circumstances this phenomenon is observed, concluding that the thermal conductivities of the materials that we ll use must have temperature dependence otherwise rectification does not occur.We then focused on two cases, the static thermal rectification and the dynamical thermal rectification. In the first case, in order to calculate the rectification factor we used the heat current equation when in the dynamic case we solved numerically the Bloch-Boltzmann-Peierls equation for the lattice and magnetic degrees of freedom. In both cases, we concluded that the highest rectification is observed in a material that is composed of the spin chain Sr_2CuO_3 and the spin ladder $Ca_9La_5Cu_{24}O_{41}$, bounded together. Lastly, we study the case that we adapt a time-dependent heat source at the left surface of our magnetic material (or a composition of magnetic materials) and we observe the temperature response at the opposite surface, trying to conclude in which cases heat propagates ballistically and in which diffusively. We pointed out that if the phonons' diffusion time is equal or smaller than the period of the heat source then the heat propagates ballistically, otherwise diffusively.

Acknowledgements

First of all, I would like to show my gratitude to my supervisor prof. Xenophon Zotos, for introducing me into the Thermodynamics and Computational physics, and I am grateful for his guidance and trust during this work.

This thesis would not have been possible without the support, help and the endless scientific discussions of my colleagues and friends Michalis Kritsotakis, Nikos Tsatrafyllis and Joniald Shena.

Last but not least, I would like to thank my family and all my friends for their moral support, and their efforts to keep me calm and concentrated during hard days when everything seemed to go extremely wrong.

Contents

1 Introduction

Efficient heat removal is crucial to the performance of many electronic devices, since overheating often leads to overall system failures. In the typical silicon semiconductors, for example, a reduction in the temperature corresponds to an exponential increase in reliability and life expectancy of the device. Another example that shows us how crucial the efficient heat removal is, is the case of the magnetic sensors in recording heads. These heads, consist of multilayers of nanoscale thin films that are very susceptible to failures caused by thermally activated processes, like interdiffusion. At higher temperatures, they can even melt.

The problem of the over-heating electronic devices is becoming more severe if we take into consideration the current trend to miniturize electronics further and further; by doing so, the power density is increased accordingly. Currently the energy density increases up to 28 % per year, showing us that self-heating will become more important, putting high pressure on research to come up with advanced cooling mechanisms and/or materials. A possible strategy for dissipating excess the heat, while at the same time protecting sensitive structures closeby in an electronic device, is to use a layer with high thermal conduction perpendicular to the surface. By doing this, we guide the heat to a heat sink and then the sensitive structures on the surface could be placed much closer, allowing further miniturization.In order to realize such a cooling device, one needs a material with three necessary properties, i) the thermal conductivity should be high, i.e. $\geq 100\, W\, m^{-1}\, K^{-1}$, ii) the thermal conductivity should be one-dimensional,

iii) the compound should be electrically insulating. Except these, it would be a great advantage if the material has a thermal conductivity that is controllable, so that the heat transport can be adjusted.

In 1997 it was established that prototype theoretical models for one-dimensional magnetic compounds show unconventional, dissipationless, thermal transport. Experimentally, in some prototype materials ($SrCuO_2$, Sr_2CuO_3 and $(Sr, Ca, La)_{14}Cu_{24}O_{41}$), especially at room temperature, an unusually large magnetic contribution to the total thermal conductivity has been observed. The magnetic heat conduction of these of these electrically insulating oxide materials is highly anisotropic, dwarfing the usual lattice contribution as the temperature rises.

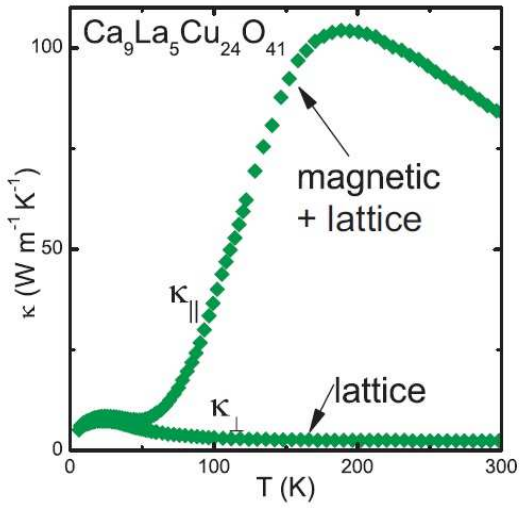

Figure 1.1: Thermal conductivity of the spin ladder compound $Ca_9La_5Cu_{24}O_{41}$ as a function of temperature. The direction parallel to the ladder has a contribution from both phonons and magnons. The directions perpendicular to the ladder only have a phonon contribution

These materials are very promising candidates for advanced cooling solutions, since they fulfil all the criteria mentioned above. i)Heat is conducted primarily along one crystal axis, so the material can thermally insulate in one directions and carry away heat along the other. ii) The thermal conductivity along one-dimensional structure is as high as $\kappa_{mag} \approx 100\ W\, m^{-1}\, K^{-1}$ at room temperature for spin ladder $Ca_9La_5Cu_{24}O_{41}$, as is shown in figure 1. iii) These compounds are electrically insulating and can therefore be used to simultaneously electrically insulate electronic circuits and transport heat. iv) Heat is carried by localised spins which might can manipulated by with magnetic fields or light. This fact, opens the possibility of having a controllable thermal conductivity

at room temperature. That can be achieved, for example, by doping the material with magnetic defects so that we ll be able to potentially tune the thermal conductivity.

The ideal situation for regulating heat flow would be a material in which κ increases when the temperature increases, such that, when used as a cooling substrate, the efficiency increases with increased heat flux, thereby acting as a negative feedback loop. In these materials the interaction between the magnetic excitations and the three-dimensional lattice excitations, can be studied relatively easily, by comparing results for different directions, since the magnetic excitations are only present in the direction along the low-dimensional structure. The interaction can give information about the coupling between the one-dimensional magnetic system and the three-dimensional lattice, and how this prevents the material from behaving like an ideal low-dimensional system.

The main goal of this thesis is to study the possibility of making a thermal diode using the magnetic materials mentioned above, and to provide useful information about how to increase the efficiency of such a rectifier.

2 Spin Chains & Spin Ladders

2.1 Basic Information about Spin chain & Ladder materials

In this chapter, we ll give a short theoretical description of magnetic materials, focussing on the spin ladder and spin chain materials. Both materials are are one-dimensional quantum magnets. Important interactions in these materials are discussed, together with the structure and the excitations.

The essential difference between three-dimensional, conventional, magnetism and ideal two- or one- dimensional magnetism is that three- dimensional magnetism deals with ordered domains, while in low-dimensional magnetism only short-range order can exist at finite temperature. This is due to an interplay between quantum and thermal fluctuations which drive the system to a disordered state, and the tendency fo the system to be in the lowest energy state, which is ordered [3]. For the one-dimensional systems, both quantum and thermal fluctuations diverge, so even at zero temperature there is no longer order.

Heat transport by magnetic excitations was originally predicted in 1936 [4].However it took almost 30 years until the first convincing experimental evidence for magnetic heat transport by classical spin waves was found in ferromagnetic yttrium-iron-garnet (YIG). The analysis of the magnetic heat conductivity, would give us valuable infor-

mation about the excitation and scattering of magnons (e.g. off defects, phonons, and electrons) as is the case for the well-understood phononic and electronic thermal conductions. However, most of the early experiments on YIG and other materials, showed that the magnetic heat conductions was present only at very low temperatures ($T < 10K$). The first material that we observed magnetic heat transport at higher temperatures ($T > 50k$), was the one-dimensional quantum antiferromagnet $KCuF_3$. The intense research on the heat transport of low-dimensional quantum spin systems, was triggered by the theoretical prediction of dissipationless heat conduction in one-dimensional antiferromagnetic Heisenberg Chains [5,6] and the discovery of huge magnetic contributions in the quantum spin ladder material $Sr_{14}Cu_{24}O_{41}$ [7-9]. Until now, the clearest experimental examples of low dimensional magnetic heat conduction are found in copper oxides (cuprate) systems.

Particular examples from the wide range of possible spin structures in cuprate systems are spin arrangements in the geometrical form of chains and the so-called two-leg ladders. Sketches of such spin arrangements are shown in figure 2.1(a)-(b).

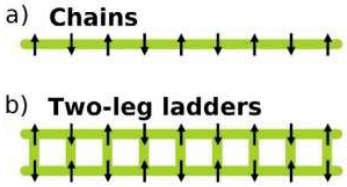

Figure 2.1: Illustration of low-dimensional spin structures: a) a spin chain, b) a two-leg spin ladder.Arrows represent localized S = 1/2 spin. Taken by [2]

Good examples for materials containing $S = 1/2$ Heisenberg chains as is shown in figure 2.1(a) are given by the compounds $SrCuO_2$ and Sr_2CuO_3, where straight Cu-O-Cu bonds and hence a strong antiferromagnetic exchange only exist alone one particular crystallographic direction; the magnetic exchange perpendicular to this direction is much weaker. Low- dimensional quantum spin models are interesting from a fundamental point of view since they give rise to very peculiar ground state properties and elementary excitations. These vary strongly from system to system. The elementary excitations, so-called spinons, are gapless, which means that it costs no energy to flip a spin, and carry a spin S=1/2. Spinons interact with structural defects and other quasiparticles, such as phonons, with a certain rate.

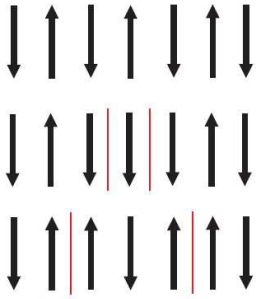

Figure 2.2: Spinons in a spin chain compound. By flipping one spin (middle pic),two excitations are created,that move outward .Picture taken from [1]

In the $(Sr, Ca, La)_{14}Cu_{24}O_{41}$ family of compounds, parallel pairs of such chains are coupled to each other, producing in straight Cu-O-Cu perpendicular to the chain direction. This spin ensemble is a so-called two-leg spin ladder, the ladder legs being formed by the two chains and the ladder rungs arising from the Cu-O-Cu bonds which connect the chains (figure 2.1(b)). A magnetic excitation (magnon) is created by flipping one spin so that the two spins in a rung are transformed from a singlet state to a triplet state. This is shown in figure 2.3.

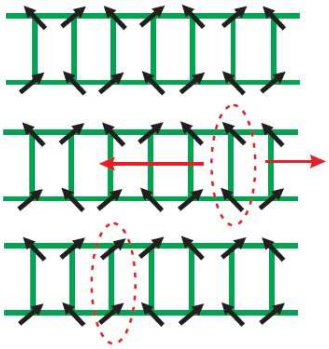

Figure 2.3: A magnon in a spin ladder compound. When we flip one spin (middle picture), an excitation is created so that the two spins on a rung are in a triplet state. This excitation can move along the ladder in two directions. Movement to the left is shown (lower picture). Picture taken from [1]

Concerning heat transport, little is known for all these magnetic systems. Often the attention in theoretical works is focussed on the possibility of ballistic magnetic heat transport in one-dimensional systems. However, in real materials scattering processes involving defects and other quasiparticles such as phonons, must play an important role and render κ_{mag} finite. Studying κ_{mag} should provide us further insight into the

nature of these scattering processes and the dissipation of heat currents.

2.2 Thermal Conductivities of the spin chain & ladder materials

2.2.1 Thermal Conductivity of the spin chains $SrCuO_2$ & Sr_2CuO_3

Figure 2.4(a) presents the total heat conductivity of $SrCuO_2$ as a function of temperature. It is measured by a conventional steady state method, in which a steady heat current flows through a brick-like sample, such that the simple equation 2.6 can be used to extract the thermal conductivity. The c-direction is parallel to the chains and has a contribution from both phonons and spinons, the a-direction is perpendicular to the chain and only has phonons. It is seen that along the chain at all temperatures above $T \approx 20K$, the spinon contribution to the thermal conductivity is much larger than the phonon contribution. Furthermore, the phonon contribution is assumed to be isotropic, making the separation of the two contribution possible.

We can understand the general behaviour of the thermal conductivity by thinking this way: at low temperature an increase of thermal conductivity with temperature is seen which is due to the increased amount of heat carriers (phonons, spinons) by thermal activation. As the amount of heat carriers increases, also the contribution of Umklapp scattering increases, leading to two processes, therefore giving a peak at certain temperature.

Figure 2.5(a) presents the total heat conductivity of Sr_2CuO_3, measured with the heat current parallel and perpendicular to the chains in the material. We focus first on the temperature dependence of the thermal conductivity perpendicular to the spin chain, κ_c, which is shown in the inset of the figure. Along this direction, the heat conductivity of this electrically insulating material is purely phononic: As a function of temperature, it shows a characteristic peak at $T = 22K$, and then strongly decreases upon further raising the temperature. The height of the peak sensitively depends on the density of impurities in the system, which generate phonon-defect scattering. This can be clearly inferred by comparing our data for a 4N purity material with that of 2N. For this lower-purity sample the overall magnitude of κ_c is strongly reduced, as is expected for typical phonon heat conductors.

The thermal conductivity parallel to the chain, κ_b, is shown in the main panel of

figure 2.5(a). κ_b exhibits a peak at the same position as observed for κ_c. However, the peak is much broader and the overall magnitude of κ_b is significantly larger than that of the purely phononic κ_c, which is the signature of a substantial magnetic contribution in this material.

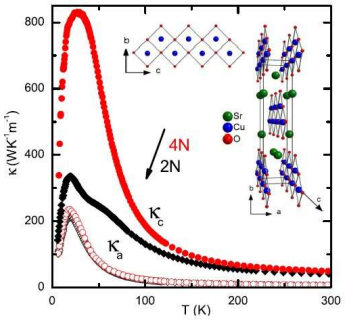

(a) Total conductivity of $SrCuO_2$

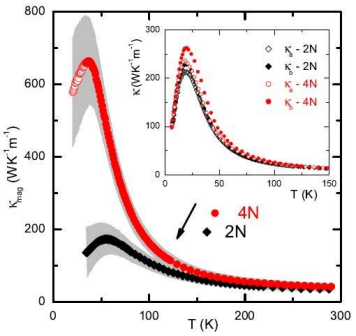

(b) Magnetic conductivity of $SrCuO_2$

Figure 2.4: (a) Closed (open) symbols represent conductivity along the c-axis (a-axis), circles (diamonds) correspond to 4N (2N) purity. Inset: crystal structure of $SrCuO_2$. (b) κ_{mag} of $SrCuO_2$ for different purities. Open sumbols represent low-T κ_{mag} which is disregarded in the further analysis. The saded areas show the uncertainty of the estimation of κ_{mag} due to the phononic background. Inset: κ_a and κ_b perpendicular to the chain for both purities. Pictures taken from [4]

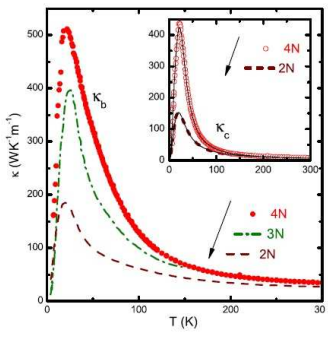

(a) Total conductivity of Sr_2CuO_3

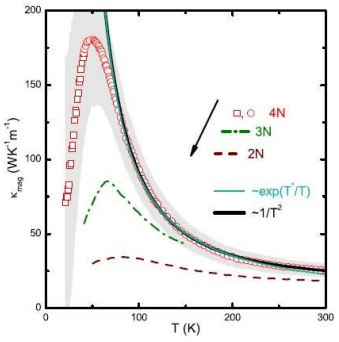

(b) Magnetic conductivity of Sr_2CuO_3

Figure 2.5: (a) Thermal Conductivity of Sr_2CuO_3 parallel to the spin chains along κ_b for various purities. Inset: thermal conductivity of Sr_2CuO_3 perpendicular to the spin chains along κ_c for 2N and 4N purity. (b) Estimated magnetic thermal conductivity of Sr_2CuO_3 for 4N (circles,squares), 3N (dash-dotted line), and 2N (dashed line) purity.

The thermal conductivity parallel to the chain is composed of a magnetic and phononic contribution, $\kappa_b = \kappa_{mag} + \kappa_{b,ph}$, assuming that b is the axe that is parallel to the chain. In order to extract the heat conductivity of the spin chain, the phononic background is approximated as $\kappa_{b,ph} \approx \kappa_c$, since at c axe that is perpendicular to the chain, the contribution to the heat conductivity is purely phononic. This assumption is reasonable, because the phononic anisotropy between κ_a and κ_c is small. Therefore $\kappa_{b,ph}$ is not expected to be much different than these. So, the spinon heat conductivity that is shown in figure 2.4(b) and figure 2.5(b), is calculated by the expression $\kappa_{mag} = \kappa_b - \kappa_c$.

2.2.2 Thermal Conductivity of the spin ladders $Ca_9La_5Cu_{24}O_{41}$ & $Sr_{14}Cu_{24}O_{41}$

The thermal conductivity of $Ca_9La_5Cu_{24}O_{41}$ & $Sr_{14}Cu_{24}O_{41}$ as a function of temperature, measured by a conventional steady state method, is shown in figures 2.6 and 2.7 . It is seen in both figures, that along the ladder at every temperature above $T > 50K$ the magnon contribution to the thermal conductivity is much larger than the phonon contribution, making the separation of the two contributions possible (again assuming that the phonon contribution is isotropic). Because the peak in κ_c lies at lower temperature for $Sr_{14}Cu_{24}O_{41}$, it is likely that the scattering processes are stronger and the mean free path somewhat shorter.

Comparing the spin ladders to the spin chain, it is seen that the magnetic contribution to the heat transport is higher at room temperature for the ladders, especially for $Ca_9La_5Cu_{24}O_{41}$. Therefore, for practical applications these materials are more promising. The spin chain however shows a much higher peak value of the thermal conductivity, which lies unfortunately at too low temperature to be interesting for most applications. The phonon thermal conductivity peaks at low temperature (≈ 30 Kelvin) and is very low at room temperature.

2.3 Thermal transport in Spin Chains & Spin Ladders

In this chapter, we ll present two theoretical descriptions of heat transport. The first one, is the well known diffusion model, which can be used for single particle macroscopic diffusive process and multi-particle diffusive processes when particles are

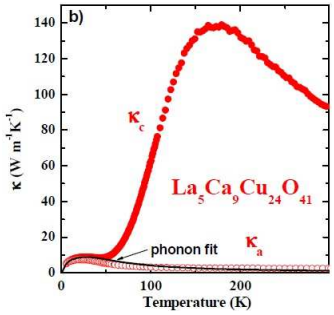

Figure 2.6: Thermal conductivity of the spin ladder compound $Ca_9La_5Cu_{24}O_{41}$ as a function of temperature. The c-direction is parallel to the ladder and has a contribution from both phonons and magnons. The a-direction and b-direction are perpendicular to the ladder and only have a phonon contribution.

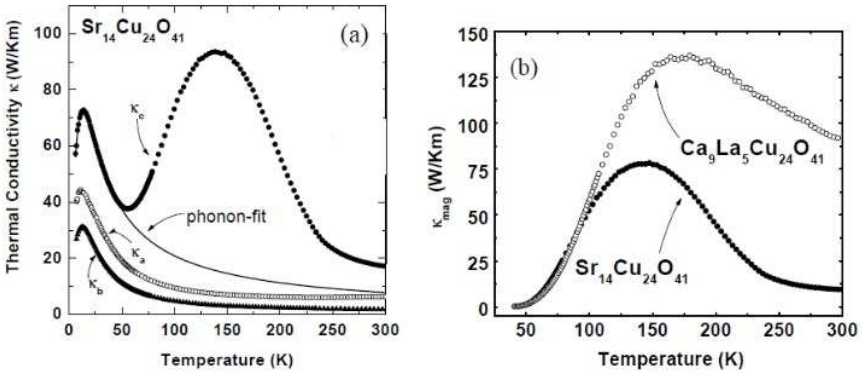

Figure 2.7: (a) Thermal conductivities of $Sr_{14}Cu_{24}O_{41}$ along all three crystallographic directions, (b) κ_{mag} for $Sr_{14}Cu_{24}O_{41}$ & $Ca_9La_5Cu_{24}O_{41}$ along the ladder. Figure taken from [5]

in thermal equilibrium. The second one, is a macroscopic diffusion model, where he have two different heat carriers that have different thermal diffusivities, and are converted into one another at certain rate.

2.3.1 One-particle one-dimensional heat conduction equation

In this case, the equation that describes the heat transport of one heat carrier in 1D is:

$$\frac{\partial T}{\partial t} = D\,\frac{\partial^2 T}{\partial x^2} \tag{2.1}$$

where

$$D = \frac{\kappa}{\rho c} \tag{2.2}$$

is called the thermal diffusion constant or thermal diffusivity (m^2/s). Thermal diffusicity is given from Equation 2.2 where, κ is the thermal conductivity ($W/(m \cdot K)$), ρ is the density (Kg/m^3), c is the specific heat capacity ($J/(Kg \cdot K)$). However, the thermal properties κ, ρ and c can depend on position and temperature.Assuming that,in general, thermal diffusivity can depend on position and temperature, the heat equation has to be modified to

$$\frac{\partial T}{\partial t} = \frac{\partial}{\partial x}(D(x,T)\frac{\partial T}{\partial x}). \tag{2.3}$$

If D is a function of position only, an analytical solution exists for a variety of initial and boundary conditions. If D depends on temperature, the situation becomes more complex and a full numerical analysis has to be performed.

2.3.1.1 Steady State Solution

If we consider a linear, steady flow of one type of heat carrier in a solid bound by a pair of parallel planes at $x = 0$ and $x = L$, the one dimensional diffusion equation becomes

$$\frac{d^2T}{dx^2} = 0 \;\Rightarrow\; \frac{dT}{dx} = constant = \frac{T_L - T_R}{L} \tag{2.4}$$

where T_R and T_L are the temperatures at the surfaces $x = 0$ and $x = L$, respectively. The equation that gives us the heat flux J is

$$J = -\kappa\frac{dT}{dx} \tag{2.5}$$

and in our case becomes

$$J = -\kappa\frac{T_L - T_R}{L}. \tag{2.6}$$

This relation is analogous to Ohm's law for the steady flow of electrical current. So, if we heat our sample homogenously over a small surface at $x = 0$, and a heat sink is connected to the small surface at $x = L$, by measuring the temperature difference at the two surfaces, κ can directly be extracted.

2.3.1.2 Dynamic solution for flash method

In most of the experiments, the thermal conductivity is determined by measuring the temperature change at a surface as a function of time. If we consider a sample with

two parallel surfaces at $x = 0$ and $x = L$ with initial temperature distribution $T(x, t)$, the temperature distribution at later time t is given by [1]

$$T(x,t) = \frac{1}{L}\int_0^L T(x,0)dx + \frac{2}{L}\sum_{i=1}^{\infty}\exp\left(\frac{-n^2\pi^2 Dt}{L^2}\right) \times cos\frac{n\pi x}{L}\int_0^L T(x,0)\, cos\frac{n\pi x}{L}dx \tag{2.7}$$

where D is the diffusion constant. If we now assume that we heat the front surface ($x = 0$) with a laser pulse of energy density Q, which is instantaneously and uniformly absorbed in a small depth μ. Taking these as notice, the initial conditions are given by

$$T(x,0) = Q/\rho C\mu \text{ for } 0 < x < \mu$$
$$T(x,0) = 0 \quad \text{for } \mu < x < L.$$

Using these initial conditions, equation 2.7 becomes

$$T(x,t) = \frac{Q}{\rho C\mu}\Big[1 + 2\sum_{i=1}^{\infty}\ cos\frac{n\pi x}{L}\frac{sin(n\pi\mu/L)}{n\pi\mu L} \times exp(\frac{-n^2\pi^2}{L^2}Dt)\Big], \tag{2.8}$$

where ρ is the density and C is the heat capacity. In most of times, only a few (like 20) terms are needed. If we now assume that μ is very small for opaque materials, then $sin(n\pi\mu/L) \approx n\pi\mu/L$. At the back surface, where $x = L$, the temperature can be expressed as

$$T_l(L,t) = T_m\Big[1 + 2\sum_{i=1}^{\infty}\ (-1)^n exp(\frac{-n^2\pi^2}{L^2}Dt)\Big] \tag{2.9}$$

where $T_l(L, t)$ is the temperature at the back surface at time t, and $T_m = Q/(\rho CL)$ is the maximum temperature at the back surface. This is the so-called Parker's formula, and it is only valid if there is just one type of heat carrier or if the various heat carriers are in thermal equilibrium.

2.3.2 Two particle one-dimensional heat conduction equation

In order to fully understand the thermal transport in the spin ladder and chain materials, the two-particle origin of the transport has to be taken into account. An important point that has to be realized, is that in experiments to determine the thermal conductivity, only the phonon temperature is directly accessible. Te temperature sensor, measures the temperature of the sample surface from the strength of the transmitted lattice vibrations. Furthermore, the heating processes mainly creates phonons, since

its more efficient than creating magnons. In the case that magnons don't interact with phonons, the only way the directly excited magnons to contribute to the measured temperature is by inelastic scattering at the surface, which is a weak process. But if there is interaction between magnons and phonons and the two carriers are not in equilibrium, the thermal conductivity measured in an experiment is not equal to the sum of thermal conductivities of the two carriers, as would be the case in a thermal equilibrium [12].

Lets suppose that we have a solid, that two types of heat carriers exist, which are not in thermal equilibrium initially and they travel diffusively through the solid. Then the coupled heat equations for the two heat carriers are given by

$$\frac{\partial T_l}{\partial t} = D_l \frac{\partial^2 T_l}{\partial x^2} - g_l(T_l - T_m) + P(x) \tag{2.10}$$

$$\frac{\partial T_m}{\partial t} = D_m \frac{\partial^2 T_m}{\partial x^2} - g_m(T_m - T_l) \tag{2.11}$$

$$\text{where } g_l = \frac{c_m}{c_{tot}\,\tau_{mp}},\ g_m = \frac{c_l}{c_{tot}\,\tau_{mp}} \text{ and } c_{tot} = c_m + c_l$$

where l stands for the lattice excitations (phonons) and m for the magnetic excitations (magnons). $P(x)$ is the rate at which phonons are created in the case we have a heat source, τ_{mp} is the thermalization time between lattice and magnetic excitations and g is the conversion rate between the two types of particles.

In the case that thermal diffusivity is a function of temperature, the former equations become

$$\frac{\partial T_l}{\partial t} = \frac{\partial}{\partial x}(D_l(T_l)\frac{\partial T_l}{\partial x}) - g_l(T_l - T_m) + P(x) \tag{2.12}$$

$$\frac{\partial T_m}{\partial t} = \frac{\partial}{\partial x}(D_m(T_m)\frac{\partial T_m}{\partial x}) - g_l(T_m - T_l). \tag{2.13}$$

2.3.2.1 Steady State Solution

Steady state method, is used in most common experimental configurations, in which we put a steady heat flow through a brick-shaped sample along the long axis. For this configuration, the effective thermal conductivity κ_{eff} and the temperature profiles of magnon and phonon systems, are analyzed by Sanders and Walton [2], assuming that thermal conductivities are constants. In a thermally isolated system, a total heat flux Q is supplied at $x = -L/2$ and absorbed at $x = +L/2$. In general, the temperature

of the phonon system $T_l(x)$ is different from the magnon system $T_m(x)$ for every x. We can find that the contribution of a small length dx to the heat flux in the magnon system is

$$dQ_m(x) = \frac{dP(x)}{A} = \frac{c_l\, c_m}{c_T} \frac{T_l(x) - T_m(x)}{\tau_{mp}} dx \tag{2.14}$$

where P is the heating power, A is the surface area, and T_l and T_m are the phonons' and magnons' temperatures, as mentioned above. We have to repeat that all the heat is coming from the phonon system, since no magnons are inserted directly.

The total magnon heat flux at any point x is given by

$$Q_m(x) = \frac{c_l\, c_m}{c_T} \frac{1}{\tau_{mp}} \int_{-L/2}^{x} [T_l(x') - T_m(x')] dx'. \tag{2.15}$$

In steady state, the magnon conductivity is also given by the heat flux equation

$$Q_m(x) = -\kappa_m \frac{dT_m(x)}{dx}. \tag{2.16}$$

If we combine and differentiate the former two equations, we find a second-order differential equation for the magnon system

$$\frac{d^2 T_m(x)}{dx^2} + \frac{c_l\, c_m}{c_T} \frac{1}{\kappa_m \tau_{mp}} [T_l(x) - T_m(x)] = 0. \tag{2.17}$$

The total heat flux Q is divided between the magnons and phonons according to the following expression

$$Q = Q_l + Q_m = -\kappa_l \frac{dT_l(x)}{dx} - \kappa_m \frac{dT_m(x)}{dx}. \tag{2.18}$$

From the above equation, we see that $T_l(x)$ is related to $T_m(x)$

$$\frac{dT_l(x)}{dx} = -\frac{Q}{\kappa_l} - \frac{\kappa_m}{\kappa_l} \frac{dT_m(x)}{dx} \tag{2.19}$$

and by solving the above equation with the boundary condition that at the center of the sample ($x = 0$), the phonon and magnon temperatures are both equal to the average sample temperature T_0, we get

$$T_l(x) = \frac{\kappa_T}{\kappa_l} T_0 - \frac{Q}{\kappa_l} x - \frac{\kappa_m}{\kappa_l} T_m(x), \tag{2.20}$$

where $\kappa_T = \kappa_l + \kappa_m$. By substituting equation (2.20) in equation (2.17), we find

$$\frac{d^2 T_m(x)}{dx^2} + A^2 (T_0 - \frac{Q}{\kappa_T} x - T_m(x)) = 0 \tag{2.21}$$

where

$$A^2 = \frac{c_l\, c_m}{c_T} \frac{\kappa_T}{\kappa_l \kappa_m} \frac{1}{\tau_{mp}}. \tag{2.22}$$

Equation (2.21) is solved with the boundary condition of equal T_l and T_m in the center of the sample, and the requirement that heat flux only enters or leaves the sample through the phonon system, therefore the magnon heat flux must be zero at both ends. Taking these boundary conditions into notice, we find the magnon temperature

$$T_m(x) = T_0 - \frac{Q}{\kappa_T}\Big(x - \frac{\sinh Ax}{A \cosh \frac{1}{2}AL}\Big). \tag{2.23}$$

By substituting this equation into equation (2.20), we find the expression for phonon temperature

$$T_l(x) = T_0 - \frac{Q}{\kappa_T}\Big(x + \frac{\kappa_m}{\kappa_l} \frac{\sinh Ax}{A \cosh \frac{1}{2}AL}\Big). \tag{2.24}$$

The parameter A, as we see from equation 2.22, is related to the coupling between magnons and phonons. If they are perfectly coupled, then $\tau_{mp} = 0$ and $A = \infty$. In this limit, the magnons' and the phonons' temperatures are the same. In the other limit where $\tau_{mp} = \infty$ and $A = 0$, the magnon temperature is constant over the whole interbal and equal to T_0.

Now,the measured *effective* thermal conductivity κ_{eff} is given by

$$\kappa_{eff} = -QL/\Delta T_l, \tag{2.25}$$

which, with $\Delta T_l = T_l - T_0$ from equation 2.24, is given by

$$\kappa_{eff} = (\kappa_l + \kappa_m)\Big(1 + \frac{\kappa_m}{\kappa_l} \frac{\tanh \frac{1}{2}AL}{\frac{1}{2}AL}\Big)^{-1}. \tag{2.26}$$

As for the dynamic solution for the flash method when two heat carriers exist, there is an analytical formula similar to Parker's that takes into account the thermalization time, but we ll not mention it, since in this work a full numerical analysis is being perfomed, that gives us the temperatures of magnons and phonons.

3
Thermal Rectification

Thermal rectification is a phenomenon in which thermal transport along a specific axis is dependent upon the sign of the temperature gradient or heat current. This phenomenon, offers improved thermal management of electronics as size scales continue to decrease and new technologies emerge by having directions of preferred thermal transport. For most applications where thermally rectifying materials could be of use they would need to exhibit one direction with high thermal conductivity to allow for efficient transport of heat from heat generating components to a sink and one direction with low conductivity to insulate the temperature and heat flux sensitive components. In the process of understanding and developing these materials, multiple mechanisms have been found which produce thermally rectifying behaviour. The one mechanism that we ll consider is when we have two dissimilar materials at a contact which have difference in temperature dependence of thermal conductivity.

A thermal rectifier is a device in which heat flows in a forward direction while it can hardly flow in the opposite direction as an analog of the diode. Devices that are composed of materials that are capable of transporting heat along a specific path with extremely high transfer rates (high conductivity) while at the same time insulating the components along the same path that are sensitive, are the ideal candidate materials for future electronic cooling applications.

We ll now study, under which circumstances we can observe the phenomenon of thermal rectification. It is pretty obvious that if we have only one material, which

has a constant thermal conductivity κ or its thermal conductivity has spatial or temperature dependence $\kappa(x, T)$, we ll not observe the rectification phenomenon since the temperature will propagate in exact the same way, regardless the position where we put the heat pulse. So, the setup that we ll study is the one that we have two bounded materials, where each one has different thermal conductivity.

The cases that we are interested in are two: the static thermal rectification and the dynamic thermal rectification. The main difference between these two cases is that in the static case, we contact our sample to two heat baths (one hot and one colder) measuring the heat current, and after that we reverse the order of the heat baths and we measure the heat current again, when at the dynamic case we put a heat pulse at the left surface of our material and measure the temperature change at the right surface and then via versa. The crucial point in order to observe the thermal rectification phenomenon is that the heat fluxes (in the static case) and the temperature change (in the dynamic case) must differ when we reverse the order of the heat baths (static case) or put the heat pulse at opposite surfaces (dynamic case).

3.1 Static Rectification

As we mentioned earlier, our material is composed of two other materials that are bounded together, and each one has different thermal conductivity. We assume that each material, has constant thermal conductivity and we ll study if it's possible to observe the phenomenon of thermal rectification under this condition.

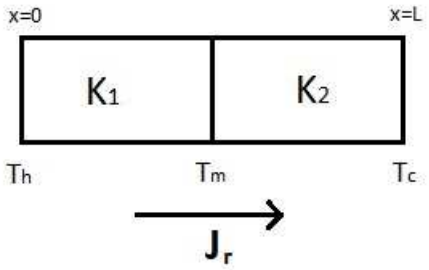

We ll calculate the heat flux J_r by integrating the Heat Flux equation:

$$J_r = -\kappa \frac{dT}{dx}. \tag{3.1}$$

We first integrate the heat flux equation from $x = 0$ to $x = L$, and we get:

$$\int_{x=0}^{x=L/2} J_r \, dx = -\int_{T_h}^{T_m} \kappa_1 \, dT(x) \;\; \Rightarrow$$

$$J_r \, L/2 = -\kappa_1 T\Big|_{T_h}^{T_m} \Rightarrow \; J_r \, L/2 = -\kappa_1 (T_m - T_h). \tag{3.2}$$

By integrating the flux equation from $x = L/2$ to $x = L$, we get :

$$J_r \, L/2 = -\kappa_2 (T_c - T_m) \tag{3.3}$$

and by abstracting Equation (3.3) from Equation (3.2) we can get an expression for the interface's temperature:

$$J_r L/2 - J_r L/2 = -\kappa_1 (T_m - T_h) + \kappa_2 (T_c - T_m) \;\Rightarrow$$

$$J_r L/2 - J_r L/2 = -\kappa_1 (T_m - T_h) + \kappa_2 (T_c - T_m) \;\Rightarrow$$

$$T_m = \frac{\kappa_1 T_h + \kappa_2 T_c}{\kappa_1 + \kappa_2}. \tag{3.4}$$

If we subtract Equation (3.2) and Equation (3.3),we can get the final expression that gives us the heat current J_r:

$$J_r L/2 + J_r L/2 = J_r L = -\kappa_1 (T_m - T_h) - \kappa_2 (T_c - T_m) \Rightarrow$$

$$J_r L = \kappa_1 T_h - \kappa_2 T_c - \kappa_1 T_m + \kappa_2 T_m \tag{3.5}$$

and by taking Equation (3.4) into account, Equation (3.5) becomes:

$$J_r L = \kappa_1 T_h - \kappa_2 T_c - \kappa_1 \frac{\kappa_1 T_h + \kappa_2 T_c}{\kappa_1 + \kappa_2} + \kappa_2 \frac{\kappa_1 T_h + \kappa_2 T_c}{\kappa_1 + \kappa_2} \Rightarrow$$

$$J_r L(\kappa_1 + \kappa_2) = \kappa_1(\kappa_1 + \kappa_2) T_h - \kappa_2(\kappa_1 + \kappa_2) T_c - \kappa_1(\kappa_1 T_h + \kappa_2 T_c) + \kappa_2(\kappa_1 T_h + \kappa_2 T_c) \Rightarrow$$

$$J_r L(\kappa_1 + \kappa_2) = \kappa_1^2 T_h + \kappa_1 \kappa_2 T_h - \kappa_1 \kappa_2 T_c - \kappa_2^2 T_c - \kappa_1^2 T_h - \kappa_1 \kappa_2 T_c + \kappa_1 \kappa_2 T_h + \kappa_2^2 T_c \Rightarrow$$

$$J_r = \frac{2\kappa_1 \kappa_2 (T_h - T_c)}{L \cdot (\kappa_1 + \kappa_2)}. \tag{3.6}$$

If we now reverse the order of the heat baths, like is shown in the following figure, and do the same calculations as before in order to find J_f we get:

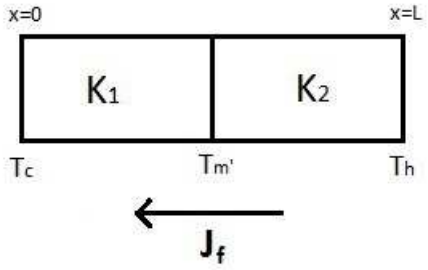

$$J_f = -\frac{2\kappa_1\kappa_2(T_h - T_c)}{L \cdot (\kappa_1 + \kappa_2)} \Rightarrow |J_f| = |J_r| \,. \tag{3.7}$$

So, we conclude that in the case that the two thermal conductivities are different but constants, we don't observe any difference in the calculated heat currents, which means that we don't have rectification. In the next section, we ll study the case that the thermal conductivities have temperature dependence, and we ll try to conclude if we can achieve thermal rectification in this case.

3.2 Dynamic Rectification

In this subsection we ll try to conclude under which circumstances we can achieve dynamic thermal rectification. In this case, we have our material and we put a heat pulse at the left surface and we measure the temperature change at the right surface, and via versa. If we observe difference in the two measured temperatures (one when we put the heat pulse at the left surface, and one when we put at the right) then we have achieved dynamic thermal rectification. In order to show which are the circumstances in order to achieve dynamic thermal rectification, we have to introduce the concept of "Reciprocity of Green's function".

The phenomenon of reciprocity, which is known in physics, also occurs in the case of heat propagation in a solid. To be more specific, if the heat source is at point 1 and at point 2 causes a temperature change ΔT, then when the source is shifted to point 2, at point 1 there occurs the same change in temperature ΔT. In this section , we want to study and conclude what form must the diffusion coefficient have in order to get a different temperature change ΔT when we shift the heat source from point 1 to point 2.

First, we assume that our diffusion coefficient has only spatial dependence and it's independent of temperature, so the diffusion equation becomes:

$$\frac{\partial T(x,t)}{\partial t} = \frac{\partial}{\partial x}(D(x)\frac{\partial T(x,t)}{\partial x}). \tag{3.8}$$

If we suppose that temperature has the following form:

$$T(x,t) = e^{\lambda t}T(x) \tag{3.9}$$

then, Equation 3.8 becomes

$$\frac{\partial}{\partial x}(D(x)\frac{\partial T(x,t)}{\partial x}) = \lambda e^{\lambda t}T(x) \quad \Rightarrow$$

$$LT(x,t) = \lambda T(x,t). \tag{3.10}$$

This is a Sturm-Liouville eigenvalue problem, where the differential operator has the form:

$$L = \frac{d}{dx}(D(x)\frac{d}{dx}) = \frac{dD(x)}{dx}\frac{d}{dx} + D(x)\frac{d^2}{dx^2}. \tag{3.11}$$

This differential operator is linear and second order.We will now check if this operator is self-adjoint:

$$\langle f, Lg\rangle = \int_a^b \overline{f(x)}[\frac{d}{dx}(D(x)\frac{dg}{dx})]\,dx = \overline{f(x)}D(x)g'(x)\Big|_a^b - \int_a^b \overline{f'(x)}D(x)g'(x)\,dx \tag{3.12}$$

and similarly we get

$$\langle Lf, g\rangle = \int_a^b \overline{\frac{d}{dx}(D(x)\frac{df}{dx})}\,g(x)\,dx = D(x)\overline{f'(x)}g(x)\Big|_a^b - \int_a^b D(x)\overline{f'(x)}g'(x)\,dx. \tag{3.13}$$

We now calculate the following expression,

$$\begin{aligned}\langle f, Lg\rangle - \langle Lf, g\rangle &= \overline{f(x)}D(x)g'(x)\Big|_a^b - D(x)\overline{f'(x)}g(x)\Big|_a^b = \\ &= \overline{f(b)}D(b)g'(b) - \overline{f(a)}D(a)g'(a) - D(b)\overline{f'(b)}g(b) + D(a)\overline{f'(a)}g(a) = \\ &= D(b)[\overline{f(b)}g'(b) - f'(b)g(b)] - D(a)[\overline{f(a)}g'(a) - f'(a)g(a)].\end{aligned} \tag{3.14}$$

Assuming that functions f, g obey the same boundary conditions (mixed Dirichlet-Neumann):

$$c_a f(a) + d_a f'(a) = 0 \Leftrightarrow c_a\overline{f(a)} + d_a\overline{f'(a)} = 0 \tag{3.15}$$

$$c_a g(a) + d_a g'(a) = 0 \tag{3.16}$$

we can prove

$$\frac{c_a\overline{f(a)}}{c_a g(a)} = \frac{-d_a\overline{f'(a)}}{-d_a g'(a)} \Rightarrow \frac{\overline{f(a)}}{g(a)} = \frac{\overline{f'(a)}}{g'(a)} \Rightarrow$$

$$\overline{f'(a)}g(a) - \overline{f(a)}g'(a) = 0. \tag{3.17}$$

Similarly we get

$$\overline{f'(b)}g(b) - \overline{f(b)}g'(b) = 0. \tag{3.18}$$

After these results, Equation 3.14 becomes

$$\langle f, Lg\rangle - \langle Lf, g\rangle = 0 \Rightarrow \langle f, Lg\rangle = \langle Lf, g\rangle \tag{3.19}$$

which means that operator L is self-adjoint on Hilbert space $\Longrightarrow$ L is a Sturm-Liouville operator.

Since operator L is self-adjoint, we can check the reciprocity and the symmetry of the Green's function. We use the Green's identity in 1D for the ODE with operators in S-L form:

$$L = \frac{d}{dx}(p(x)\frac{d}{dx}) + q(x),$$

which is:

$$\langle u, Lv\rangle - \langle Lu, v\rangle = \left[p(x)(\overline{u}\frac{dv}{dx} - v\frac{\overline{du}}{dx})\right]_a^b \tag{3.20}$$

which is equal to zero when L is a self adjoint operator, as we showed earlier.

We now take $v = G(x, x_1)$ and $u = G(x, x_2)$, which both satisfy boundary conditions of the form of Equation 3.15. Furthermore , since $Lv = \delta(x - x_1)$, we use Green's identity and we get:

$$\langle G(x, x_2), LG(x, x_1)\rangle - \langle LG(x, x_2), G(x, x_1)\rangle =$$

$$= \int_a^b \left[\overline{G(x, x_2)}LG(x, x_1) - \overline{LG(x, x_2)}G(x, x_1)\right]dx = 0 \Leftrightarrow$$

$$\Leftrightarrow \int_a^b \left[\overline{G(x, x_2)}\delta(x - x_1) - \overline{LG(x, x_2)}G(x, x_1)\right]dx = 0 \Leftrightarrow$$

$$\Leftrightarrow \int_a^b \overline{G(x, x_2)}\delta(x - x_1)dx = \int_a^b \overline{LG(x, x_2)}G(x, x_1)dx. \tag{3.21}$$

Therefore, from the sifting property of the Dirac function, we get:

$$\overline{G(x_1,x_2)} = \int_a^b \overline{LG(x,x_2)}G(x,x_1)dx = \overline{\int_a^b LG(x,x_2)\overline{G(x,x_1)}dx} =$$

$$= \overline{\int_a^b \delta(x-x_2)} = \overline{\overline{G(x_2,x_1)}} = G(x_2,x_1) \Leftrightarrow$$

$$\Leftrightarrow \overline{G(x_1,x_2)} = G(x_2,x_1). \tag{3.22}$$

Physically, the above result says that the response at x_1 due to a concentrated source at x_2 is the same as the response at x_2 due to a concentrated source at x_1. Of course, we would have concluded to the same result if the Diffusion coefficient was a constant.

Note that, this is all reliant on the fact that the operator is fully self-adjoint.If the given problem is self-adjoint, the operators L and $\tilde{L}$ coincide. In this case the Green's function $\widetilde{G}$ of the adjoint problem must coincide with G since the solution of the given differential equation is unique and allows the existence of a single Green's function only.

Concluding, we just showed that when the diffusion equation is linear, shifting the heat source from point 1 to point 2, gives us the same temperature change ΔT at points 2 and 1 respectively. So if we want to see different temperature change when we shift the heat source, the differential operator (Equation 3.11) must be non-linear, which is achieved when the diffusion coefficient is temperature dependent.

Assuming that the diffusion coefficient has the following form:

$$D(T) = D_0 + \eta T \tag{3.23}$$

the differential operator (Equation 3.11) becomes:

$$L = \frac{d}{dx}(D(T)\frac{d}{dx}) = \frac{dD(T)}{dx}\frac{d}{dx} + D(T)\frac{d^2}{dx^2} \tag{3.24}$$

which is clearly a non-linear operator. So our problem is not self-adjoint anymore, which leads us to two different Green's functions that do not coincide,

$$\overline{G(x_1,x_2)} \neq G(x_2,x_1). \tag{3.25}$$

The above result says that the response at x_1 due to a concentrated source at x_2 is different as the response at x_2 due to a concentrated source at x_1.

4 Static Thermal Rectification

In the previous chapter we showed that if our two bounded materials have constant thermal conductivities, then we can't observe the phenomenon of thermal rectification. So, our next move is to study if we ll achieve thermal rectification in the case where our two materials' thermal conductivities are not constants, but they have dependence on temperature.

4.1 Static Thermal Rectification

We demonstrate the thermal rectification in a device made of two magnetic materials, one is spin chain material and the other is spin ladder (we ll examine several cases of different materials). We consider the heat current density J through the bar made of materials A and B bonded at the center. J is described by Fourier's law,

$$J = -\kappa(T(x))\frac{dT(x)}{dx} \tag{4.1}$$

where κ represents the thermal conductivity as a function of position $T(x)$. Here, we suppose that the material A exhibits a high κ at low temperature T_L, and a relatively low κ at high temperature T_H, while the material B displays the opposite property.Then, we provide two heat baths with T_H and T_L. When the materials A and B are connected to the heat baths with T_L and T_H,respectively, a total thermal conductance of the sample should be relatively high leading to a high heat current density

J_f through Eq. 4.1 (we call this direction the forward direction, see the lower left panel in figure 4.1). On the other hand, if the boundary conditions are reversed, the total thermal conductance becomes smaller than the other one, resulting in a smaller heat current density J_r than J_f. Thus, the rectifying coefficient defined by the ratio of $|J_f|$ to $|J_r|$,

$$R = \frac{|J_f|}{|J_r|}, \tag{4.2}$$

should be above one. If its value is one, then the values of the heat fluxes are equal and no rectification occurs.

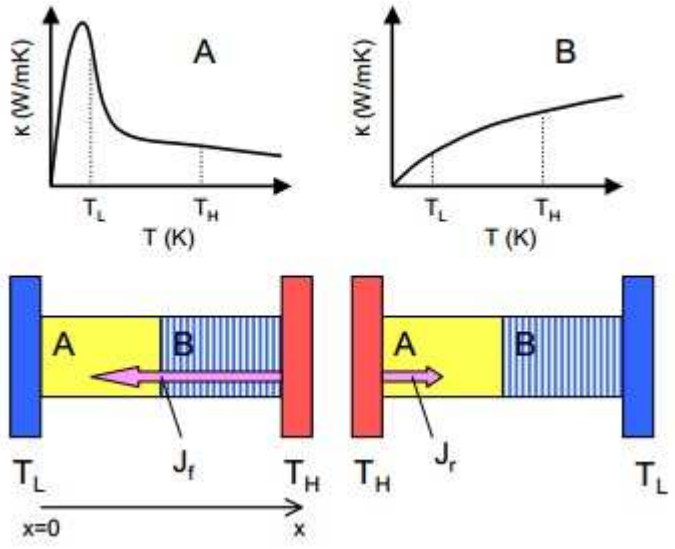

Figure 4.1: Top panels: Schematic figures of the thermal conductivity that is required for thermal rectification. Bottom panels: conceptual diagrams of the thermal rectification in bonded materials. Picture taken from [10]

We ll examine 2 special cases of thermal conductivity's form: the first one is when the thermal conductivity has linear dependence of temperature and the other is when has quadratic dependence of temperature.

4.1.1 Thermal Conductivity - Linear Form

At this point, we assume that material's A thermal conductivity can be written as

$$\kappa_1 = \kappa_{10} + \lambda(T - T_0) \tag{4.3}$$

and material's B as

$$\kappa_2 = \kappa_{20} + \mu(T - T_0), \tag{4.4}$$

where κ_{10}, κ_{20}, λ, μ and T_0 are constants. These constants have to be found from the figures that give us the temperature dependence of the thermal conductivity of these materials.More specifically, assume the case of Equation 4.3, κ_{10} is the thermal conductivity of the sample when $T = T_0$,where T_0 is the initial temperature of our material,before the connection with the heat baths. When we talk about material A,we are referring to a spin chain material and when we talk about material B, we are referring to a spin ladder material.

The main point is to find analytical expressions for J_f and J_r, as described before, when thermal conductivity is not constant but depends from temperature. The next step after this one is to calculate the Rectification factor R, which was represented in Equation 4.2. We now introduce T_m, which is the temperature at the centre of our bounded material and L which of course is the length of our bounded material. We ll first find J_f and then we ll do the analogous calculations to find J_r.

So, for J_r from Eq. (4.1) we get

$$J_r\, dx = -\kappa(T)\, T(x). \tag{4.5}$$

Next step is to integrate Equation 4.5 from $x = 0$ to $x = L$, but to simplify the calculations we ll split this integration into 2 parts. First, we ll integrate from $x = 0$ to $x = L/2$ (which is the center of our material where temperature is T_m) and then we ll do a second integration from $x = L/2$ to $x = L$. After these two steps, we ll have 2 equations with 2 unknown parameters, J_r and T_m.We ll then solve them to find T_m and after that step, we ll get the final expression for J_r. From $x = 0$ to $x = L/2$ we have the material A, so we ll use κ_1 (Equation 4.3) as the thermal conductivity $\kappa(T)$ in Equation 4.5. Similarly, we ll use κ_2 (Equation 4.4) as $\kappa(T)$ when we ll integrate from $x = L/2$ to $x = L$.

So, our first move is to integrate Equation 4.5 from $x = 0$ to $x = L/2$, taking notice that since we examine the forward direction, the hot heat bath T_h is at $x = 0$ and the cold heat bath is at $x = L$,

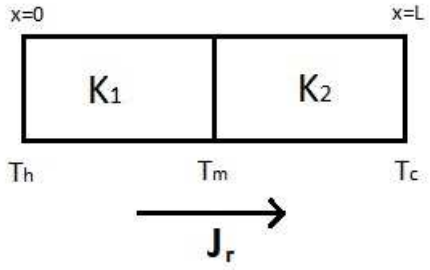

$$\int_{x=0}^{x=L/2} J_r\, dx = -\int_{T_h}^{T_m} \kappa_1(T)\, dT(x) \;\Rightarrow$$

$$J_r\, L/2 = -\int_{T_h}^{T_m} \left(\kappa_{10} + \lambda(T - T_0)\right) dT(x) = -\kappa_{10} \int_{T_h}^{T_m} dT(x) - \lambda \int_{T_h}^{T_m} (T - T_0)\, dT(x) \;\Rightarrow$$

$$J_r\, L/2 = -\kappa_{10} T\Big|_{T_h}^{T_m} - \frac{\lambda}{2} T^2\Big|_{T_h}^{T_m} + \lambda T_0\, T\,\Big|_{T_h}^{T_m} \;\Rightarrow$$

$$J_r\, L/2 = -\kappa_{10}(T_m - T_h) + \lambda T_0 (T_m - T_h) - \frac{\lambda}{2}(T_m^2 - T_h^2). \tag{4.6}$$

If we now integrate Equation 4.5 from $x = L/2$ to $x = L$, we get

$$\int_{x=L/2}^{x=L} J_r\, dx = -\int_{T_m}^{T_c} k_2(T)\, dT(x) \;\Rightarrow$$

$$J_r\, L/2 = -\int_{T_m}^{T_c} \left(\kappa_{20} + \lambda(T - T_0)\right) dT(x) \;\Rightarrow$$

$$J_r\, L/2 = -\kappa_{20}(T_c - T_m) + \mu T_0 (T_c - T_m) - \frac{\mu}{2}(T_c^2 - T_m^2). \tag{4.7}$$

Our next move is to abstract Equation 4.7 from Equation 4.6,

$$J_r L/2 - JL/2 = -\kappa_{10}(T_m - T_h) + \lambda T_0 (T_m - T_h) - \frac{\lambda}{2}(T_m^2 - T_h^2) + \kappa_{20}(T_c - T_m) - \mu T_0 (T_c - T_m) + \frac{\mu}{2}(T_c^2 - T_m^2) \;\Rightarrow$$

$$-\kappa_{10}(T_m - T_h) + \lambda T_0 (T_m - T_h) - \frac{\lambda}{2}(T_m^2 - T_h^2) + \kappa_{20}(T_c - T_m) - \mu T_0 (T_c - T_m) + \frac{\mu}{2}(T_c^2 - T_m^2) = 0 \;\Rightarrow$$

$$-\frac{1}{2}(\mu+\lambda)T_m^2+(-\kappa_{10}-\kappa_{20}+\lambda T_0+\mu T_0)T_m+$$
$$+(-\lambda T_0\,T_h-\mu T_0 T_c+\frac{\lambda}{2}T_h^2+\kappa_{10}T_h+\frac{\mu}{2}T_c^2+\kappa_{20}T_c)=0. \quad (4.8)$$

The Equation 4.8 can be simplified to the following form

$$\alpha T_m^2+\beta T_m+\gamma=0, \quad (4.9)$$

where

$$\alpha=-\frac{1}{2}(\mu+\lambda)$$
$$\beta=-\kappa_{10}-\kappa_{20}+\lambda T_0+\mu T_0$$
$$\gamma=-\lambda T_0\,T_h-\mu T_0 T_c+\frac{\lambda}{2}T_h^2+\kappa_{10}T_h+\frac{\mu}{2}T_c^2+\kappa_{20}T_c.$$

Equation 4.8 / 4.9 is a quadratic equation and it's roots are given by

$$T_{m\pm}=\frac{-\beta\pm\sqrt{\beta^2-4\alpha\gamma}}{2\alpha}. \quad (4.10)$$

Every parameter that is in the coefficients α, β and γ is known, so it is very easy to extract T_{m+} and T_{m-} from Equation 4.10. As we ll see later, when we ll put the real values of these parameters in Equation 4.10, only one of the two values of T_m will be acceptable, since the second one is either bigger than T_h or smaller than T_c. T_m is the temperature at the center of our bounded material, so it's pretty logical to have a value between our two heat baths T_h and T_c.

Next step after finding the right T_m value, is to find the final expression for J_r. By adding the corresponding sides of Equations 4.6 and 4.7 together, we form the following equation

$$J_r L=-\kappa_{10}(T_m-T_h)+\lambda T_0(T_m-T_h)-\frac{\lambda}{2}(T_m^2-T_h^2)$$
$$-\kappa_{20}(T_c-T_m)+\mu T_0(T_c-T_m)-\frac{\mu}{2}(T_c^2-T_m^2), \quad (4.11)$$

which is the final expression that gives us J_r, since all the parameters are known.

We ll now find J_f using the previous method, but now we integrate from $x=L$ to $x=0$, taking notice that the heat baths are the same, in reversed order (the hot heat bath T_h is at $x=L$ and the cold heat bath is at $x=0$).

So,by integrating Eq. (4.5) from $x=L$ to $x=L/2$, we get:

$$J_f\,L/2=-\kappa_{20}(T_{m'}-T_h)+\mu T_0(T_{m'}-T_h)-\frac{\mu}{2}(T_{m'}^2-T_h^2). \quad (4.12)$$

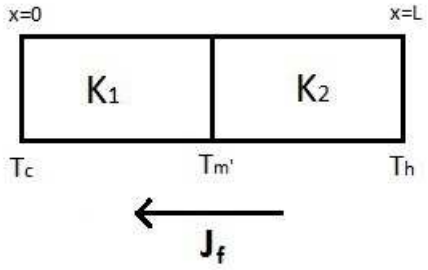

By integrating Equation 4.5 from $x = L/2$ to $x = 0$, we get

$$J_f\, L/2 = -\kappa_{10}(T_c - T_{m'}) + \lambda T_0(T_c - T_{m'}) - \frac{\lambda}{2}(T_c^2 - T_{m'}^2). \tag{4.13}$$

If we abstract Equation 4.13 from Equation 4.12, we get the expression that gives us $T_{m'}$:

$$-\frac{1}{2}(\mu+\lambda)T_{m'}^2 + (-\kappa_{10} - \kappa_{20} + \lambda T_0 + \mu T_0)T_{m'} + (-\lambda T_0\, T_c - \mu T_0 T_h + \frac{\lambda}{2}T_c^2 + \kappa_{10}T_c + \frac{\mu}{2}T_h^2 + \kappa_{20}T_h) = 0. \tag{4.14}$$

The Equation 4.14 can be simplified to the following form

$$\alpha' T_{m'}^2 + \beta' T_{m'} + \gamma' = 0, \tag{4.15}$$

where

$$\alpha' = -\frac{1}{2}(\mu+\lambda)$$

$$\beta' = -\kappa_{10} - \kappa_{20} + \lambda T_0 + \mu T_0$$

$$\gamma' = -\lambda T_0\, T_c - \mu T_0 T_h + \frac{\lambda}{2}T_c^2 + \kappa_{10}T_c + \frac{\mu}{2}T_h^2 + \kappa_{20}T_h.$$

Equation 4.14 / 4.15 is a quadratic equation and its roots are given by

$$T_{m'\pm} = \frac{-\beta' \pm \sqrt{\beta'^2 - 4\alpha'\gamma'}}{2\alpha'}. \tag{4.16}$$

Every parameter that is in the coefficients α', β' and γ' is known, so it is very easy to extract $T_{m'+}$ and $T_{m'-}$ from Equation 4.16. If we put the real values of these parameters in Equation 4.16, only one of the two values of $T_{m'}$ will be acceptable, since the second one is either bigger than T_h or smaller than T_c. $T_{m'}$ is the temperature at the center of our bounded material, so it's pretty logical to have a value between our two heat baths T_h and T_c.

Next step and final step after finding the right $T_{m'}$ value, is to find the final expression for J_f. By adding the corresponding sides of Equations 4.12 and 4.13 together, we form the following equation

$$J_f L = -\kappa_{20}(T_{m'} - T_h) + \mu T_0(T_{m'} - T_h) - \frac{\mu}{2}(T_{m'}^2 - T_h^2) \\ - \kappa_{10}(T_c - T_{m'}) + \lambda T_0(T_c - T_{m'}) - \frac{\lambda}{2}(T_c^2 - T_{m'}^2), \quad (4.17)$$

which is the final expression that gives us J_f, since all the parameters are known.

Finally, we can calculate the Rectification factor, Equation 4.2, since we got the expressions for heat current for both directions (Equations 4.11 & 4.17).

4.1.2 Thermal Conductivity - Linear & Quadratic Form

We consider another special case, where material A's thermal conductivity has linear dependence on temperature (same as before), but material B's thermal conductivity has quadratic dependence on temperature. More specifically, the thermal conductivities have the following forms:

$$\kappa_1 = \kappa_{10} + \lambda(T - T_0) \quad (4.18)$$

and material's B as

$$\kappa_2 = \kappa_{20} + \mu(T - T_0)^2, \quad (4.19)$$

where κ_{10}, κ_{20}, λ, μ and T_0 are known constants.

We are following the same formalism as the one we used in the previous paragraph, wanting to export analytical expressions for J_f (heat pulse propagates in forward direction) and J_r (heat pulse propagates in backward direction) in order to calculate the Rectification coefficient R, Equation 4.2.

So,we ll start with the forward direction, integrating Equation 4.5 from $x = 0$ to $x = L/2$, where we can use the result of Equation 4.6:

$$J_r\, L/2 = -\kappa_{10}(T_m - T_h) + \lambda T_0(T_m - T_h) - \frac{\lambda}{2}(T_m^2 - T_h^2). \quad (4.20)$$

Our next step is to integrate Equation 4.5 from $x = L/2$ to $x = L$. In that case, we ll obtain the same result as Equation 4.7:

$$\int_{x=L/2}^{x=L} J_r\, dx = -\int_{T_m}^{T_c} \kappa_2(T)\, dT(x) \;\Rightarrow$$

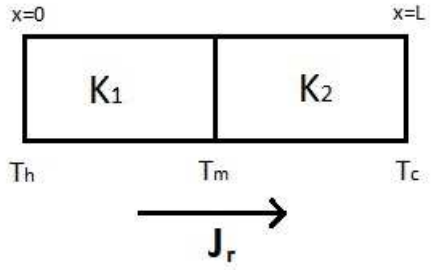

$$J_r\,L/2 = -\int_{T_m}^{T_c} (\kappa_{20} + \mu(T - T_0)^2)\,dT(x) = -\kappa_{20}\int_{T_m}^{T_c} dT(x) - \mu\int_{T_m}^{T_c}(T - T_0)^2\,dT(x) \;\Rightarrow$$

$$J_r\,L/2 = -\kappa_{20}\int_{T_m}^{T_c} dT(x) - \mu\int_{T_m}^{T_c}(T^2 - 2T\,T_0 + {T_0}^2)\,dT(x) \;\Rightarrow$$

$$J_r\,L/2 = -\kappa_{20}T\Big|_{T_m}^{T_c} - \frac{\mu}{3}T^3\Big|_{T_m}^{T_c} + 2\mu T_0\frac{T^2}{2}\Big|_{T_m}^{T_c} - \mu{T_0}^2\,T\Big|_{T_m}^{T_c} \;\Rightarrow$$

$$J_r\,L/2 = -\kappa_{20}(T_c - T_m) - \frac{\mu}{3}(T_c^3 - T_m^3) + \mu T_0(T_c^2 - T_m^2) - \mu T_0^2(T_c - T_m). \tag{4.21}$$

We now abstract Equation 4.21 from Equation 4.20 in order to get an expression,where our only unknown parameter is T_m,

$$J_rL/2 - J_rL/2 = -\kappa_{10}(T_m - T_h) + \lambda T_0(T_m - T_h) - \frac{\lambda}{2}(T_m^2 - T_h^2)$$
$$+ \kappa_{20}(T_c - T_m) + \frac{\mu}{3}(T_c^3 - T_m^3) - \mu T_0(T_c^2 - T_m^2) + \mu T_0^2(T_c - T_m) \;\Rightarrow$$

$$-\frac{\mu}{3}T_m^3 + (\mu T_0 - \frac{\lambda}{2})T_m^2 + (-\kappa_{10} + \lambda T_0 - \mu T_0^2 - k_{20})T_m$$
$$+ (\kappa_{10}T_h + \frac{\mu}{3}T_c^3 - \mu T_0T_c^2 + \mu T_0^2T_c + \kappa_{20}T_c + \frac{\lambda}{2}T_h^2 - \lambda T_0T_h) = 0. \tag{4.22}$$

Equation 4.22 can be rewritten to the simpler form

$$\alpha T_m^3 + \beta T_m^2 + \gamma T_m + \delta = 0 \tag{4.23}$$

where

$$\alpha = -\frac{\mu}{3}$$

$$\beta = \mu T_0 - \frac{\lambda}{2}$$

$$\gamma = -k_{10} + \lambda T_0 - \mu T_0^2 - \kappa_{20}$$

$$\delta = \kappa_{10} T_h + \frac{\mu}{3} T_c^3 - \mu T_0 T_c^2 + \mu T_0^2 T_c + \kappa_{20} T_c + \frac{\lambda}{2} T_h^2 - \lambda T_0 T_h.$$

Equation 4.23 is a cubic equation that has 3 roots. When we find the 3 roots, we keep the one that satisfies the following inequality, $T_h > T_m > T_c$. After finding the value of T_m, our final move for obtaining the expression which gives us the value of the forward heat current, is to subtract Equation 4.20 and Equation 4.21, getting

$$J_r \cdot L = -\kappa_{10}(T_m - T_h) + \lambda T_0 (T_m - T_h) - \frac{\lambda}{2}(T_m^2 - T_h^2) \\ - \kappa_{20}(T_c - T_m) - \frac{\mu}{3}(T_c^3 - T_m^3) + \mu T_0 (T_c^2 - T_m^2) - \mu T_0^2 (T_c - T_m). \quad (4.24)$$

We obtained the expression for J_r and now we ll find the corresponding expression for J_f, where the heat pulse propagates forward.

In order to find the J_f, we set our heat baths in reversed order (T_h is at $x = L$ and T_c is at $x = 0$) and we integrate Equation 4.5 from $x = L$ to $x = 0$.

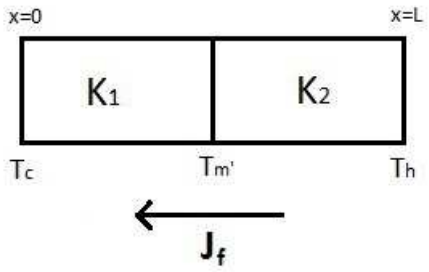

Our first move is to integrate from $x = L$ to $x = L/2$ and the result we ll get, is the same as Equation 4.21:

$$J_f \, L/2 = -\kappa_{20}(T_{m'} - T_h) - \frac{\mu}{3}(T_{m'}^3 - T_h^3) + \mu T_0 (T_{m'}^2 - T_h^2) - \mu T_0^2 (T_{m'} - T_h). \quad (4.25)$$

We continue with the integration from $x = L/2$ to $x = 0$, which will have the same result as Equation 4.20:

$$J_f \, L/2 = -\kappa_{10}(T_c - T_{m'}) + \lambda T_0 (T_c - T_{m'}) - \frac{\lambda}{2}(T_c^2 - T_{m'}^2). \quad (4.26)$$

We now abstract Equation 4.26 from Equation 4.25 in order to get an expression,where our only unknown parameter is T_m,

$$J_f L/2 - J_f L/2 = -\kappa_{20}(T_{m'} - T_h) - \frac{\mu}{3}(T_{m'}^3 - T_h^3) + \mu T_0(T_{m'}^2 - T_h^2) - \mu T_0^2(T_{m'} - T_h) + k_{10}(T_c - T_{m'}) - \lambda T_0(T_c - T_{m'}) + \frac{\lambda}{2}(T_c^2 - T_{m'}^2) \Rightarrow$$

$$-\frac{\mu}{3}T_{m'}^3 + (\mu T_0 - \frac{\lambda}{2})T_{m'}^2 + (-\kappa_{20} + \lambda T_0 - \mu T_0^2 - \kappa_{10})T_{m'} + (\kappa_{20}T_h + \frac{\mu}{3}T_h^3 - \mu T_0 T_h^2 + \mu T_0^2 T_h + \kappa_{10}T_c + \frac{\lambda}{2}T_c^2 - \lambda T_0 T_c) = 0. \quad (4.27)$$

Equation 4.22 can be rewritten to the simpler form

$$\alpha' T_{m'}^3 + \beta' T_{m'}^2 + \gamma' T_{m'} + \delta' = 0 \quad (4.28)$$

where

$$\alpha' = -\frac{\mu}{3}$$
$$\beta' = \mu T_0 - \frac{\lambda}{2}$$
$$\gamma' = -\kappa_{20} + \lambda T_0 - \mu T_0^2 - \kappa_{10}$$
$$\delta' = \kappa_{20}T_h + \frac{\mu}{3}T_h^3 - \mu T_0 T_h^2 + \mu T_0^2 T_h + \kappa_{10}T_c + \frac{\lambda}{2}T_c^2 - \lambda T_0 T_c.$$

Equation 4.28 is a cubic equation that has 3 roots. When we find the 3 roots, we keep the one that satisfies the following inequality, $T_h > T_{m'} > T_c$. After finding the value of $T_{m'}$, our final move for obtaining the expression which gives us the value of the backward heat current, is to subtract Equation 4.25 and Equation 4.26, getting:

$$J_f \cdot L = -\kappa_{20}(T_{m'} - T_h) - \frac{\mu}{3}(T_{m'}^3 - T_h^3) + \mu T_0(T_{m'}^2 - T_h^2) - \mu T_0^2(T_{m'} - T_h) - \kappa_{10}(T_c - T_{m'}) + \lambda T_0(T_c - T_{m'}) - \frac{\lambda}{2}(T_c^2 - T_{m'}^2). \quad (4.29)$$

Using Equation 4.2, we can calculate the Rectification factor, since we got the expressions for heat current for both directions (Equations 4.24 & 4.29).

4.2 Experimental Static Rectification

We ll now put real values in the above equations and we ll calculate the rectification that some bounded spin chain-ladder materials present.

4.2.1 case 1: Sr_2CuO_3 - $Ca_9La_5Cu_{24}O_{41}$ compound

The first case that we ll study, is the Sr_2CuO_3 (Spin chain - Material A) - $Ca_9La_5Cu_{24}O_{41}$ (Spin ladder - Material B) bounded material.

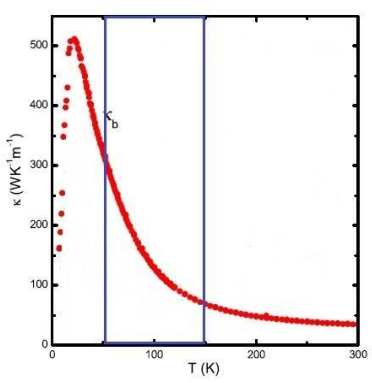

(a) Total thermal conductivity of Sr_2CuO_3

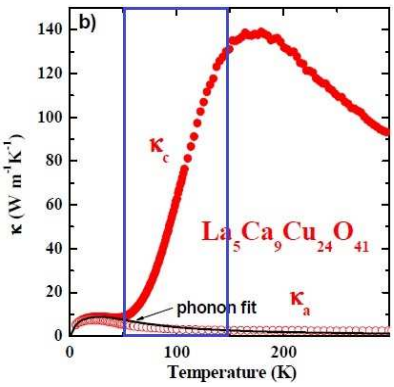

(b) Total thermal conductivity of $Ca_9La_5Cu_{24}O_{41}$

Figure 4.2: The blue boxes in the above figures, show us the range of temperatures that we ll take into account when we ll calculate the thermal rectification. The left surface of each box, corresponds to the low temperature heat bath $T_c = 75\,K$ and the right surface the high temperature heat bath $T_h = 125\,K$.

As we see in figure 4.2, these two materials fulfil the 2 criteria that we mentioned above. Material A (the spin chain) exhibits a high κ at low temperatures (near the T_c) and low κ at high temperatures (near T_h), when material B exhibits low κ near T_c and high κ near T_h. From the above figure, we can extract the thermal conductivity for each material, in the form of Equations 4.2 and 4.3.So, we get:

$$\kappa_1 = 135\frac{W}{m\,K} - 2\cdot(T - T_0)\,\frac{W}{m\,K^2} \tag{4.30}$$

$$\kappa_2 = 63\frac{W}{m\,K} + 1.7 \cdot (T - T_0)\,\frac{W}{m\,K^2}, \tag{4.31}$$

where $T_0 = 100\,K$ for both materials. Now, since both materials have thermal conductivities that have linear dependence on temperature, we can use the results 4.11 and 4.17 in order to calculate the two heat currents, J_r and J_f. After this calculation, we can easily extract the rectification factor from Equation 4.2. In order to calculate J_r from Equation 4.11, we have to find T_m first. Taking into account that $\kappa_{10} = 135\frac{W}{m\,K}$, $\kappa_{20} = 63\frac{W}{m\,K}$, $\lambda = -2\frac{W}{m\,K^2}$ and $\mu = +1.7\frac{W}{m\,K^2}$ we get:

$$\alpha = -\frac{1}{2}(\mu + \lambda) = 0.15\,\frac{W}{m\,K^2}$$

$$\beta = -\kappa_{10} - \kappa_{20} + \lambda T_0 + \mu T_0 = -228\,\frac{W}{m\,K}$$

$$\gamma = -\lambda T_0\,T_h - \mu T_0 T_c + \frac{\lambda}{2}T_h^2 + \kappa_{10}T_h + \frac{\mu}{2}T_c^2 + \kappa_{20}T_c = 23006.25\,\frac{W}{m}.$$

By putting α, β and γ into equation 4.10 we get T_{m+} and T_{m-}:

$$T_{m\pm} = \frac{-\beta \pm \sqrt{\beta^2 - 4\alpha\gamma}}{2\alpha} \Rightarrow$$

$$T_{m+} = 1411.33\,K, \tag{4.32}$$

$$T_{m-} = 108.67\,K. \tag{4.33}$$

Only T_{m-} is acceptable since $T_c < T_{m-} < T_h$, when $T_{m+} \gg T_h$, which is not logical. Now from Equation 4.11, since we found T_m, we can find J_r which is

$$J_r L = 3308.40\,\frac{W}{m}. \tag{4.34}$$

Similarly, we ll calculate J_f. From Equation 4.15 we will find $T_{m'}$ taking into notice that:

$$\alpha' = -\frac{1}{2}(\mu + \lambda) = 0.15\,\frac{W}{m\,K^2}$$

$$\beta' = -\kappa_{10} - \kappa_{20} + \lambda T_0 + \mu T_0 = -228\,\frac{W}{m\,K}$$

$$\gamma' = -\lambda T_0\,T_c - \mu T_0 T_h + \frac{\lambda}{2}T_c^2 + \kappa_{10}T_c + \frac{\mu}{2}T_h^2 + \kappa_{20}T_h = 19406.25\,\frac{W}{m}.$$

By putting α', β' and γ' into Equation 4.16, we get

$$T_{m'+} = 1429.50\,K \tag{4.35}$$

$$T_{m'-} = 90.50\,K. \tag{4.36}$$

As before, only $T_{m'-}$ is acceptable since $T_c < T_{m'-} < T_h$, when $T_{m'+} \gg T_h$, which is not logical. Now from Equation 4.17, since we found T'_m, we can find J_f which is

$$J_f L = 5255.71\,\frac{W}{m}. \tag{4.37}$$

Now, since we know J_r and J_f, we can calculate the rectification factor from Equation 4.2, which is equal to:

$$R = \frac{|J_f|}{|J_r|} = \frac{5255.71}{3308.40} = 1.59 \tag{4.38}$$

4.2.2 case 2: Sr_2CuO_3 - $Sr_{14}Cu_{24}O_{41}$ compound

The second case that we will study is the Sr_2CuO_3 (Spin chain - Material A) - $Sr_{14}Cu_{24}O_{41}$ (Spin ladder - Material B) bounded material.

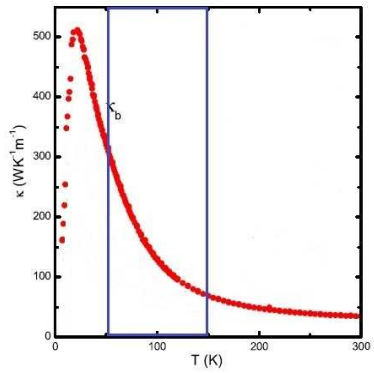

(a) Total thermal conductivity of Sr_2CuO_3

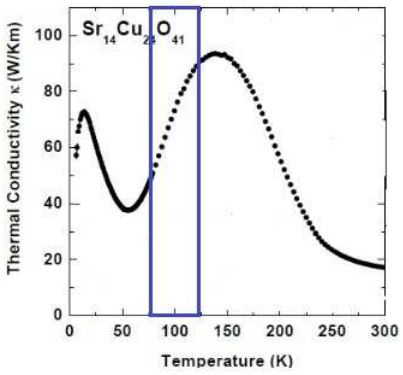

(b) Total thermal conductivity of $Sr_{14}Cu_{24}O_{41}$

Figure 4.3: The blue boxes in the above figures, show us the range of temperatures that we ll take into account when we ll calculate the thermal rectification. The left surface of each box, corresponds to the low temperature heat bath $T_c = 75\,K$ and the right surface the high temperature heat bath $T_h = 125K$.

From the figure 4.3, we can extract the thermal conductivity for each material, in the form of Equations 4.2 and 4.3.So, we get:

$$\kappa_1 = 135\frac{W}{m\,K} - 2\cdot(T - T_0)\,\frac{W}{m\,K^2} \tag{4.39}$$

$$\kappa_2 = 75\frac{W}{m\,K} + 0.9\cdot(T - T_0)\,\frac{W}{m\,K^2}, \tag{4.40}$$

where $T_0 = 100\ K$ for both materials. In order to calculate the thermal rectification factor we follow the same procedure as before.We will first find T_m and then we will calculate J_r from Equation 4.11 taking into account that $\kappa_{10} = 135\frac{W}{m\,K}$, $\kappa_{20} = 75\frac{W}{m\,K}$, $\lambda = -2\frac{W}{m\,K^2}$ and $\mu = +0.9\frac{W}{m\,K^2}$. We ll now find the coefficients of Equation 4.10:

$$\alpha = -\frac{1}{2}(\mu + \lambda) = 0.55\,\frac{W}{m\,K^2}$$

$$\beta = -\kappa_{10} - \kappa_{20} + \lambda T_0 + \mu T_0 = -320\,\frac{W}{m\,K}$$

$$\gamma = -\lambda T_0\,T_h - \mu T_0 T_c + \frac{\lambda}{2}T_h^2 + \kappa_{10}T_h + \frac{\mu}{2}T_c^2 + \kappa_{20}T_c = 27656.25\,\frac{W}{m}.$$

By putting α, β and γ into Equation 4.10 we get T_{m+} and T_{m-}:

$$T_{m\pm} = \frac{-\beta \pm \sqrt{\beta^2 - 4\alpha\gamma}}{2\alpha} \Rightarrow$$

$$T_{m+} = 476.23\ K, \tag{4.41}$$

$$T_{m-} = 105.59\ K. \tag{4.42}$$

Only T_{m-} is acceptable since $T_c < T_{m-} < T_h$, when $T_{m+} \gg T_h$, which is not logical. Now from Equation 4.11, since we found T_m, we can find J_r which is

$$J_r L = 4053.75\,\frac{W}{m}. \tag{4.43}$$

Similarly, we ll calculate J_f. From Equation 4.15 we will find $T_{m'}$ taking into notice that:

$$\alpha' = -\frac{1}{2}(\mu + \lambda) = 0.55\,\frac{W}{m\,K^2}$$

$$\beta' = -\kappa_{10} - \kappa_{20} + \lambda T_0 + \mu T_0 = -320\,\frac{W}{m\,K}$$

$$\gamma' = -\lambda T_0\,T_c - \mu T_0 T_h + \frac{\lambda}{2}T_c^2 + \kappa_{10}T_c + \frac{\mu}{2}T_h^2 + \kappa_{20}T_h = 24656.25\,\frac{W}{m}.$$

By putting α', β' and γ' into equation 4.16, we get

$$T_{m'+} = 490.40\ K \tag{4.44}$$

$$T_{m'-} = 91.41\ K. \tag{4.45}$$

As before, only $T_{m'-}$ is acceptable since $T_c < T_{m'-} < T_h$, when $T_{m'+} \gg T_h$, which is not logical. Now from Equation 4.17, since we found T'_m, we can find J_f which is

$$J_f L = 5534.14\ \frac{W}{m}. \tag{4.46}$$

Now, since we know J_r and J_f, we can calculate the rectification factor from Equation 4.2, which is equal to:

$$R = \frac{|J_f|}{|J_r|} = \frac{5534.14}{4053.75} = 1.37. \tag{4.47}$$

As we notice, the rectification factor in the second case of materials, is smaller than the first case.

4.2.3 case 3: $SrCuO_2$ - $Ca_9La_5Cu_{24}O_{41}$ compound

The third case that we will study is the $SrCuO_2$ (Spin chain - Material A) - $Ca_9La_5Cu_{24}O_{41}$ (Spin ladder - Material B) bounded material.

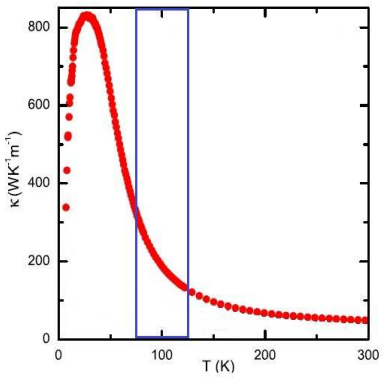

(a) Total thermal conductivity of $SrCuO_2$

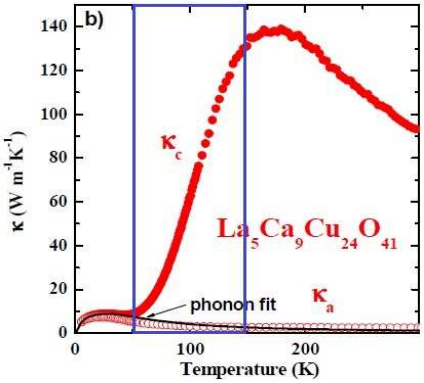

(b) Total thermal conductivity of $Ca_9La_5Cu_{24}O_{41}$

Figure 4.4: The left surface of each blue box, corresponds to the low temperature heat bath $T_c = 75\ K$ and the right surface the high temperature heat bath $T_h = 125K$.

From the figure 4.4, we can extract the thermal conductivity for each material, in the form of Equations 4.2 and 4.3.So, we get:

$$\kappa_1 = 190\frac{W}{m\,K} - 2.1 \cdot (T - T_0)\,\frac{W}{m\,K^2} \tag{4.48}$$

$$\kappa_2 = 63\frac{W}{m\,K} + 1.7 \cdot (T - T_0)\,\frac{W}{m\,K^2}, \tag{4.49}$$

where $T_0 = 100\ K$ for both materials. In order to calculate the thermal rectification factor we follow the same procedure as before.We will first find T_m and then we will calculate J_r from Equation 4.11 taking into account that $\kappa_{10} = 190\frac{W}{m\,K}$, $\kappa_{20} = 63\frac{W}{m\,K}$, $\lambda = -2.1\frac{W}{m\,K^2}$ and $\mu = +1.7\frac{W}{m\,K^2}$. We ll now find the coefficients of Equation 4.10:

$$\alpha = -\frac{1}{2}(\mu + \lambda) = 0.2\,\frac{W}{m\,K^2}$$

$$\beta = -\kappa_{10} - \kappa_{20} + \lambda T_0 + \mu T_0 = -293\,\frac{W}{m\,K}$$

$$\gamma = -\lambda T_0\,T_h - \mu T_0 T_c + \frac{\lambda}{2}T_h^2 + \kappa_{10}T_h + \frac{\mu}{2}T_c^2 + \kappa_{20}T_c = 30350.0\,\frac{W}{m}.$$

By putting α, β and γ into Equation 4.10 we get T_{m+} and T_{m-}:

$$T_{m\pm} = \frac{-\beta \pm \sqrt{\beta^2 - 4\alpha\gamma}}{2\alpha} \Rightarrow$$

$$T_{m+} = 1352.83\ K, \tag{4.50}$$

$$T_{m-} = 112.17\ K. \tag{4.51}$$

Only T_{m-} is acceptable since $T_c < T_{m-} < T_h$, when $T_{m+} \gg T_h$, which is not logical. Now from Equation 4.11, since we found T_m, we can find J_r which is

$$J_r L = 3873.12\,\frac{W}{m}. \tag{4.52}$$

Similarly, we ll calculate J_f. From equation 4.15 we will find $T_{m'}$ taking into notice that:

$$\alpha' = -\frac{1}{2}(\mu + \lambda) = 0.2\,\frac{W}{m\,K^2}$$

$$\beta' = -\kappa_{10} - \kappa_{20} + \lambda T_0 + \mu T_0 = -293\,\frac{W}{m\,K}$$

$$\gamma' = -\lambda T_0\,T_c - \mu T_0 T_h + \frac{\lambda}{2}T_c^2 + \kappa_{10}T_c + \frac{\mu}{2}T_h^2 + \kappa_{20}T_h = 24000.0\,\frac{W}{m}.$$

By putting α', β' and γ' into Equation 4.16, we get

$$T_{m'+} = 1377.91\ K \tag{4.53}$$

$$T_{m'-} = 87.09\ K. \tag{4.54}$$

As before, only $T_{m'-}$ is acceptable since $T_c < T_{m'-} < T_h$, when $T_{m'+} \gg T_h$, which is not logical. Now from equation 4.17, since we found T'_m, we can find J_f which is

$$J_f L = 5555.96\ \frac{W}{m}. \tag{4.55}$$

Now, since we know J_r and J_f, we can calculate the rectification factor from Equation 4.2, which is equal to:

$$R = \frac{|J_f|}{|J_r|} = \frac{5555.96}{3873.12} = 1.43. \tag{4.56}$$

4.2.4 case 4: $SrCuO_2$ - $Sr_{14}Cu_{24}O_{41}$ compound

The third case that we will study is the $SrCuO_2$ (Spin chain - Material A) - $Sr_{14}Cu_{24}O_{41}$ (Spin ladder - Material B) bounded material.

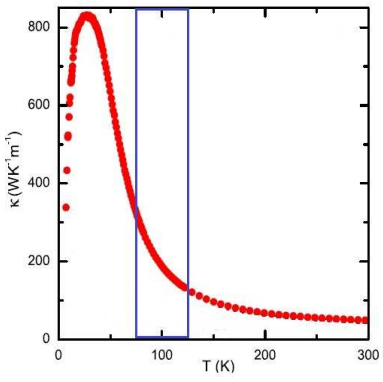

(a) Total thermal conductivity of $SrCuO_2$

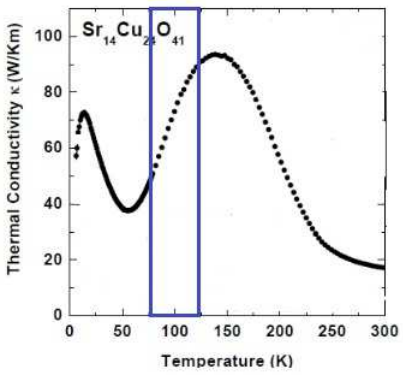

(b) Total thermal conductivity of $Sr_{14}Cu_{24}O_{41}$

Figure 4.5: The left surface of each blue box, corresponds to the low temperature heat bath $T_c = 75\ K$ and the right surface the high temperature heat bath $T_h = 125K$.

From the figure 4.5, we can extract the thermal conductivity for each material, in the form of equations 4.2 and 4.3.So, we get:

$$\kappa_1 = 190\frac{W}{m\,K} - 2.1 \cdot (T - T_0)\,\frac{W}{m\,K^2} \tag{4.57}$$

$$\kappa_2 = 75\frac{W}{m\,K} + 0.9 \cdot (T - T_0)\,\frac{W}{m\,K^2}, \tag{4.58}$$

where $T_0 = 100\ K$ for both materials. In order to calculate the thermal rectification factor we follow the same procedure as before.We will first find T_m and then we will calculate J_r from Equation 4.11 taking into account that $\kappa_{10} = 190\frac{W}{m\,K}$, $\kappa_{20} = 75\frac{W}{m\,K}$, $\lambda = -2.1\frac{W}{m\,K^2}$ and $\mu = +0.9\frac{W}{m\,K^2}$. We ll now find the coefficients of Equation 4.10:

$$\alpha = -\frac{1}{2}(\mu + \lambda) = 0.6\,\frac{W}{m\,K^2}$$

$$\beta = -\kappa_{10} - \kappa_{20} + \lambda T_0 + \mu T_0 = -385\,\frac{W}{m\,K}$$

$$\gamma = -\lambda T_0\,T_h - \mu T_0 T_c + \frac{\lambda}{2}T_h^2 + \kappa_{10}T_h + \frac{\mu}{2}T_c^2 + \kappa_{20}T_c = 35000.0\,\frac{W}{m}.$$

By putting α, β and γ into Equation 4.10 we get T_{m+} and T_{m-}:

$$T_{m\pm} = \frac{-\beta \pm \sqrt{\beta^2 - 4\alpha\gamma}}{2\alpha} \Rightarrow$$

$$T_{m+} = 532.02\ K, \tag{4.59}$$

$$T_{m-} = 109.64\ K. \tag{4.60}$$

Only T_{m-} is acceptable since $T_c < T_{m-} < T_h$, when $T_{m+} \gg T_h$, which is not logical. Now from Equation 4.11, since we found T_m, we can find J_r which is

$$J_r L = 4717.90\,\frac{W}{m}. \tag{4.61}$$

Similarly, we ll calculate J_f. From Equation 4.15 we will find $T_{m'}$ taking into notice that:

$$\alpha' = -\frac{1}{2}(\mu + \lambda) = 0.6\,\frac{W}{m\,K^2}$$

$$\beta' = -\kappa_{10} - \kappa_{20} + \lambda T_0 + \mu T_0 = -385\,\frac{W}{m\,K}$$

$$\gamma' = -\lambda T_0\,T_c - \mu T_0 T_h + \frac{\lambda}{2}T_c^2 + \kappa_{10}T_c + \frac{\mu}{2}T_h^2 + \kappa_{20}T_h = 29250.0\,\frac{W}{m}.$$

By putting α', β' and γ' into Equation 4.16, we get

$$T_{m'+} = 553.61\ K \tag{4.62}$$

$$T_{m'-} = 88.06\ K. \tag{4.63}$$

As before, only $T_{m'-}$ is acceptable since $T_c < T_{m'-} < T_h$, when $T_{m'+} \gg T_h$, which is not logical. Now from equation 4.17, since we found T'_m, we can find J_f which is

$$J_f L = 5975.36\ \frac{W}{m}. \tag{4.64}$$

Now, since we know J_r and J_f, we can calculate the rectification factor from equation 4.2, which is equal to:

$$R = \frac{|J_f|}{|J_r|} = \frac{5975.36}{4717.90} = 1.27. \tag{4.65}$$

We will now study two more cases, in which the ladder's material thermal conductivity has quadratic dependence on temperature, when chain's material has linear dependence on temperature.

4.2.5 case 5: Sr_2CuO_3 - $Sr_{14}Cu_{24}O_{41}$ compound

The fifth case that we will study is the Sr_2CuO_3 (Spin chain - Material A) - $Sr_{14}Cu_{24}O_{41}$ (Spin ladder - Material B) bounded material, but now the spin ladder's thermal conductivity has quadratic dependence on temperature.

From the figure 4.6, we can extract the thermal conductivity for each material, in the form of equations 4.18 and 4.19.So, we get:

$$\kappa_1 = 80\frac{W}{m\,K} - 0.8 \cdot (T - T_0)\ \frac{W}{m\,K^2} \tag{4.66}$$

$$\kappa_2 = 94\frac{W}{m\,K} - 0.01 \cdot (T - T_0)^2\ \frac{W}{m\,K^3}, \tag{4.67}$$

where $T_0 = 140\ K$ for both materials.

We will first find T_m from Equation 4.23 and then we will calculate J_r from Equation 4.24 taking into account that $\kappa_{10} = 80\frac{W}{m\,K}$, $\kappa_{20} = 94\frac{W}{m\,K}$, $\lambda = -0.8\frac{W}{m\,K^2}$ and $\mu = -0.01\frac{W}{m\,K^3}$. We ll now find the coefficients of equation 4.23):

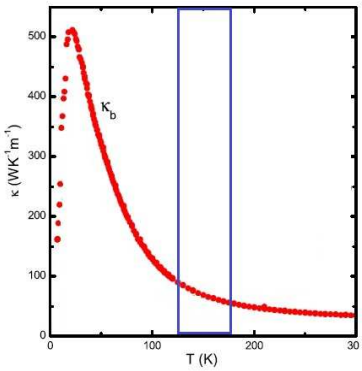

(a) Total thermal conductivity of Sr_2CuO_3

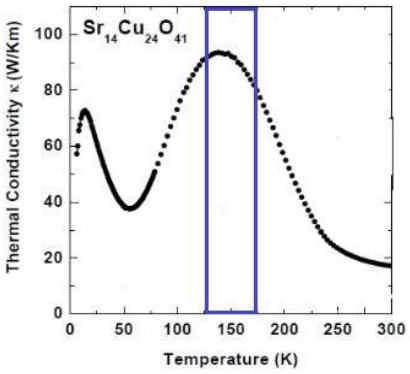

(b) Total thermal conductivity of $Sr_{14}Cu_{24}O_{41}$

Figure 4.6: The left surface of each blue box, corresponds to the low temperature heat bath $T_c = 125\,K$ and the right surface the high temperature heat bath $T_h = 175K$.

$$\alpha = -\frac{\mu}{3} = 0.003\frac{W}{m\,K^3}$$

$$\beta = \mu T_0 - \frac{\lambda}{2} = -1\frac{W}{m\,K^2}$$

$$\gamma = -k_{10} + \lambda T_0 - \mu T_0^2 - \kappa_{20} = -90\frac{W}{m\,K}$$

$$\delta = \kappa_{10}T_h + \frac{\mu}{3}T_c^3 - \mu T_0 T_c^2 + \mu T_0^2 T_c + \kappa_{20}T_c + \frac{\lambda}{2}T_h^2 - \lambda T_0 T_h = 23964.58\frac{W}{m}$$

By putting α, β, γ and δ into equation 4.23 and solving it, we get T_{m1}, T_{m2} and T_{m3}:

$$T_{m1} = -161.03\,K, \tag{4.68}$$

$$T_{m2} = 139.98\,K. \tag{4.69}$$

$$T_{m3} = 354.38\,K \tag{4.70}$$

Only T_{m2} is acceptable since $T_c < T_{m2} < T_h$, when $T_{m3} \gg T_h$ and $T_{m1} \ll T_c$ which are not logical. Now from equation (4.24), since we found T_m, we can find J_r which is

$$J_r L = 3708.47\,\frac{W}{m}. \tag{4.71}$$

Similarly, we ll calculate J_f. From Equation 4.28 we will find $T_{m'}$ taking into notice that:

$$\alpha' = -\frac{\mu}{3} = 0.003\frac{W}{m\,K^3}$$

$$\beta' = \mu T_0 - \frac{\lambda}{2} = -1\frac{W}{m\,K^2}$$

$$\gamma' = -\kappa_{20} + \lambda T_0 - \mu T_0^2 - \kappa_{10} = -90\frac{W}{m\,K}$$

$$\delta' = \kappa_{20}T_h + \frac{\mu}{3}T_h^3 - \mu T_0 T_h^2 + \mu T_0^2 T_h + \kappa_{10}T_c + \frac{\lambda}{2}T_c^2 - \lambda T_0 T_c = 24910.42\frac{W}{m}$$

By putting α', β', γ' and δ' into Equation4.28, we get

$$T_{m'1} = -163.04\,K \tag{4.72}$$

$$T_{m'2} = 144.90\,K. \tag{4.73}$$

$$T_{m'3} = 351.47\,K. \tag{4.74}$$

As before, only $T_{m'2}$ is acceptable since $T_c < T_{m'2} < T_h$, when $T_{m'3} \gg T_h$ and $T_{m'1} \ll T_c$, which are not logical. Now from Equation 4.29, since we found T'_m, we can find J_f which is

$$J_f L = 4359.27\,\frac{W}{m}. \tag{4.75}$$

Now, since we know J_r and J_f, we can calculate the rectification factor from equation 4.2, which is equal to:

$$R = \frac{|J_f|}{|J_r|} = \frac{4359.27}{3708.47} = 1.18. \tag{4.76}$$

4.2.6 case 6: $SrCuO_2$ - $Ca_9La_5Cu_{24}O_{41}$ compound

The sixth and the last case that we will study is the $SrCuO_2$ (Spin chain - Material A) - $Ca_9La_5Cu_{24}O_{41}$ (Spin ladder - Material B) bounded material, but now the spin ladder's thermal conductivity has quadratic dependence on temperature, as the previous case.

From the figure 4.7, we can extract the thermal conductivity for each material, in the form of Equations 4.18 and 4.19.So, we get:

$$\kappa_1 = 60\frac{W}{m\,K} - 0.3\cdot(T - T_0)\,\frac{W}{m\,K^2} \tag{4.77}$$

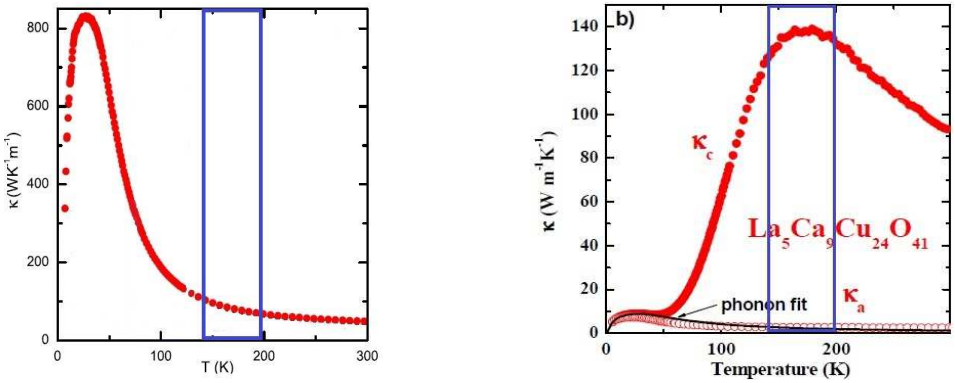

(a) Total thermal conductivity of $SrCuO_2$

(b) Total thermal conductivity of $Ca_9La_5Cu_{24}O_{41}$

Figure 4.7: The left surface of each blue box, corresponds to the low temperature heat bath $T_c = 140\,K$ and the right surface the high temperature heat bath $T_h = 200K$.

$$\kappa_2 = 138\frac{W}{m\,K} - 0.02 \cdot (T - T_0)^2\,\frac{W}{m\,K^3}, \tag{4.78}$$

where $T_0 = 170\,K$ for both materials.

We will first find T_m from Equation 4.23 and then we will calculate J_r from Equation 4.24 taking into account that $\kappa_{10} = 60\frac{W}{m\,K}$, $\kappa_{20} = 138\frac{W}{m\,K}$, $\lambda = -0.3\frac{W}{m\,K^2}$ and $\mu = -0.02\frac{W}{m\,K^3}$. We ll now find the coefficients of Equation 4.23:

$$\alpha = -\frac{\mu}{3} = 0.007\frac{W}{m\,K^3}$$

$$\beta = \mu T_0 - \frac{\lambda}{2} = -3.25\frac{W}{m\,K^2}$$

$$\gamma = -k_{10} + \lambda T_0 - \mu T_0^2 - \kappa_{20} = 329\frac{W}{m\,K}$$

$$\delta = \kappa_{10}T_h + \frac{\mu}{3}T_c^3 - \mu T_0 T_c^2 + \mu T_0^2 T_c + \kappa_{20}T_c + \frac{\lambda}{2}T_h^2 - \lambda T_0 T_h = 2946.67\frac{W}{m}$$

By putting α, β, γ and δ into equation 4.23 and solving it, we get T_{m1}, T_{m2} and T_{m3}:

$$T_{m1} = -8.27\,K, \tag{4.79}$$

$$T_{m2} = 166.14\,K. \tag{4.80}$$

$$T_{m3} = 306.42\,K \tag{4.81}$$

Only T_{m2} is acceptable since $T_c < T_{m2} < T_h$, when $T_{m3} \gg T_h$ and $T_{m1} \ll T_c$ which are not logical. Now from Equation 4.24, since we found T_m, we can find J_r which is

$$J_r L = 5326.54\,\frac{W}{m}. \tag{4.82}$$

Similarly, we ll calculate J_f. From Equation 4.28 we will find $T_{m'}$ taking into notice that:

$$\alpha' = -\frac{\mu}{3} = 0.007\frac{W}{m\,K^3}$$

$$\beta' = \mu T_0 - \frac{\lambda}{2} = -3.25\frac{W}{m\,K^2}$$

$$\gamma' = -\kappa_{20} + \lambda T_0 - \mu T_0^2 - \kappa_{10} = 329\frac{W}{m\,K}$$

$$\delta' = \kappa_{20} T_h + \frac{\mu}{3} T_h^3 - \mu T_0 T_h^2 + \mu T_0^2 T_h + \kappa_{10} T_c + \frac{\lambda}{2} T_c^2 - \lambda T_0 T_c = 7266.67\frac{W}{m}$$

By putting α', β', γ' and δ' into Equation 4.28, we get

$$T_{m'1} = -18.55\,K \tag{4.83}$$

$$T_{m'2} = 193.19\,K. \tag{4.84}$$

$$T_{m'3} = 289.64\,K. \tag{4.85}$$

As before, only $T_{m'2}$ is acceptable since $T_c < T_{m'2} < T_h$, when $T_{m'3} \gg T_h$ and $T_{m'1} \ll T_c$, which are not logical. Now from Equation 4.29, since we found T'_m, we can find J_f which is

$$J_f L = 4088.65\,\frac{W}{m}. \tag{4.86}$$

This is not the result that we were waiting because, as we mentioned before, we expect that J_f will be bigger than J_r. The reason that this is not happening is that these two materials that are bounded together, don't fulfil the two criteria that are needed for thermal rectification. To be more specific, material B that should present high κ at high temperatures and low κ at low temperatures (when material A should present the opposite properties), presents high κ at both low and high temperatures. As we see, the conductivity of material B near the T_c is $\kappa \approx 120\frac{W}{m \cdot K}$ which is way

higher than material's A at low temperatures ($\kappa \approx 70\frac{W}{m \cdot K}$). So, the last compound that we studied is not a good candidate for thermal rectifier.

Concluding, we notice that the higher rectification factor is achieved in case 1. The reason why the rectification factor in case 1 is higher than in the case 2 when the spin ladder material is the same, is the difference in the conductivities in the spin chain materials. We remind that in order to achieve rectification, as for the spin chain material, it must has high κ at low temperatures and low κ at high temperatures. We notice that the spin chain material in case 3, has a very large conductance ($\kappa \approx 140\frac{W}{m \cdot K}$) even at high temperatures, which at the same time is even higher than spin ladder's conductance at high temperatures in the same material, which is $\kappa \approx 105\frac{W}{m \cdot K}$. This doesn't happen in case 1, where spin chain's thermal conductance at high temperatures ($\kappa \approx 80\frac{W}{m \cdot K}$) is lower than spin ladder's conductance at the same temperature range ($\kappa \approx 110\frac{W}{m \cdot K}$).

The most crucial point that makes the materials good or bad candidates for thermal rectifier, is the non-linear's term coefficient. When the coefficient is big, then we notice biggest difference in thermal conductivity's values at high and low temperatures. We have to clarify at this point, that when thermal conductivity has the form of Equation 4.3, it has linear dependence on temperature, but in general the thermal conductivity is non-linear, since $\sim T$ term in heat flux equation, is non-linear. To be more specific, we have the heat flux equation:

$$J = -\kappa(T)\,\frac{dT}{dx} = -(\kappa_{10} + \lambda(T - T_0))\frac{dT}{dx} = -(\kappa_{10} - \lambda T_0)\frac{dT}{dx} - \lambda T\frac{dT}{dx}. \tag{4.87}$$

It is clear now, that heat flux equation that we are solving in order to calculate the thermal rectification is non-linear, since $\sim T\frac{dT}{dx}$ is non-linear term.

4.3 Static Rectification Study via Sander's & Walton's method

In the previous section, we calculated the static rectification in a material which was composed of two other materials bounded together, by integrating the heat flux equation from $x = 0$ to $x = L$, and from $x = L$ to $x = 0$ respectively. The point here is that by doing so, we didn't take into consideration many valuable parameters of the 2 materials and the fact that the heat in these materials propagates via two heat carriers,

the magnons and the phonons. As we mentioned in previous sections, the total thermal conductivity in each material can be separated into two thermal conductivities, one is for the magnon system and the other for the phonon system. The sum of these two different conductivities gives us the total one. The parameters that we didnt take into consideration before, is the specific heat of the two heat carriers (which is different in each material for each heat carrier) and the thermalization time τ_{mp} between the two carriers.

First, lets assume that we have only one material (spin chain or spin ladder), and we ll try to find an analytical expression that will give us the temperature profile of each carrier, taking into consideration all these parameters mentioned above. If that's possible, we ll continue to find the temperature profile in a material that is composed of two others and we ll calculate the thermal rectification.

Expressing the total conductivity as a simple sum of the magnon and phonon conductivities, implicitly assumes that the temperature gradient in the phonon system is the same as that in the magnon system. Since thermal transport is inherently a nonequilibrium phenomenon, that is not necessarily the case. In a thermally isolated system, the difference between the magnon and the phonon temperatures, T_m and T_p, would decay exponentially. The magnon-phonon relaxation time τ_{mp} is defined by

$$\frac{d}{dt}\Delta T = -\frac{\Delta T}{\tau_{mp}} \tag{4.88}$$

where $\Delta T = T_p - T_m$. It is easy to show from Equation 4.88 that T_m and T_p approach each other. Especially, in the case that T_m approaches T_p, we have

$$-c_m \frac{dT_m}{dt} = c_p \frac{dT_p}{dt} \;\Rightarrow\; \frac{dT_m}{dt} = -\frac{c_p}{c_m}\frac{dT_p}{dt}. \tag{4.89}$$

From the left-hand side expression of the Equation 4.88, we can take

$$\frac{d}{dt}\Delta T = \frac{d}{dt}(T_p - T_m) \;\Rightarrow\; \frac{dT_p}{dt} - \frac{dT_m}{dt} = -\frac{\Delta T}{\tau_{mp}}, \tag{4.90}$$

so if we enter Equation 4.89 into Equation 4.90, we will have

$$\frac{dT_p}{dt} - (-\frac{c_p}{c_m}\frac{dT_p}{dt}) = \frac{dT_p}{dt}(1 + \frac{c_p}{c_m}) = \frac{dT_p}{dt}(\frac{c_p + c_m}{c_m}) \;\Rightarrow$$

$$\frac{dT_p}{dt}(\frac{c_T}{c_m}) = -\frac{\Delta T}{\tau_{mp}} \;\Rightarrow\; \frac{dT_p}{dt} = \frac{c_m}{c_T}\frac{T_m - T_p}{\tau_{mp}}, \tag{4.91}$$

where c_m and c_p are the specific heats of the magnon and phonon systems, and $c_T = c_p + c_m$. Using the same logic, we can derive a similar equation for the case that T_p approaches T_m

$$\frac{dT_m}{dt} = \frac{c_p}{c_T}\frac{T_p - T_m}{\tau_{mp}}. \tag{4.92}$$

Now consider a thermal conductivity sample of length L and cross-sectional area A, with the heat flow along the x direction. A total heat flux Q is supplied at $x = -\frac{1}{2}L$, and absorbed at $x = \frac{1}{2}L$. In general, the temperature of the magnon system $T_m(x)$ at any point x will differ from that of the phonons $T_p(x)$. If there were no heat flow down the sample through the magnon system, the magnon temperature at each point would come into equilibrium with the phonon temperature, as in Equation 4.92.

Therefore, in volume element $A\,dx$ of the sample, the amount of heat per unit time flowing into the magnon system from the phonon system would be

$$dP_m(x) = c_m\frac{dT_m(x)}{dt}A\,dx = \frac{c_p c_m}{c_T}\frac{T_p(x) - T_m(x)}{\tau_{mp}}\,A\,dx, \tag{4.93}$$

where the specific heat is now explicitly the heat capacity per unit volume.

However, if the magnon system has a finite conductivity k_m, the heat which flows into it will be conducted along the sample and a steady state will be reached. The contribution of a small length dx to the heat flux in the magnon system is

$$dQ_m(x) = \frac{dP_m(x)}{A} = \frac{c_p c_m}{c_T}\frac{T_p(x) - T_m(x)}{\tau_{mp}}\,dx. \tag{4.94}$$

Therefore, the total magnon heat flux at any point x is given by

$$Q_m(x) = \frac{c_p c_m}{c_T}\frac{1}{\tau_{mp}}\int_{-L/2}^{x}[T_p(x') - T_m(x')]\,dx'. \tag{4.95}$$

But, by definition of the magnon conductivity,

$$Q_m(x) = -k_m(x)\frac{dT_m(x)}{dx}. \tag{4.96}$$

This is the point where we stray from Mr D.J. Sanders' and Mr D. Walton's way of finding the phonon and magnon temperature distribution profile. Mr Sanders and Mr Walton considered that magnon's thermal conductivity is a constant k_m, when we consider that it has a temperature dependence, $k_m(T_m)$.

Combining Equations 4.95 and 4.96, we get

$$k_m(T_m)\frac{dT_m}{dx} + \frac{c_m c_p}{c_T}\frac{1}{\tau_{mp}}\int_{-L/2}^{x}[T_p(x') - T_m(x')]\,dx' = 0 \;\Rightarrow$$

$$\frac{k_m(T_m)}{c_m}\frac{dT_m}{dx} + \frac{c_p}{c_T}\frac{1}{\tau_{mp}}\int_{-L/2}^{x}[T_p(x') - T_m(x')]\,dx' = 0 \;\Rightarrow$$

$$D_m(T_m)\frac{dT_m}{dx} + \frac{c_p}{c_T}\frac{1}{\tau_{mp}}\int_{-L/2}^{x}[T_p(x') - T_m(x')]\,dx' = 0. \tag{4.97}$$

As we know, thermal diffusivity is the thermal conductivity divided by density and specific heat capacity at constant pressure. Therefore, the product of density and specific heat capacity can be considered as the volumteric heat capacity. In a more mathematical language,

$$D = \frac{k}{\rho c_P} = \frac{k}{c}.$$

In our case, we considered the following expression

$$D_m(T_m) = \frac{k_m(T)}{c_m} \tag{4.98}$$

in order to get Equation 4.97. At this point, we have to emphasize that we assumed that only magnon thermal diffusivity has a spatial dependence. Phonon thermal conductivity on the other hand, is constant.

By differentiating Equation 4.97 we get

$$\frac{d}{dx}(D_m(T)\frac{dT_m(x)}{dx}) + \frac{c_p}{c_T}\frac{1}{\tau_{mp}}(T_p(x) - T_m(x)) = 0. \tag{4.99}$$

The total heat flux Q is divided between the magnons and the phonons according to

$$Q = Q_p(x) + Q_m(x) = -k_p\frac{dT_p(x)}{dx} - k_m(x)\frac{dT_m(x)}{dx} \;\Rightarrow$$

$$Q = -k_p\frac{dT_p(x)}{dx} - c_m D_m(T_m)\frac{dT_m(x)}{dx}. \tag{4.100}$$

Therefore, $T_p(x)$ is related to $T_m(x)$ by

$$\frac{dT_p}{dx} = -\frac{Q}{k_p} - \frac{c_m}{k_p}D_m(T_m)\frac{dT_m}{dx}, \tag{4.101}$$

with the boundary condition that at the center of the sample, the phonon and magnon temperatures are both equal to the average sample temperature T_0; i.e.,

$$T_m(0) = T_p(0) = T_0. \tag{4.102}$$

We will now solve Equation (4.101)

$$\int \frac{dT_p}{dx}dx = \int(-\frac{Q}{k_p} - \frac{c_m}{k_p}D_m(T_m)\frac{dT_m}{dx})dx \;\Rightarrow$$

$$T_p(x) = -\frac{Q}{k_p}x - \frac{c_m}{k_p}\int D_m(T_m)dT_m(x). \tag{4.103}$$

At this point, we consider that magnon thermal diffusivity $D_m(x)$ has the following form

$$D_m(T_m) = D_0 + \alpha T_m(x), \tag{4.104}$$

where D_0 and α are constants. Now,we put Equation 4.104 into 4.103 and we get

$$T_p(x) = -\frac{Q}{k_p}x - \frac{c_m}{k_p}\int (D_0 + \alpha T_m(x))dT_m(x) \;\Rightarrow$$

$$T_p(x) = -\frac{Q}{k_p}x - \frac{c_m}{k_p}D_0 T_m(x) - \alpha\frac{c_m}{k_p}\int T_m(x)dT_m(x) + C \;\Rightarrow$$

$$T_p(x) = -\frac{Q}{k_p}x - \frac{c_m}{k_p}D_0 T_m(x) - \frac{\alpha}{2}\frac{c_m}{k_p}T_m^2(x) + C\,. \tag{4.105}$$

We ll use the boundary condition 4.102 in order to neglect the constant of integration C that exists in Equation 4.105

$$T_p(0) = -\frac{c_m}{k_p}D_0 T_m(0) - \frac{\alpha}{2}\frac{c_m}{k_p}T_m^2(0) + C \;\Rightarrow$$

$$T_0 = -\frac{c_m}{k_p}D_0 T_0 - \frac{\alpha}{2}\frac{c_m}{k_p}T_0^2 + C \;\Rightarrow$$

$$C = T_0 + \frac{c_m}{k_p}D_0 T_0 + \frac{\alpha}{2}\frac{c_m}{k_p}T_0^2 \;\Rightarrow$$

$$C = T_0\big(\frac{c_m}{k_p}(D_0 + \frac{\alpha}{2}T_0) + 1\big) \tag{4.106}$$

Substituting 4.104 & 4.105 into 4.99, the differential equation for $T_m(x)$ becomes

$$\underbrace{\frac{d}{dx}\Big(D_m(x)\frac{dT_m(x)}{dx}\Big)}_{\text{term \#1}} + \frac{c_p}{c_T}\frac{1}{\tau_{mp}}\Big(-\frac{Q}{k_p}x - \frac{c_m}{k_p}D_0 T_m(x) - \frac{\alpha}{2}\frac{c_m}{k_p}T_m^2(x) + C - T_m(x)\Big) = 0\,. \tag{4.107}$$

We work $Term\ \#1$ separately

$$\frac{d}{dx}(D_m(x)\frac{dT_m(x)}{dx}) = \frac{dD_m(x)}{dx}\frac{dT_m(x)}{dx} + D_m(x)\frac{d^2T_m(x)}{dx^2} \;\Rightarrow$$

$$\frac{d}{dx}(D_m(x)\frac{dT_m(x)}{dx}) = \frac{d}{dx}(D_0 + \alpha T_m(x))\frac{dT_m}{dx} + (D_0 + \alpha T_m(x))\frac{d^2T_m(x)}{dx^2} \;\Rightarrow$$

$$\frac{d}{dx}(D_m(x)\frac{dT_m(x)}{dx}) = \alpha(\frac{dT_m}{dx})^2 + D_0\frac{d^2T_m}{dx^2} + \alpha T_m\frac{d^2T_m}{dx^2}\,. \tag{4.108}$$

Substituting Equation 4.108 into 4.107 we get the final form of the equation that gives us $T_m(x)$

$$\alpha(\frac{dT_m}{dx})^2 + D_0\frac{d^2T_m}{dx^2} + \alpha T_m\frac{d^2T_m}{dx^2} + \frac{c_p}{c_T}\frac{1}{\tau_{mp}}\Big(-\frac{Q}{k_p}x - \frac{c_m}{k_p}D_0T_m(x) - \frac{\alpha}{2}\frac{c_m}{k_p}T_m^2(x) + C - T_m(x)\Big) = 0. \tag{4.109}$$

Equation 4.109 can be written in a simpler form

$$y'^2 + \widetilde{\alpha}y'' + yy'' + \beta x + \gamma y + \delta y^2 + \epsilon y + \zeta = 0 \tag{4.110}$$

where

$$\widetilde{\alpha} \equiv \frac{D_0}{\alpha}$$

$$\beta \equiv -\frac{c_p}{c_T}\frac{1}{\tau_{mp}}\frac{Q}{k_p}\frac{1}{\alpha}$$

$$\gamma \equiv -\frac{c_p}{c_T}\frac{1}{\tau_{mp}}\frac{c_m}{k_p}\frac{D_0}{\alpha}$$

$$\delta \equiv -\frac{c_p}{c_T}\frac{1}{\tau_{mp}}\frac{c_m}{2k_p}$$

$$\epsilon \equiv -\frac{c_p}{c_T}\frac{1}{\tau_{mp}}\frac{1}{\alpha}$$

$$\zeta \equiv \frac{c_p}{c_T}\frac{1}{\tau_{mp}}\frac{C}{\alpha}.$$

Equation 4.110 is a non-linear equation that cannot be solved analytically. So, we can't continue to study the static thermal rectification in these materials by using this method, that was first used from D. J. Sanders and D. Walton. In the next section we ll calculate numerically the dynamic rectification in these materials, taking in mind all the microscopic parameters that we mentioned earlier.

5 Dynamic Thermal Rectification

5.1 Thermal Rectification

In this section, we ll study the dynamic heat transfer in the magnetic materials that we were talking in the previous paragraph. We have, as we mentioned from the start of this work, two bounded magnetic materials, in which we ll put a heat pulse at the one surface and then we ll calculate the temperature change over time, at the opposite surface. By doing this twice (one for the left surface , calculating the temperature change at the right surface and via versa), we ll calculate the thermal rectification factor, which we ll compare it with the one that we extracted in the static heat transfer in each case.

The heat transport in these compounds that we are referring to, can be described by a two-temperature (2T) model, obtained by phase space integration of the Bloch-Boltzmann-Peierls equation for the lattice $(l, phonons)$ and magnetic $(m, magnons)$ degrees of freedom:

$$C_l \frac{\partial T_l}{\partial t} = \frac{\partial}{\partial x}(k_l(x)\frac{\partial T_l}{\partial x}) - \frac{C_l \cdot C_m}{C_l + C_m}\frac{1}{\tau_{mp}}(T_l - T_m) \tag{5.1}$$

$$C_m \frac{\partial T_m}{\partial t} = \frac{\partial}{\partial x}(k_m(x)\frac{\partial T_m}{\partial x}) - \frac{C_l \cdot C_m}{C_l + C_m}\frac{1}{\tau_{mp}}(T_m - T_l). \tag{5.2}$$

Here, t is time; x is the coordinate alone the spin ladder or chain; $T_{l,m}$, $C_{l,m}$ and $k_{l,m}$ are

the temperature, specific heat, and thermal conductivity for the lattice and magnetic subsystems; and the $\frac{C_l \cdot C_m}{C_l + C_m}\frac{1}{\tau_{mp}}$ term is the coupling constant.

The reduced equations that we solve in this toy model, taking into account that $[D] = \frac{L^2}{T}$, can be found:

$$C_l\frac{\partial T_l}{\partial t} = \frac{\partial}{\partial x}(k_l(x)\frac{\partial T_l}{\partial x}) - \frac{C_l \cdot C_m}{C_l + C_m}\frac{1}{\tau_{mp}}(T_l - T_m) \;\Rightarrow$$

$$\frac{\partial T_l}{\partial t} = \frac{\partial}{\partial x}((\frac{k_l(x)}{C_l})\frac{\partial T_l}{\partial x}) - \frac{C_m}{C_l + C_m}\frac{1}{\tau_{mp}}(T_l - T_m) \;\Rightarrow$$

$$\frac{\partial T_l}{\partial t} = \frac{\partial}{\partial x}(D_l(x)\frac{\partial T_l}{\partial x}) - \frac{C_m}{C_l + C_m}\frac{1}{\tau_{mp}}(T_l - T_m) \;\Rightarrow$$

$$\frac{\partial T_l}{\partial t} = \frac{\partial}{\partial x}(\frac{D_l(x)}{L^2/L^2}\frac{\partial T_l}{\partial x}) - \frac{C_m}{C_l + C_m}\frac{1}{\tau_{mp}}(T_l - T_m) \;\Rightarrow$$

$$\frac{\partial T_l}{\partial t} = \frac{\partial}{\partial(\frac{x}{L})}(\frac{D_l(x)}{L^2}\frac{\partial T_l}{\partial(\frac{x}{L})}) - \frac{C_m}{C_l + C_m}\frac{1}{\tau_{mp}}(T_l - T_m) \;\Rightarrow$$

$$\frac{\partial T_l}{\partial t} = \frac{\partial}{\partial \xi}(\frac{1}{\tau_l}\frac{\partial T_l}{\partial \xi}) - \frac{C_m}{C_l + C_m}\frac{1}{\tau_{mp}}(T_l - T_m) \tag{5.3}$$

and similarly for magnons,

$$\frac{\partial T_m}{\partial t} = \frac{\partial}{\partial \xi}(\frac{1}{\tau_m}\frac{\partial T_m}{\partial \xi}) - \frac{C_l}{C_l + C_m}\frac{1}{\tau_{mp}}(T_m - T_l), \tag{5.4}$$

where $\xi = x/L$ and $0 < \xi < 1$.

5.1.1 Tridiagonal System

If we use the backward difference at time t_{j+1} and a second-order central difference for space derivative at position x_i (The Backward Time, Centered Space Method "BTCS") and the equation that gives us the heat current:

$$J = -k_l(x)\frac{dT_l}{dx} = -C_l \cdot D_l(x)\frac{dT_l}{dx},$$

from Equations 5.1 and 5.2 we get the recurrence equation:

$$C_l\frac{T_i^{j+1} - T_i^j}{dt} = \frac{J_{i,i+1} - J_{i-1,i}}{h} - \frac{C_l \cdot C_m}{C_l + C_m}\frac{1}{\tau_{mp}}(T_l^j - T_m^j). \tag{5.5}$$

This is an implicit method for solving the one-dimensional diffusion equation. Implicit methods find a solution by solving an equation involving both the current state of the system and the later one. Mathematically if $Y(t)$ is the current system state and $Y(t+dt)$ is the state at the later time (dt is a small time step), for the implicit method one solves the equation:

$$G(Y(t),\, Y(t+dt)) = 0$$

in order to find $Y(t+dt)$.

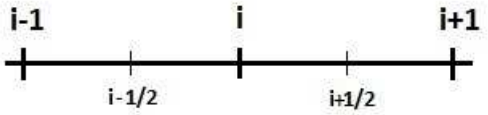

Figure 5.1: The stencil of our problem

From Equation 5.5 we get:

$$C_l \frac{T_i^{j+1} - T_i^j}{dt} = \frac{(C_l \cdot D^l_{(i+1/2)} \frac{T_{i+1}^{j+1} - T_i^{j+1}}{h}) - (C_l \cdot D^l_{(i-1/2)} \frac{T_i^{j+1} - T_{i-1}^{j+1}}{h})}{h} - \\ - \frac{C_l \cdot C_m}{C_l + C_m} \frac{1}{\tau_{mp}} (T^j_{l,i} - T^j_{m,i}) \;\Rightarrow$$

$$\frac{T_i^{j+1} - T_i^j}{dt} = \frac{(D^l_{(i+1/2)} \frac{T_{i+1}^{j+1} - T_i^{j+1}}{h}) - (D^l_{(i-1/2)} \frac{T_i^{j+1} - T_{i-1}^{j+1}}{h})}{h} - \\ - \frac{C_m}{C_l + C_m} \frac{1}{\tau_{mp}} (T^j_{l,i} - T^j_{m,i}) \;\Rightarrow$$

$$T_i^{j+1} - T_i^j = \frac{dt}{h^2} \Big[(D^l_{(i+1/2)} (T_{i+1}^{j+1} - T_i^{j+1}) - D^l_{(i-1/2)} (T_i^{j+1} - T_{i-1}^{j+1}) \Big] - \\ - \frac{C_m}{C_l + C_m} \frac{1}{\tau_{mp}} (T^j_{l,i} - T^j_{m,i}) \;\Rightarrow$$

$$T_i^j - \frac{C_m}{C_l + C_m} \frac{1}{\tau_{mp}} (T^j_{l,i} - T^j_{m,i}) = T_i^{j+1} - \frac{dt}{h^2} \Big[(D^l_{(i+1/2)} (T_{i+1}^{j+1} - T_i^{j+1}) - \\ - D^l_{(i-1/2)} (T_i^{j+1} - T_{i-1}^{j+1}) \Big] \;\Rightarrow$$

$$T_i^j - \frac{C_m}{C_l + C_m}\frac{1}{\tau_{mp}}(T_{l,i}^j - T_{m,i}^j) = T_{i+1}^{j+1}(-\frac{dt}{h^2}\, D_{(i+1/2)}^l) + \\ + T_i^{j+1}(1 + \frac{dt}{h^2}(\, D_{(i+1/2)}^l + D_{(i-1/2)}^l) + T_{i-1}^{j+1}(-\frac{dt}{h^2}\, D_{(i-1/2)}^l) \Rightarrow \quad (5.6)$$

$$\left(\widetilde{T_i^j}\right) = \left(A\right) \cdot \left(T_i^{j+1}\right) \quad (5.7)$$

where A is a tridiagonal matrix (which is known), T_i^j is the "current" Temperature which is also known, and we solve numerically this tridiagonal system in order to find the later Temperature T_i^{j+1}. At this point, emphasize the fact that we solve this tridiagonal system twice, once for phonons' system and once for magnons' system, since these two systems are coupled. Another useful notation is that in the Equation 5.6, wherever we see the diffusion coefficient, we replace it with the diffusion time of each carrier, according with the equation $D_i = \frac{1}{\tau_i}$, as we showed in the reduced dynamic Equations 5.3 and 5.4 .

5.1.2 Energy Conservation

Energy in a system like these that we are studying is conserved, since it's closed system. We will now prove it analytically, assuming that at first we have only one magnetic material.

The heat transport in the materials, as we mentioned earlier, are given by Equations 5.1 and 5.2:

$$C_l\frac{\partial T_l}{\partial t} = \frac{\partial}{\partial x}(k_l(x)\frac{\partial T_l}{\partial x}) - \frac{C_m C_l}{C_m + C_l}\frac{1}{\tau_{mp}}(T_l - T_m)$$

$$C_m\frac{\partial T_m}{\partial t} = \frac{\partial}{\partial x}(k_m(x)\frac{\partial T_m}{\partial x}) + \frac{C_m C_l}{C_m + C_l}\frac{1}{\tau_{mp}}(T_l - T_m).$$

In the Equations 5.1 and 5.2, we can go from temperatures to energies, knowing that:

$$D_i(x) = \frac{k_i(x)}{C_i} \quad (5.8)$$

and

$$C_i \cdot T_i = E_i \quad , \quad (5.9)$$

where $D_i(x)$ is the diffusion coefficient, E_i is the energy and the subscript i can be equal to l if we are referring to lattice, or m if we are referring to magnons. So from

Equation 5.1 using Equations 5.8 and 5.9, we can get:

$$\frac{\partial(C_l \cdot T_l)}{\partial t} = \frac{\partial}{\partial x}(D_l(x)\frac{\partial(C_l \cdot T_l)}{\partial x}) - \frac{C_m C_l}{C_m + C_l}\frac{1}{\tau_{mp}}(T_l - T_m) \Rightarrow$$

$$\frac{\partial E_l}{\partial t} = \frac{\partial}{\partial x}(D_l(x)\frac{\partial E_l}{\partial x}) - \frac{C_m C_l}{C_m + C_l}\frac{1}{\tau_{mp}}(T_l - T_m) \tag{5.10}$$

and similarly from Equation 5.2 we get:

$$\frac{\partial E_m}{\partial t} = \frac{\partial}{\partial x}(D_m(x)\frac{\partial E_m}{\partial x}) - \frac{C_m C_l}{C_m + C_l}\frac{1}{\tau_{mp}}(T_l - T_m)\,. \tag{5.11}$$

By adding the last 2 equations together, we have as result:

$$\frac{\partial E_l}{\partial t} + \frac{\partial E_m}{\partial t} = \frac{\partial(E_l + E_m)}{\partial t} = \frac{\partial}{\partial x}(D_l(x)\frac{\partial E_l}{\partial x}) + \frac{\partial}{\partial x}(D_m(x)\frac{\partial E_m}{\partial x}) \Rightarrow$$

$$\frac{\partial E}{\partial t} = \frac{\partial}{\partial x}(D_l(x)\frac{\partial E_l}{\partial x}) + \frac{\partial}{\partial x}(D_m(x)\frac{\partial E_m}{\partial x}), \tag{5.12}$$

where E is the total Energy of our system.

In order to find if our energy is conserved, we integrate Equation 5.12 with respect to x, assuming that our material's length is L :

$$\frac{\partial}{\partial t}\int_0^L E\,dx = \int_0^L \frac{\partial}{\partial x}(D_l(x)\frac{\partial E_l}{\partial x})\,dx + \int_0^L \frac{\partial}{\partial x}(D_m(x)\frac{\partial E_m}{\partial x})\,dx \Rightarrow$$

$$\frac{\partial}{\partial t}\int_0^L E\,dx = D_l(x)\frac{\partial E_l}{\partial x}\Big|_0^L + D_m(x)\frac{\partial E_m}{\partial x}\Big|_0^L \Rightarrow$$

$$\frac{\partial}{\partial t}\int_0^L E\,dx = D_l(L)\frac{\partial E_l}{\partial x}\Big|_L - D_l(0)\frac{\partial E_l}{\partial x}\Big|_0 + D_m(L)\frac{\partial E_m}{\partial x}\Big|_L - D_m(0)\frac{\partial E_m}{\partial x}\Big|_0\,. \tag{5.13}$$

Knowing that the magnons are insulated on the surfaces $x = 0$ and $x = L$:

$$\frac{\partial E_m}{\partial x}\Big|_0 = \frac{\partial E_m}{\partial x}\Big|_L = 0\ ,$$

Equation (5.13) becomes:

$$\frac{\partial}{\partial t}\int_0^L E\,dx = D_l(L)\frac{\partial E_l}{\partial x}\Big|_L - D_l(0)\frac{\partial E_l}{\partial x}\Big|_0. \tag{5.14}$$

By using the heat current equation, the above equation becomes

$$\frac{\partial}{\partial t}\int_0^L E\,dx = D_l(L)\frac{\partial E_l}{\partial x}\Big|_L - D_l(0)\frac{\partial E_l}{\partial x}\Big|_0 = J\big|_0 - J\big|_L = 0, \tag{5.15}$$

since the material is not attached to any heat baths and that means that we don't have heat current flowing along our material.

We ll now examine the case where our sample consists of 2 materials that are bounded together. Each material has both phonons and magnons as heat transport carriers, so, in general the diffusion coefficients and the specific heats are different for each carrier in each material. Coupling or thermalization time τ_{mp} ll be different in each material too, since the one material can be spin ladder and the other spin chain.

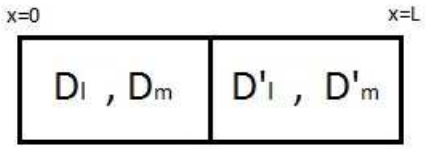

In this case, our results for each material will be similar to what we showed earlier (Equation 5.9) but now the integration limits will be different and there will be extra boundary conditions in the interface, where $x = L/2$. For the first material, where $0 < x < L/2$, from Equation 5.8 we get:

$$\frac{\partial}{\partial t}\int_0^{L/2} E\,dx = D_l(L/2)\frac{\partial E_l}{\partial x}\Big|_{L/2} - D_l(0)\frac{\partial E_l}{\partial x}\Big|_0 + D_m(L/2)\frac{\partial E_m}{\partial x}\Big|_{L/2} - D_m(0)\frac{\partial E_m}{\partial x}\Big|_0 . \tag{5.16}$$

Magnons, as we said before, are insulated on the surfaces at $x = 0$ and $x = L$, but not in the interface, which has as result that the term $\frac{\partial E_m}{\partial x}\Big|_{L/2}$ isn't equal to zero. After that notation, Equation 5.16 becomes:

$$\frac{\partial}{\partial t}\int_0^{L/2} E\,dx = D_l(L/2)\frac{\partial E_l}{\partial x}\Big|_{L/2} - D_l(0)\frac{\partial E_l}{\partial x}\Big|_0 + D_m(L/2)\frac{\partial E_m}{\partial x}\Big|_{L/2}. \tag{5.17}$$

Similarly, for the second material, where $L/2 < x < L$, from Equation 5.8 we get:

$$\frac{\partial}{\partial t}\int_{L/2}^{L} E\,dx = \widetilde{D}_l(L)\frac{\partial E_l}{\partial x}\Big|_L - \widetilde{D}_l(L/2)\frac{\partial E_l}{\partial x}\Big|_{L/2} + \widetilde{D}_m(L)\frac{\partial E_m}{\partial x}\Big|_L - \widetilde{D}_m(L/2)\frac{\partial E_m}{\partial x}\Big|_{L/2}, \tag{5.18}$$

but as we explained before, magnons are insulated on the surfaces so:

$$\widetilde{D}_m(L)\frac{\partial E_m}{\partial x}\Big|_L = 0 \ ,$$

and because of this statement, Equation (5.18) becomes:

$$\frac{\partial}{\partial t}\int_{L/2}^{L} E\,dx = \widetilde{D}_l(L)\frac{\partial E_l}{\partial x}\Big|_L - \widetilde{D}_l(L/2)\frac{\partial E_l}{\partial x}\Big|_{L/2} - \widetilde{D}_m(L/2)\frac{\partial E_m}{\partial x}\Big|_{L/2}. \tag{5.19}$$

By adding Equations 5.17 and 5.19, we get

$$\frac{\partial}{\partial t}\int_0^{L/2} E\,dx + \frac{\partial}{\partial t}\int_{L/2}^{L} E\,dx = D_l(L/2)\frac{\partial E_l}{\partial x}\Big|_{L/2} - D_l(0)\frac{\partial E_l}{\partial x}\Big|_0 + D_m(L/2)\frac{\partial E_m}{\partial x}\Big|_{L/2} + \widetilde{D}_l(L)\frac{\partial E_l}{\partial x}\Big|_L - \widetilde{D}_l(L/2)\frac{\partial E_l}{\partial x}\Big|_{L/2} - \widetilde{D}_m(L/2)\frac{\partial E_m}{\partial x}\Big|_{L/2} \Rightarrow$$

$$\frac{\partial}{\partial t}\int_0^{L} E\,dx = D_l(L/2)\frac{\partial E_l}{\partial x}\Big|_{L/2} - D_l(0)\frac{\partial E_l}{\partial x}\Big|_0 + D_m(L/2)\frac{\partial E_m}{\partial x}\Big|_{L/2} + \widetilde{D}_l(L)\frac{\partial E_l}{\partial x}\Big|_L - \widetilde{D}_l(L/2)\frac{\partial E_l}{\partial x}\Big|_{L/2} - \widetilde{D}_m(L/2)\frac{\partial E_m}{\partial x}\Big|_{L/2}. \quad (5.20)$$

Taking in mind that in the interface the heat current for each carrier must be continuous, then from the following equation that gives us the current:

$$J_i = -k_i(x)\frac{dT_i}{dx} = -D_i(x)\cdot C_i\frac{dT_i}{dx} = -D_i(x)\frac{dE_i}{dx},$$

we get the following boundary conditions on the interface of our material ($x = L/2$):

- $D_l(L/2)\frac{\partial E_l}{\partial x}\Big|_{L/2} = \widetilde{D}_l(L/2)\frac{\partial E_l}{\partial x}\Big|_{L/2}$
- $D_m(L/2)\frac{\partial E_m}{\partial x}\Big|_{L/2} = \widetilde{D}_m(L/2)\frac{\partial E_m}{\partial x}\Big|_{L/2}$.

By using these 2 boundaries conditions, Equation 5.20 becomes:

$$\frac{\partial}{\partial t}\int_0^{L} E\,dx = \widetilde{D}_l(L)\frac{\partial E_l}{\partial x}\Big|_L - D_l(0)\frac{\partial E_l}{\partial x}\Big|_0 = J\big|_0 - J\big|_L = 0 \quad (5.21)$$

since our material is not contacted to any heat baths, so we don't have heat current flowing along our material. As we see, energy is conserved in our system, as we expected.

5.2 Dynamic Rectification Results

We ll now study the same cases that we studied in the Static rectification section, solving the toy model we mentioned earlier numerically. Then, we ll extract a thermal rectification factor for each case, and we ll compare it with the static one.

The main differences between static and dynamic rectification are:

- in the static rectification our sample is contacted to two heat baths (one hot heat bath at the left surface and one cold at the right surface) that leads to a heat current that flows along our material, when in the dynamic rectification case, we have no heat baths but we put a heat pulse at the left surface and we measure the temperature at the right surface and via versa
- in the static case, we solve the heat flux equation, when at at the dynamic case we solve Bloch-Boltzmann-Peierls equation for each heat carrier (Equations 5.1 and 5.2)
- in the static case we only need the each material's total thermal conductivity in order to extract the rectification factor, when at the dynamic case, we need the thermal diffusivity (which is extracted by the thermal conductivity as we ll show below), the specific heats for each heat carrier (phonons and magnons) in each material (these parameters are different in spin chain and spin ladder materials) and the thermalization time between the two heat carriers, which is different in each material too
- in static case the rectification factor is defined by the ratio of $|J_f|$ to $|J_r|$, when in the dynamic case we define the rectification factor as the ratio τ_f to τ_r, where τ in each case (r refers to backward heat propagation when f to forward propagation) is the the time of $1/2$ increase of T_l at $\xi = 1$.

5.2.1 case 1: Sr_2CuO_3 - $Ca_9La_5Cu_{24}O_{41}$ compound

The first case that we will study is the Sr_2CuO_3 (Spin chain - Material A) - $Ca_9La_5Cu_{24}O_{41}$ (Spin ladder - Material B) bounded material.

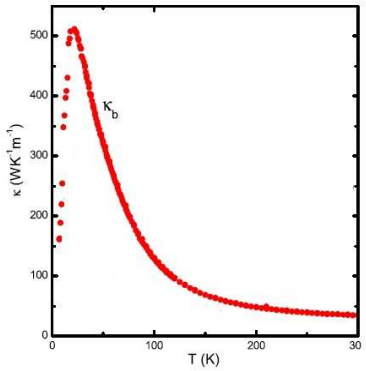

(a) Total thermal conductivity of Sr_2CuO_3

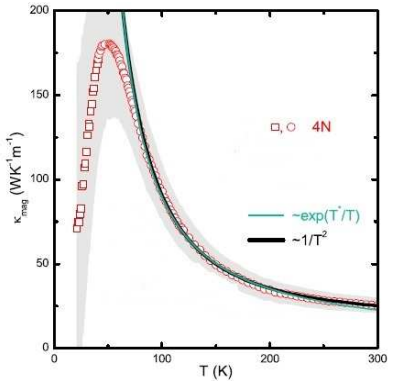

(b) Magnetic thermal conductivity of Sr_2CuO_3

Figure 5.2: These two diagrams show us the total and the magnetic conductivity of Sr_2CuO_3. In order to extract the phononic conductivity, we abstract the magnetic conductivity from the total one and the remaining is the phononic since $\kappa \approx \kappa_{mag} + \kappa_{ph}$.

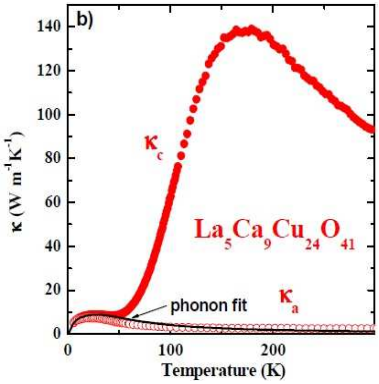

Figure 5.3: This diagram shows us the total and the phononic conductivity of $Ca_9La_5Cu_{24}O_{41}$. To find the magnetic contribution to total conductivity, we just abstract the phononic from the total.

The bounded material is in equilibrium at $T_0 = 100K$ and in order to make our numerical calculations, we have to extract the phononic and the magnetic diffusivities from the corresponding thermal conductivities. To accomplish this, we have first to extract the magnetic and phononic conductivity in each material.

We can find from the figure 5.2 that in the temperature range of 75 K to 125 K for the spin chain material (Sr_2CuO_3), the phononic and the magnetic conductivities have the linear form:

$$\kappa_{ph} = 55\frac{W}{m\,K} - 0.8 \cdot (T - T_0)\,\frac{W}{m\,K^2} \tag{5.22}$$

$$\kappa_m = 80\frac{W}{m\,K} - 1.6 \cdot (T - T_0)\,\frac{W}{m\,K^2}. \tag{5.23}$$

The specific heats for the two heat carriers in the spin chain material are:

$$C_p = 2.83 \cdot 10^6 \frac{J}{K\,m^3} \tag{5.24}$$

and

$$C_m = 3 \cdot 10^4 \frac{J}{K\,m^3}. \tag{5.25}$$

Knowing these two parameters, we can extract each carrier's thermal diffusivity from the equation $\kappa_i = C_i \cdot D_i$. So, starting from phononic conductivity we have:

$$\kappa_{ph} = 55\frac{W}{m\,K} - 0.8 \cdot (T - T_0)\,\frac{W}{m\,K^2} \Rightarrow$$

$$\kappa_{ph} = 2.83 \cdot 10^6 \frac{J}{K\,m^3}\left(\frac{55}{2.83 \cdot 10^6}\frac{m^2}{s} - \frac{0.8}{2.83 \cdot 10^6}\frac{m^2}{s\,K}(T - T_0)\right) \Rightarrow$$

$$\kappa_{ph} = C_p\left(\frac{55}{2.83 \cdot 10^6}\frac{10^6\,mm^2}{s} - \frac{0.8}{2.83 \cdot 10^6}\frac{10^6\,mm^2}{s\,K}(T - T_0)\right) \Rightarrow$$

$$\kappa_{ph} = C_p(\underbrace{19.4\frac{mm^2}{s} - 0.3 \cdot (T - T_0)\frac{mm^2}{s\,K}}_{D_p}).$$

By doing the same calculation for the magnetic diffusivity using the Equations 5.23 and 5.25 we get :

$$\kappa_m = C_m(\underbrace{2666.6\frac{mm^2}{s} - 53 \cdot (T - T_0)\frac{mm^2}{s\,K}}_{D_m}).$$

So the phonon and magnetic diffusivities of the spin chain material are

$$D_p = 19.4\frac{mm^2}{s} - 0.3 \cdot (T - T_0)\frac{mm^2}{s\,K} \tag{5.26}$$

$$D_m = 2666.6\frac{mm^2}{s} - 53 \cdot (T - T_0)\frac{mm^2}{s\,K}. \tag{5.27}$$

We notice that there is a huge value difference between the magnetic and phononic diffusivities and this is explained by the fact that magnetic specific heat is 2 magnitudes of order smaller than the phononic specific heat, which results in higher values when we calculate the ratios. The last parameter that we ll put into our numerical calculations, regarding the spin chain material, is the thermalization time which is $\tau_{mp} = 10^{-12}s$.

We ll now do the same calculations for the spin ladder ($Ca_9La_5Cu_{24}O_{41}$) material, in order to extract the phonons' and magnons' diffusivities that we ll put into our numerical calculations.

From figure 5.3, we can extract the magnon and phonon thermal conductivity in the temperature range of $75K$ to $125K$, which are:

$$\kappa_{ph} = 4\frac{W}{m\,K} - 0.02 \cdot (T - T_0)\,\frac{W}{m\,K^2} \tag{5.28}$$

$$\kappa_m = 60\frac{W}{m\,K} + 1.2 \cdot (T - T_0)\,\frac{W}{m\,K^2}. \tag{5.29}$$

The specific heats of the two heat carriers in the spin ladder material are different from these in the spin chain material, and have the values:

$$C_p = 2.86 \cdot 10^6\frac{J}{K\,m^3} \tag{5.30}$$

$$C_m = 1.5 \cdot 10^5\frac{J}{K\,m^3}. \tag{5.31}$$

By using the specific heats, we can extract the diffusivities from the thermal conductivities, as we did before for the spin chain material, so we get:

$$D_p = 1.4\frac{mm^2}{s} - 0.07 \cdot (T - T_0)\frac{mm^2}{s\,K} \tag{5.32}$$

$$D_m = 400\frac{mm^2}{s} + 8 \cdot (T - T_0)\frac{mm^2}{s\,K}. \tag{5.33}$$

The last parameter that we need for our numerical analysis is the thermalization time of the two heat carriers in the spin ladder material, which can be found in the bibliography

and has the value $\tau_{mp} = 4 \cdot 10^{-4} s$. As we notice, the coupling time between the two carrier is much smaller in the spin chain material than the ladder one.

We put all these parameters (the thermal diffusivities, the specific heats and the thermalization times for both materials) into our fortran program that solves the tridiagonal system (Equation 5.7) that we mentioned earlier, and by applying a heat pulse at the left surface of our material, we measure the temperature change at the right surface and via versa. Then, we measure the time of 1/2 increase of T_l in both surfaces and we calculate the rectification factor.

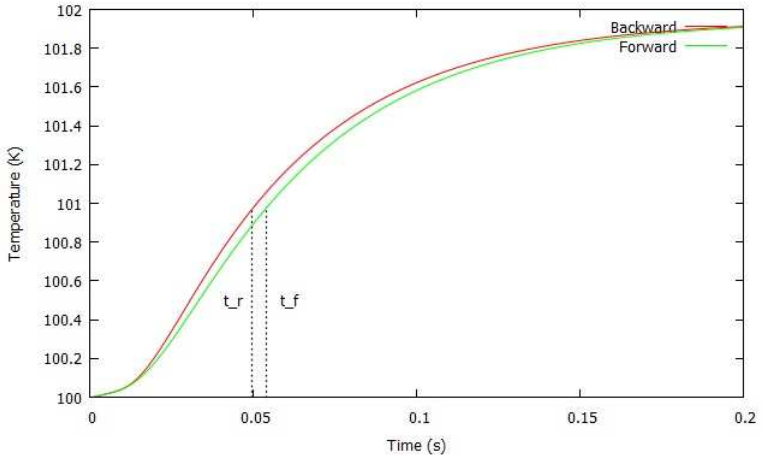

Figure 5.4: This figure shows us the phonons' temperature change when we put a heat pulse at the right surface and we measure the change at the left surface of our material (Forward direction - Green line) and via versa (Backward/Reversed direction - Red line). We can see the 1/2 temperature increase time for each direction, τ_f and τ_r.

We can find the 1/2 temperature increase time for each direction from the plot data, and their values are $\tau_f = 0.0538s$ and $\tau_r = 0.0494s$. So we can find the dynamic rectification factor which is

$$R_{dyn} = \frac{\tau_f}{\tau_r} = \frac{0.0538s}{0.0494s} = 1.089 \approx 1.09. \tag{5.34}$$

5.2.2 case 2: Sr_2CuO_3 - $Sr_{14}Cu_{24}O_{41}$ compound

The second case that we will study is the Sr_2CuO_3 (Spin chain - Material A) - $Sr_{14}Cu_{24}O_{41}$ (Spin ladder - Material B) bounded material.

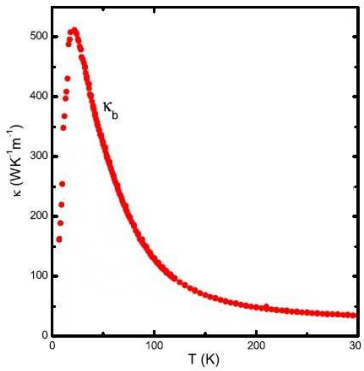

(a) Total thermal conductivity of Sr_2CuO_3

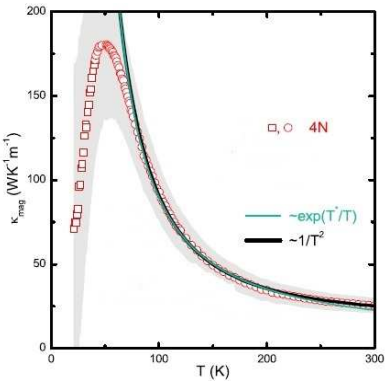

(b) Magnetic thermal conductivity of Sr_2CuO_3

Figure 5.5: These two diagrams show us the total and the magnetic conductivity of Sr_2CuO_3. In order to extract the phononic conductivity, we abstract the magnetic conductivity from the total one and the remaining is the phononic since $\kappa \approx \kappa_{mag} + \kappa_{ph}$.

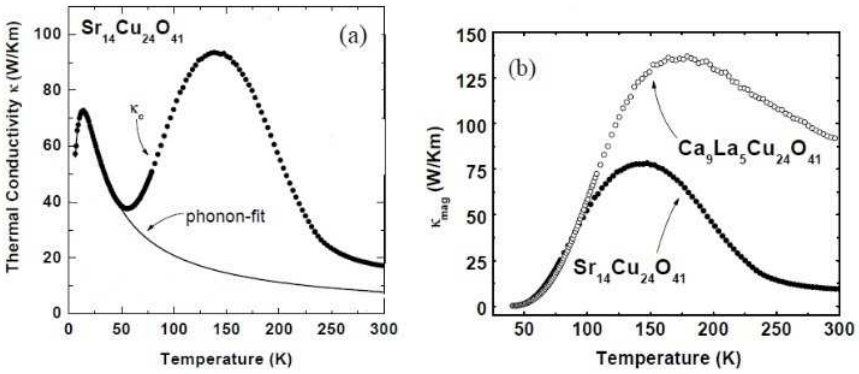

Figure 5.6: The diagram (a) shows us the total and the phononic conductivity of $Sr_{14}Cu_{24}O_{41}$ when the diagram (b) shows us the magnetic contribution to the total conductivity.

The spin chain material (Sr_2CuO_3) is the same as in the case 1, so we know all the parameters (Specific heats, thermal diffusivities for the two heat carriers and the thermalization time) we need for our numerical calculation:

$$C_p = 2.83 \cdot 10^6 \frac{J}{K\ m^3},$$

$$C_m = 3 \cdot 10^4 \frac{J}{K\ m^3},$$

$$D_p = 19.4\frac{mm^2}{s} - 0.3 \cdot (T - T_0)\frac{mm^2}{s\,K},$$
$$D_m = 2666.6\frac{mm^2}{s} - 53 \cdot (T - T_0)\frac{mm^2}{s\,K},$$

and

$$\tau_{mp} = 10^{-12}s$$

These thermal diffusivities, as we mentioned in case 1, correspond to the temperature range of $75K$ to $125k$.

The spin ladder ($SR_{14}Cu_{24}O_{41}$) material is different from the one in case 1, so we have to do all the calculations that we did before in order to extract the phonons' and magnons' diffusivities that we ll put into our numerical calculations.

From figure 5.6, we can extract the magnon and phonon thermal conductivity in the temperature range of $75K$ to $125K$, which are:

$$\kappa_{ph} = 21\frac{W}{m\,K} - 0.3 \cdot (T - T_0)\,\frac{W}{m\,K^2} \tag{5.35}$$

$$\kappa_m = 52\frac{W}{m\,K} + 1.0 \cdot (T - T_0)\,\frac{W}{m\,K^2}. \tag{5.36}$$

The specific heats of the two heat carriers in the spin ladder material are (as we mentioned in case 1):

$$C_p = 2.86 \cdot 10^6\frac{J}{K\,m^3}$$

$$C_m = 1.5 \cdot 10^5\frac{J}{K\,m^3}.$$

By using the specific heats, we can extract the diffusivities from the thermal conductivities, so we get:

$$\kappa_{ph} = 21\frac{W}{m\,K} - 0.3 \cdot (T - T_0)\,\frac{W}{m\,K^2} \Rightarrow$$
$$\kappa_{ph} = 2.86 \cdot 10^6\frac{J}{K\,m^3}\Big(\frac{21}{2.86 \cdot 10^6}\frac{m^2}{s} - \frac{0.3}{2.86 \cdot 10^6}\frac{m^2}{s\,K}(T - T_0)\Big) \Rightarrow$$
$$\kappa_{ph} = C_p\Big(\frac{21}{2.83 \cdot 10^6}\frac{10^6\,mm^2}{s} - \frac{0.3}{2.83 \cdot 10^6}\frac{10^6\,mm^2}{s\,K}(T - T_0)\Big) \Rightarrow$$

$$\kappa_{ph} = C_p\Big(\underbrace{7.3\frac{mm^2}{s} - 0.1 \cdot (T - T_0)\frac{mm^2}{s\,K}}_{D_p}\Big).$$

By doing the same calculation for the magnetic diffusivity using the Equations 5.36 and 5.31 we get :

$$\kappa_m = C_m(\underbrace{346.6\frac{mm^2}{s} + 6.6 \cdot (T - T_0)\frac{mm^2}{s\,K}}_{D_m}).$$

So, the thermal diffusivities for our two heat carriers in the spin ladder material, are:

$$D_p = 7.3\frac{mm^2}{s} - 0.1 \cdot (T - T_0)\frac{mm^2}{s\,K} \tag{5.37}$$

$$D_m = 346.6\frac{mm^2}{s} + 6.6 \cdot (T - T_0)\frac{mm^2}{s\,K}. \tag{5.38}$$

The thermalization time for the spin ladder is $\tau_{mp} = 4 \cdot 10^{-4}s$,so by solving numerically the tridiagonal system (Equation 5.7) we get the figure that shows us the temperature change in our material, when we put a heat pulse in each surface.

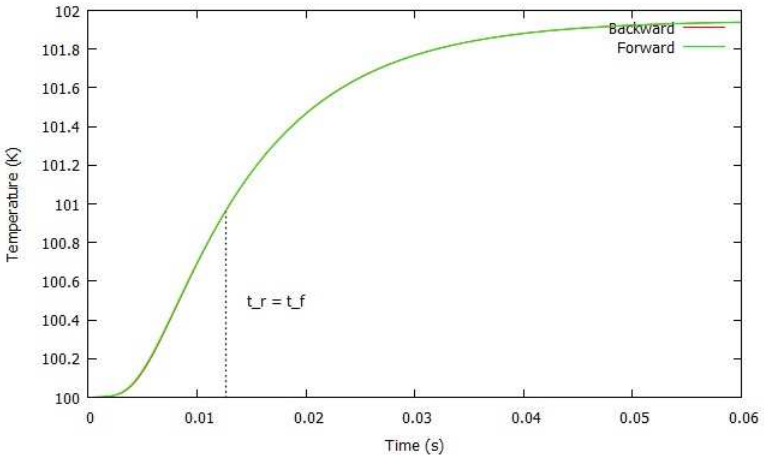

Figure 5.7: This figure shows us the phonons' temperature change when we put a heat pulse at the right surface and we measure the change at the left surface of our material (Forward direction - Green line) and via versa (Backward/Reversed direction - Red line). We can see the 1/2 temperature increase time for each direction, τ_f and τ_r.

As we see in the figure 5.7, the heat propagates the same way for both directions. The 1/2 temperature increase time for each direction is the same, $\tau_f = \tau_r = 0.0127s$, that leads to a rectification factor $R_{dyn} = 1$, which means that we have no rectification. In the static case, we found a Rectification factor whose value is $R_{stat} = 1.37$, and as we see, in the static study rectification occurs, when in the dynamic study does not.

5.2.3 case 3: $SrCuO_2$ - $Ca_9La_5Cu_{24}O_{41}$ compound

The third case that we will study is the $SrCuO_2$ (Spin chain - Material A) - $Ca_9La_5Cu_{24}O_{41}$ (Spin ladder - Material B) bounded material.

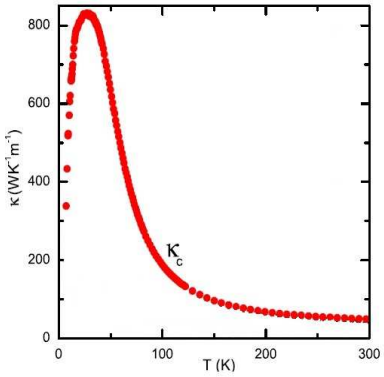

(a) Total thermal conductivity of $SrCuO_2$

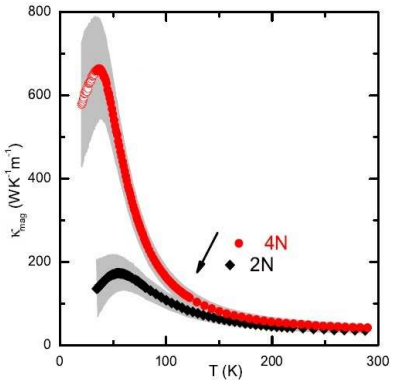

(b) Magnetic thermal conductivity of $SrCuO_2$

Figure 5.8: These two diagrams show us the total and the magnetic conductivity of $SrCuO_2$. In order to extract the phononic conductivity, we abstract the magnetic conductivity from the total one and the remaining is the phononic since $\kappa \approx \kappa_{mag} + \kappa_{ph}$. We are interested for the $4N$ purity's conductivity.

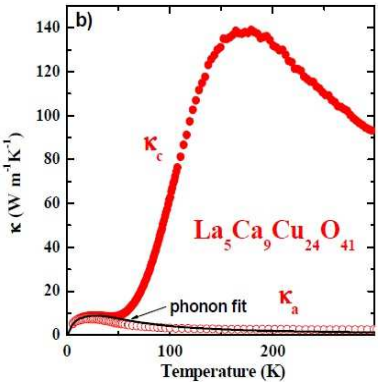

Figure 5.9: The diagram (a) shows us the total and the phononic conductivity of $Ca_9La_5Cu_{24}O_{41}$ when the diagram (b) shows us the magnetic contribution to the total conductivity.

We can find from the figure 5.8 that in the temperature range of $75\,K$ to $125\,K$ for the spin chain material ($SrCuO_2$), the phononic and the magnetic conductivities have the linear form:

$$\kappa_{ph} = 30\frac{W}{m\,K} - 0.3 \cdot (T - T_0)\,\frac{W}{m\,K^2} \tag{5.39}$$

$$\kappa_m = 160\frac{W}{m\,K} - 1.9 \cdot (T - T_0)\,\frac{W}{m\,K^2}. \tag{5.40}$$

The specific heats for the two heat carriers in the spin chain material are:

$$C_p = 2.83 \cdot 10^6 \frac{J}{K\,m^3} \tag{5.41}$$

and

$$C_m = 3 \cdot 10^4 \frac{J}{K\,m^3}. \tag{5.42}$$

Knowing these two parameters, we can extract each carrier's thermal diffusivity from the equation $\kappa_i = C_i \cdot D_i$, as we did before. So, starting from phononic conductivity we have:

$$\kappa_{ph} = 30\frac{W}{m\,K} - 0.3 \cdot (T - T_0)\,\frac{W}{m\,K^2} \Rightarrow$$

$$\kappa_{ph} = 2.83 \cdot 10^6 \frac{J}{K\,m^3}\left(\frac{30}{2.83 \cdot 10^6}\frac{m^2}{s} - \frac{0.3}{2.83 \cdot 10^6}\frac{m^2}{s\,K}(T - T_0)\right) \Rightarrow$$

$$\kappa_{ph} = C_p\left(\frac{30}{2.83 \cdot 10^6}\frac{10^6\,mm^2}{s} - \frac{0.3}{2.83 \cdot 10^6}\frac{10^6\,mm^2}{s\,K}(T - T_0)\right) \Rightarrow$$

$$\kappa_{ph} = C_p\Big(\underbrace{10.6\frac{mm^2}{s} - 0.1 \cdot (T - T_0)\frac{mm^2}{s\,K}}_{D_p}\Big).$$

By doing the same calculation for the magnetic diffusivity using the Equations 5.40 and 5.42 we get :

$$\kappa_m = C_m\Big(\underbrace{5333.0\frac{mm^2}{s} - 62 \cdot (T - T_0)\frac{mm^2}{s\,K}}_{D_m}\Big). \tag{5.43}$$

So the phonon and magnetic diffusivities of the spin chain material are

$$D_p = 10.6\frac{mm^2}{s} - 0.1 \cdot (T - T_0)\frac{mm^2}{s\,K} \tag{5.44}$$

$$D_m = 5333.0\frac{mm^2}{s} - 62 \cdot (T - T_0)\frac{mm^2}{s\,K}. \tag{5.45}$$

The last parameter that we ll put into our numerical calculations, regarding the spin chain material, is the thermalization time which is $\tau_{mp} = 10^{-12}s$.

We have made the calculations for the spin ladder ($Ca_9La_5Cu_{24}O_{41}$) material in *case 1*, so the thermal diffusivites are:

$$D_p = 1.4\frac{mm^2}{s} - 0.07 \cdot (T - T_0)\frac{mm^2}{s\,K} \tag{5.46}$$

$$D_m = 400\frac{mm^2}{s} + 8 \cdot (T - T_0)\frac{mm^2}{s\,K}. \tag{5.47}$$

The last parameter that we need for our numerical analysis is the thermalization time of the two heat carriers in the spin ladder material, which can be found in the bibliography and has the value $\tau_{mp} = 4 \cdot 10^{-4}s$.

We put all these parameters (the thermal diffusivities, the specific heats and the thermalization times for both materials) into our fortran program that solves the tridiagonal system (Equation 5.7) that we mentioned earlier, and by applying a heat pulse at the left surface of our material, we measure the temperature change at the right surface and via versa. Then, we measure the time of 1/2 increase of T_l in both surfaces and we calculate the rectification factor.

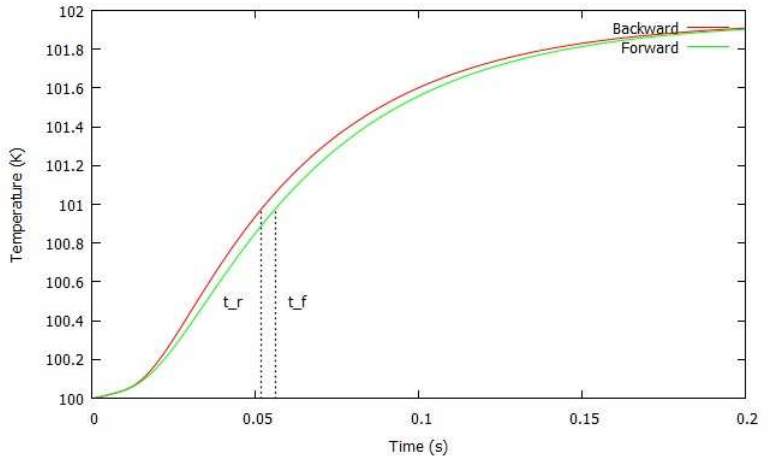

Figure 5.10: This figure shows us the phonons' temperature change when we put a heat pulse at the right surface and we measure the change at the left surface of our material (Forward direction - Green line) and via versa (Backward/Reversed direction - Red line). We can see the 1/2 temperature increase time for each direction, τ_f and τ_r.

We can find the 1/2 temperature increase time for each direction from the plot data, and their values are $\tau_f = 0.0561s$ and $\tau_r = 0.0518s$. So we can find the dynamic

rectification factor which is

$$R_{dyn} = \frac{\tau_f}{\tau_r} = \frac{0.0561s}{0.0518} = 1.083 \approx 1.08. \tag{5.48}$$

5.2.4 case 4: $SrCuO_2$ - $Sr_{14}Cu_{24}O_{41}$ compound

The fourth case that we will study is the $SrCuO_2$ (Spin chain - Material A) - $Sr_{14}Cu_{24}O_{41}$ (Spin ladder - Material B) bounded material.

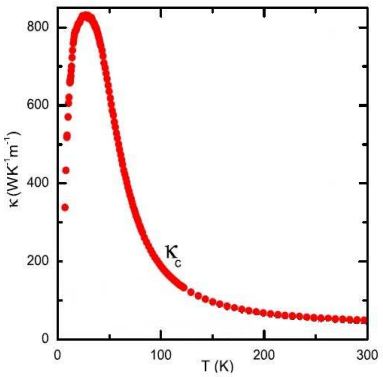

(a) Total thermal conductivity of $SrCuO_2$

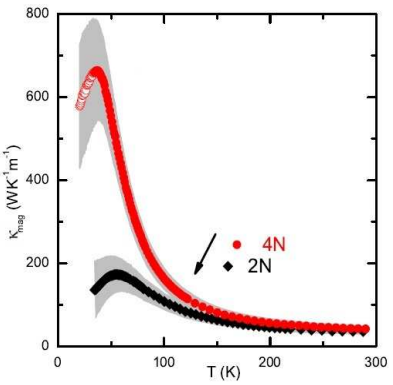

(b) Magnetic thermal conductivity of $SrCuO_2$

Figure 5.11: These two diagrams show us the total and the magnetic conductivity of $SrCuO_2$. In order to extract the phononic conductivity, we abstract the magnetic conductivity from the total one and the remaining is the phononic since $\kappa \approx \kappa_{mag} + \kappa_{ph}$. We are interested for the $4N$ purity's conductivity.

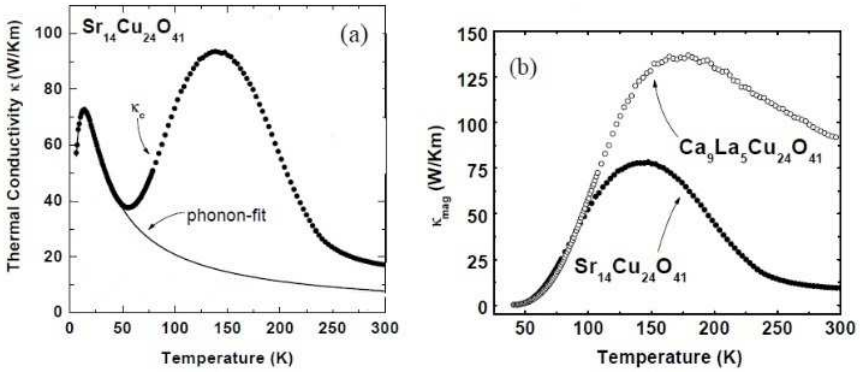

Figure 5.12: The diagram (a) shows us the total and the phononic conductivity of $Sr_{14}Cu_{24}O_{41}$ when the diagram (b) shows us the magnetic contribution to the total conductivity.

We have made the calculations and found the thermal diffusivities for both materials, within the $75K$-$125K$ range, which are for the chain material

$$D_p = 10.6\frac{mm^2}{s} - 0.1 \cdot (T - T_0)\frac{mm^2}{s\,K} \tag{5.49}$$

$$D_m = 5333.0\frac{mm^2}{s} - 62 \cdot (T - T_0)\frac{mm^2}{s\,K}. \tag{5.50}$$

and for the ladder material:

$$D_p = 7.3\frac{mm^2}{s} - 0.1 \cdot (T - T_0)\frac{mm^2}{s\,K} \tag{5.51}$$

$$D_m = 346.6\frac{mm^2}{s} + 6.6 \cdot (T - T_0)\frac{mm^2}{s\,K}. \tag{5.52}$$

We put all these parameters (the thermal diffusivities, the specific heats and the thermalization times for both materials) into our fortran program that solves the tridiagonal system (Equation 5.7) that we mentioned earlier, and by applying a heat pulse at the left surface of our material, we measure the temperature change at the right surface and via versa. Then, we measure the time of $1/2$ increase of T_l in both surfaces and we calculate the rectification factor.

As we see from the figure 5.13, the $1/2$ temperature increase time, is the same for both directions of propagation, $\tau_r = \tau_f = 0.0163s$ which leads to a rectification factor $R_{dyn} = 1$. That means that we haven't rectification in this case, when at the static study rectification occurs for this compound.

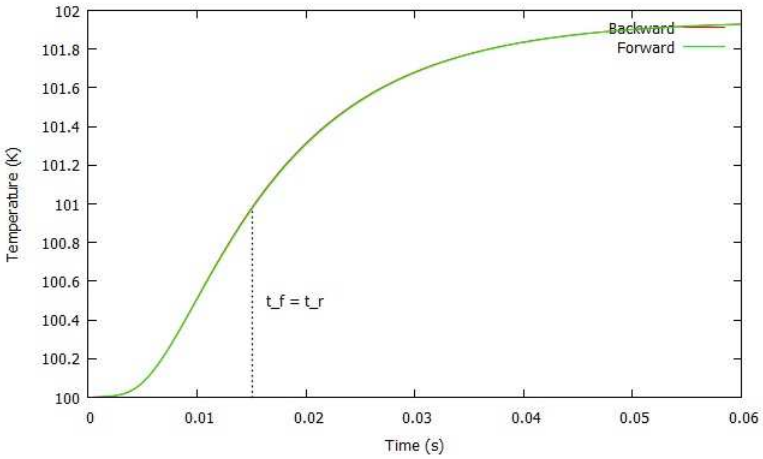

Figure 5.13: This figure shows us the phonons' temperature change when we put a heat pulse at the right surface and we measure the change at the left surface of our material (Forward direction - Green line) and via versa (Backward/Reversed direction - Red line). We can see the 1/2 temperature increase time for each direction, τ_f and τ_r.

5.2.5 case 5: Sr_2CuO_3 - $Sr_{14}Cu_{24}O_{41}$ compound

The fifth case that we will study is the $SrCuO_2$ (Spin chain - Material A) - $Sr_{14}Cu_{24}O_{41}$ (Spin ladder - Material B) bounded material. The differences between this case and the previous, is that in this one, spin ladder's magnetic thermal conductivity has quadratic dependence on temperature and that the temperature range, where we study the thermal rectification, is between $125K$-$175K$.

From the Figures 5.14 and 5.15, we can extract the thermal conductivity for each heat carrier, for both materials. We start from the spin chain material, and the thermal conductivities within the range of $125K$ - $175K$ are:

$$\kappa_{ph} = 25\frac{W}{m\,K} - 0.3 \cdot (T - T_0)\,\frac{W}{m\,K^2} \tag{5.53}$$

$$\kappa_{m} = 55\frac{W}{m\,K} - 0.5 \cdot (T - T_0)\,\frac{W}{m\,K^2}, \tag{5.54}$$

where $T_0 = 140K$. Knowing the specific heats for the two heat carriers in the spin chain material, we calculate the thermal diffusivities like we did in the previous cases:

$$\kappa_{ph} = 25\frac{W}{m\,K} - 0.3 \cdot (T - T_0)\,\frac{W}{m\,K^2} \Rightarrow$$

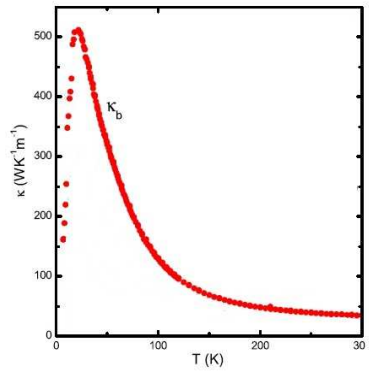

(a) Total thermal conductivity of Sr_2CuO_3

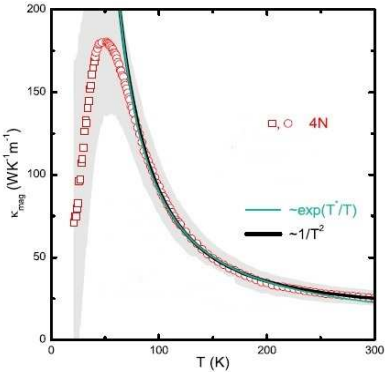

(b) Magnetic thermal conductivity of Sr_2CuO_3

Figure 5.14: These two diagrams show us the total and the magnetic conductivity of Sr_2CuO_3. In order to extract the phononic conductivity, we abstract the magnetic conductivity from the total one and the remaining is the phononic since $\kappa \approx \kappa_{mag} + \kappa_{ph}$. We are interested for the $4N$ purity's conductivity.

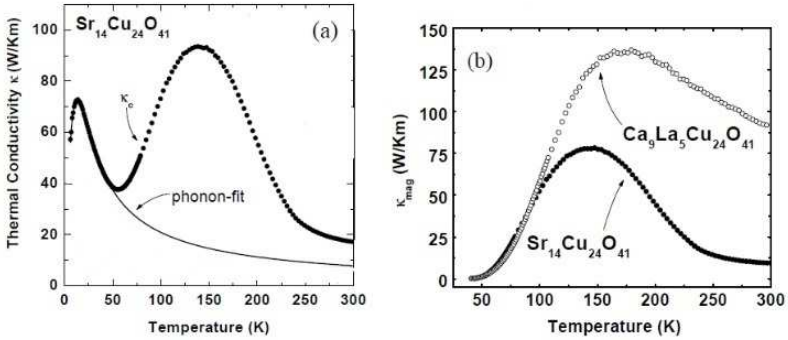

Figure 5.15: The diagram (a) shows us the total and the phononic conductivity of $Sr_{14}Cu_{24}O_{41}$ when the diagram (b) shows us the magnetic contribution to the total conductivity.

$$\kappa_{ph} = 2.83 \cdot 10^6 \frac{J}{K\, m^3}\left(\frac{25}{2.83 \cdot 10^6}\frac{m^2}{s} - \frac{0.3}{2.83 \cdot 10^6}\frac{m^2}{s\, K}(T - T_0)\right) \Rightarrow$$

$$\kappa_{ph} = C_p\left(\frac{25}{2.83 \cdot 10^6}\frac{10^6\, mm^2}{s} - \frac{0.3}{2.83 \cdot 10^6}\frac{10^6\, mm^2}{s\, K}(T - T_0)\right) \Rightarrow$$

$$\kappa_{ph} = C_p\Big(\underbrace{8.8\frac{mm^2}{s} - 0.1 \cdot (T - T_0)\frac{mm^2}{s\, K}}_{D_p}\Big).$$

Doing the same calculation for the magnetic thermal conductivity in the spin chain material, results:

$$\kappa_m = C_m(\underbrace{1833\frac{mm^2}{s} - 17\cdot(T-T_0)\frac{mm^2}{s\,K}}_{D_p})$$

where $T_0 = 140K$.

As for the spin ladder material, $Sr_{14}Cu_{24}O_{41}$, we can extract the thermal conductivity for each heat carrier from figure 5.15 within the $125K$-$175K$ temperature range, which are:

$$\kappa_{ph} = 16\frac{W}{m\,K} - 0.12\cdot(T-T_0)\,\frac{W}{m\,K^2} \tag{5.55}$$

$$\kappa_m = 78\frac{W}{m\,K} - 0.01\cdot(T-T_0)^2\,\frac{W}{m\,K^3}. \tag{5.56}$$

By knowing that in the spin ladder, the specific heats for phonons and magnons are $C_p = 2.86\cdot 10^6 J/K\cdot m^3$ and $C_m = 1.5\cdot 10^5 J/K\cdot m^3$, using the previous method to extract the thermal diffusivities leads us to the results:

$$D_p = 5.6\frac{mm^2}{s} - 0.04\cdot(T-T_0)\frac{mm^2}{s\,K} \tag{5.57}$$

$$D_m = 520.0\frac{mm^2}{s} - 0.06\cdot(T-T_0)^2\frac{mm^2}{s\,K^2}. \tag{5.58}$$

As we mentioned at the start of this case study, all thermal diffusivities except the magnons' one in the spin ladder that has quadratic dependence on temperature, depend linearly on temperature. We now put all these parameters (the thermal diffusivities, the specific heats and the thermalization times for both materials) into our fortran program that solves the tridiagonal system (Equation 5.7) that we mentioned earlier, and by applying a heat pulse at the left surface of our material, we measure the temperature change at the right surface and via versa. Then, we measure the time of 1/2 increase of T_l in both surfaces and we calculate the rectification factor.

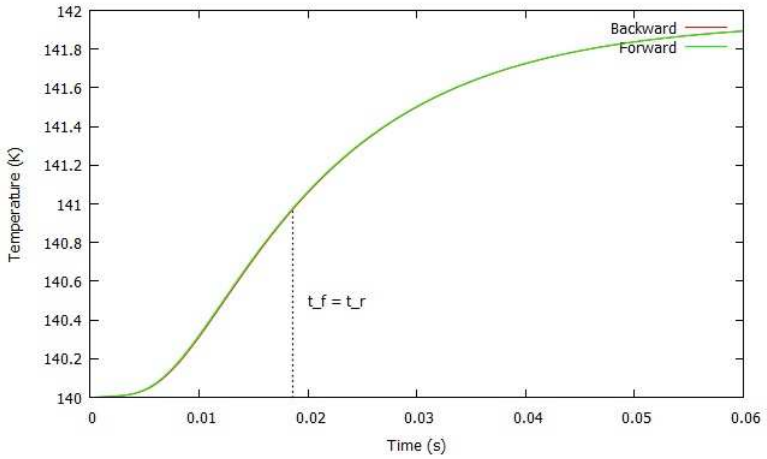

Figure 5.16: This figure shows us the phonons' temperature change when we put a heat pulse at the right surface and we measure the change at the left surface of our material (Forward direction - Green line) and via versa (Backward/Reversed direction - Red line). We can see the 1/2 temperature increase time for each direction, τ_f and τ_r.

As we see from the figure 5.16, the 1/2 temperature increase time, is the same for both directions of propagation, $\tau_r = \tau_f = 0.0186s$ which leads to a rectification factor $R_{dyn} = 1$. That means that we haven't rectification in this case, when at the static study, rectification occurs for this compound.

5.2.6 Discussion

Why dynamic rectification factors are much smaller that the static ones?
At this point, we have to emphasize the main difference between the static and the dynamic rectification. In the static one, we only use the total thermal conductivity for each material, and we integrate the heat flux equation. On the other hand, in the dynamic rectification, we solve numerically a coupled system of two diffusion equations, taking in mind the dynamic parameters that we know from the microscopic study of the materials, such as the thermal conductivity of each heat carrier in both materials, the specific heats of the heat carriers and the coupling time that shows us how much time is needed for the two heat carriers to interact. As we see, in the static we neglect a lot of information about our materials and maybe this is a reason that we see much divergence in our results between the static and the dynamic case, which leads in much more "promising" results.

But let's try to explain why in the dynamic rectification study, we observe that the heat propagates, in almost every case, by the same way in both directions. We ll show moments of the heat that propagates (for both directions) in our material due to the phonons and magnons and we ll try to explain why the 1/2 increase time of T_l is almost the same in both directions. The following figures correspond to case's 1 thermal diffusivities.

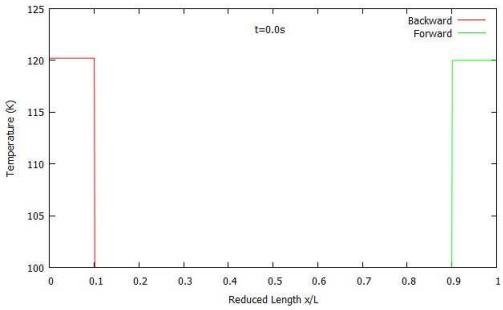

Figure 5.17: Phonons' Temperature versus reduced length $\xi = x/L$, at time $t = 0s$

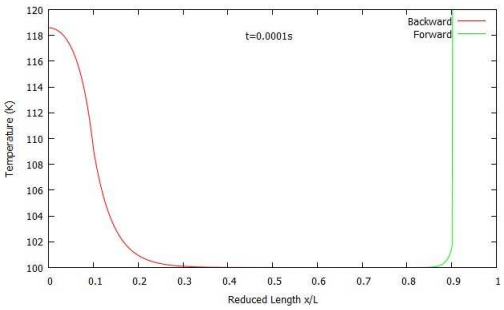

(a) Phonons' Temperature versus reduced length $\xi = x/L$

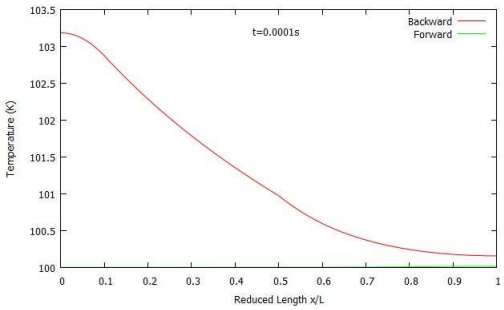

(b) Magnons' Temperature versus reduced length $\xi = x/L$

Figure 5.18: Temperature of each carrier versus reduced length $\xi = x/L$,at time $t = 0.0001s$

Figure 5.17 shows us the moment when $t = 0s$, which is when we put the heat pulse at the surfaces. We have to point out that these are two different subcases, one is when we put the heat pulse at the left surface and measure the temperature increase at the opposite and via versa, that are plotted simultaneously. The next moment is when $t = 0.0001s$ (figure 5.18), and as we see, when the heat pulse is putted at the chain material, the phonons' temperature (figure 5.18(a)) diffuses faster than when is putted in the ladder material where temperature's diffusion is extremely small. This happens for two

reasons, the first one is because of the difference in the phonons' thermal diffusivity in the two bounded materials (in the chain material $D_p \approx 19\, mm^2/s$ when in the ladder material $D_p \approx 1.4\, mm^2/s$) and the second reason is because of the thermalization time in these two materials. The thermalization time in the chain material is much smaller than in the ladder material, $\tau_{chain} \ll \tau_{ladder}$, and that leads the heat to transfer from the phonon system to the magnon one faster in the chain material, as it is shown in figure 5.18(a), where we observe a 3-degrees increase in magnons' temperature when the pulse is putted at the chain material. At the same time, we observe that when the heat pulse is putted at the ladder material, magnons' temperature increase for less than 0.1 degrees. We notice that in the magnon system, the heat diffuses extremely fast and that is because of the big values of the magnons' diffusivities in both materials ($D_m \approx 2500 mm^2/s$ in the chain material and $D_m \approx 400 mm^2/s$ in the ladder material).

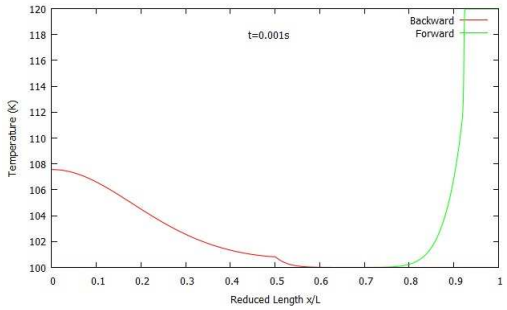

(a) Phonons' Temperature versus reduced length $\xi = x/L$

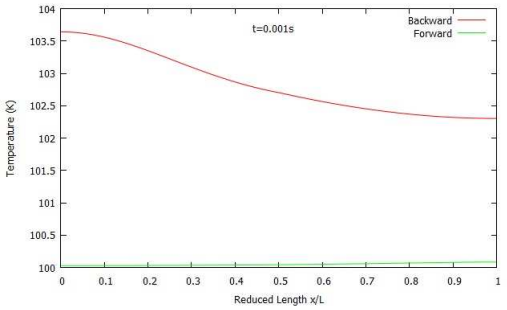

(b) Magnons' Temperature versus reduced length $\xi = x/L$

Figure 5.19: Temperature of each carrier versus reduced length $\xi = x/L$,at time $t = 0.001s$

By observing the figures 5.19 and 5.20, we can see that when the heat pulse is putted in the chain material, the heat diffuses much faster than when is putted in the ladder material, and the two reasons that cause this is the bigger phonon diffusivity in the chain material and the smaller thermalization time in the chain material that leads the heat to the magnon system, as we mentioned earlier. At the two moments that are shown in these two figures, we notice that there is a big difference in the temperature in the magnon systems for the two directions. This happens because at the chain material the coupling time is much more smaller than the ladder's one, so the heat transfers faster in the magnon system and diffuses pretty fast due to the high magnon diffusivities.At the same time in the ladder material, the coupling time is way bigger that the τ_{chain} and if we add the fact that the phonon's system diffusivity is

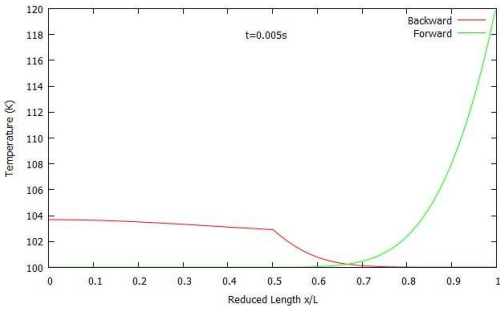

(a) Phonons' Temperature versus reduced length $\xi = x/L$

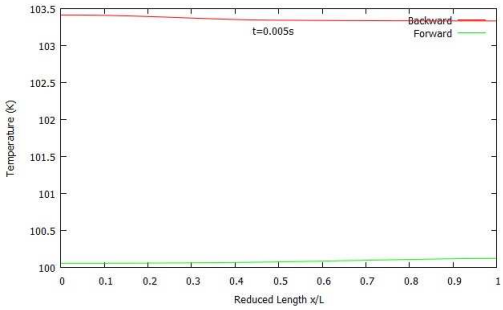

(b) Magnons' Temperature versus reduced length $\xi = x/L$

Figure 5.20: Temperature of each carrier versus reduced length $\xi = x/L$,at time $t = 0.005s$

way too small,most of the heat stays in the phonon system that diffuses too slowly (comparing to the chain material) and only a small part of it transfers to the magnon system causing the magnons' temperature to increase for 0.2 Kelvin degrees.

As for the phonon system , which interests us the most since we measure the phonon temperature increase at the opposite surfaces, we observe something interesting that we have to point it out. Despite the fact that in the chain material the heat diffuses pretty fast in the phonon system, when it reaches the interface (where the ladder material begins, at $\xi = 0.5$) the heat there diffuses very slowly (due to the small D_p in the ladder material) causing the phonon's temperature to slowly increase. So, we don't still see an increase in the phonons' temperature at the opposite surfaces since despite the direction, the phonons' temperature increases slowly at the opposite surfaces.

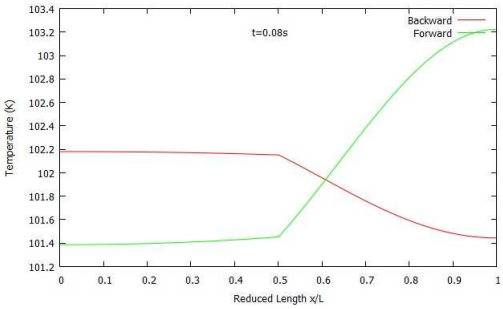

(a) Phonons' Temperature versus reduced length $\xi = x/L$

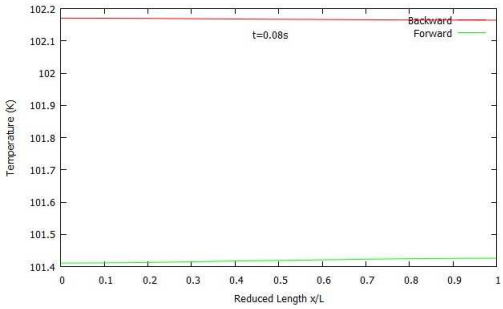

(b) Magnons' Temperature versus reduced length $\xi = x/L$

Figure 5.21: Temperature of each carrier versus reduced length $\xi = x/L$,at time $t = 0.08s$

The last figure (Figure 5.21), corresponds to a moment where we observe a difference in the phonons' temperature at the two opposite surfaces. As we see, despite the fact that the two bounded materials have different dynamic parameters, the heat reaches the opposite surface from the one that we put the heat pulse, in almost the same time for both directions. The result is to observe a very small rectification for all the cases we studied for these 4 materials (every case's moment figures are similar to these we showed).

After we studied these cases, a new question arises. "Which dynamic parameter is crucial for seeing intense rectification phenomena?". The answer to this question lies at the "Reciprocity and symmetry of the Green's function" section, where we showed that in order to observe thermal rectification, our diffusion coefficients must be non linear. That means that they must have the following form : $D = D_0 + \eta \cdot T$, which depends linearly on temperature, but in general D is non linear. So, the bigger the non linear coefficient η becomes, the bigger the linearity is, which leads to a big rectification factor.

Lets study the following setup of spin chain-ladder bounded material:

	Spin Chain Material	Spin Ladder Material
D_p	$5\,\frac{mm^2}{s} + 20 \cdot (T - T_0)\,\frac{mm^2}{s \cdot K}$	$100\,\frac{mm^2}{s} - 4.9 \cdot (T - T_0)\,\frac{mm^2}{s \cdot K}$
D_m	$5\,\frac{mm^2}{s} + 20 \cdot (T - T_0)\,\frac{mm^2}{s \cdot K}$	$0.1\,\frac{mm^2}{s} + 15 \cdot (T - T_0)\,\frac{mm^2}{s \cdot K}$

where as we see, the non linear coefficients are much bigger than these in cases 1-5. These coefficients values aren't random and the logic behind this choice will explained now. In the static rectification study, we studied cases of two bounded materials,where the one exhibits a high κ at low temperatures and high κ at high temperatures and the second material had the opposite properties. This leads us to two different heat fluxes when we place a hot heat bath at the left surface and a cold heat bath at the right surface and via versa, and because of that we observed the rectification phenomenon. The difference now is that in each material we have two heat carriers, each one having its own thermal conductivity, so we have to think a little different. We want our chain material, which is a material with very small thermalization time if we compare it with the one in the ladder material ($\tau_{chain} \ll \tau_{ladder}$), to exhibit high diffusivity in both phonons' and magnons' system at high temperatures and low diffusivity at low temperatures. On the other hand we want our ladder's material phonons' system to exhibit low diffusivity at high temperatures and high diffusivity at low temperatures,

when the magnons' system should exhibit low diffusivity at low temperatures and high diffusivity at high temperatures.

When we put the heat pulse at the spin chain material, we expect to diffuse pretty fast since the D_p is big in high temperatures and at the same time, since the coupling time is pretty small and a big portion of the heat will be transfered to magnons' systen, magnons will diffuse pretty fast too (D_m is big in high T). At the time that the heat pulse will reach the interface (at the start the temperature at the interface will be small but it will keep increasing), it will diffuse fast since the ladder's D_p is high at low temperatures causing the heat to reach the opposite surface in short time. If we now put the heat pulse at the spin ladder material, we observe that the phonons will diffuse at very slow rates, since D_p is small at high temperatures. At the same time, the coupling time is much bigger in the ladder material, so the heat will remain much more time in the phonon system that diffuses slowly. At a time, the heat will reach the interface, where the spin chain ladder exhibits low diffusivity at low temperatures in both phonons' and magnons' system, which will stall the heat propagation.

So in general we expect that in the backward direction (when we put the heat pulse at the chain material) the heat pulse will propagate faster than in the forward direction (when we put the heat pulse at the ladder material). We will put these thermal diffusivities that are shown in the above table into our program and we ll see if the result agrees with our speculations.

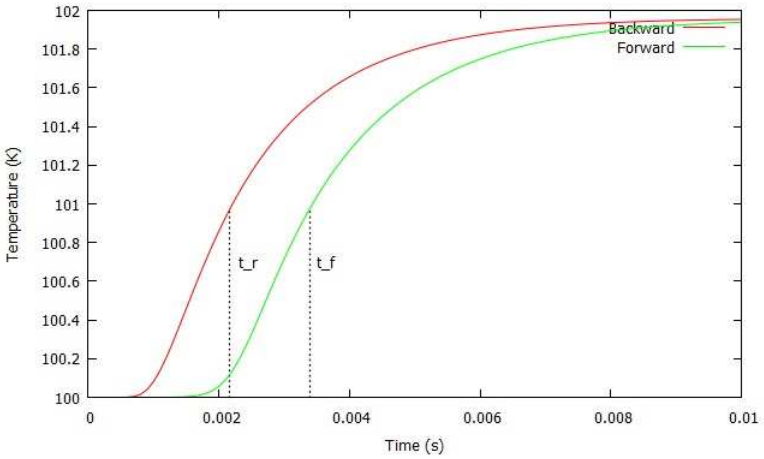

Figure 5.22: This figure shows us the phonons' temperature change when we put a heat pulse at the right surface and we measure the change at the left surface of our material (Forward direction - Green line) and via versa (Backward/Reversed direction - Red line). We can see the 1/2 temperature increase time for each direction, τ_f and τ_r.

From figure 5.22, we can measure the 1/2 temperature increase times for both directions which are $\tau_f = 0.00340s$ for the forward direction and $\tau_r = 0.00216s$ for the backward/reversed direction. The rectification factor is:

$$R_{dyn} = \frac{\tau_f}{\tau_r} = \frac{0.00340s}{0.00216s} = 1.57\,. \tag{5.59}$$

As we see, the setup we studied leads to a high rectification factor, if we compare it with the previous dynamical results (cases 1-5). This results shows us that we have to search for materials that their thermal conductivities have steeper slopes, which means that the thermal diffusivity's non linear term coefficient will be high in value. The last case we studied, we showed that the bigger the non linear's term coefficient is, results to more intense non linear phenomena, which in our case is the phenomenon of thermal rectification.

The question that arises now is: "Are there materials whose thermal conductivity's slope is as steep as we mentioned in the last case that we studied?". The answer to this question is yes. Recently, the family of vanadium oxides has been studied in some works, where they used these materials to study the thermal rectification phenomenon. The heat in these materials is carried by two heat carriers, the phonons and the electrons. The interesting thing that they showed in these materials, is that when the insulator-to-metal transition occurs in thin films of polycrystalline VO_2, the thermal conductance is increased by 60% due to the phase transition (which occurs close to $\sim 340\,K$). So the thermal conductance's slope is pretty steep, thing that we are searching for.

As we just showed, thermal rectification is a subject that is being studied by a lot of scientific teams, and the discovery of materials that their thermal conductivity's slopes are as steep as possible, will help us to get more promising results at creating a thermal rectifier.

6 Temperature Response due to time-dependent heat source

In the last chapter of this work, we ll study the temperature response at the right surface of a material, when at the left surface we have adapted a time-dependent heat source.

6.1 1 Material

6.1.1 One heat carrier

At first, we suppose that we have one material, tha has only one heat carrier, phonons. Our material is at Equilibrium at $T = 100K$ and we adapt at the left surface a time dependent heat source that has the following form

$$Source = 5 \cdot sin(\frac{2\pi}{T} \cdot t), \tag{6.1}$$

where 5 is the amplitude (the peak deviation of the function from zero) and T is the period. By doing our numerical calculations, we observe the temperature response at the opposite surface versus time, wanting to see in which cases the heat propagates diffusivily and in which ballistically.

case i:

We suppose that the period of the heat source is $T = 0.1s$ and the diffusion constant of the phonons is $D_p = 100\ \frac{mm^2}{s}$ which corresponds ,as we showed in the Dynamic Rectification section when we showed the reduced dynamic equations, to a diffusion time of $\tau_p = \frac{1}{D_p} = 0.01s$.

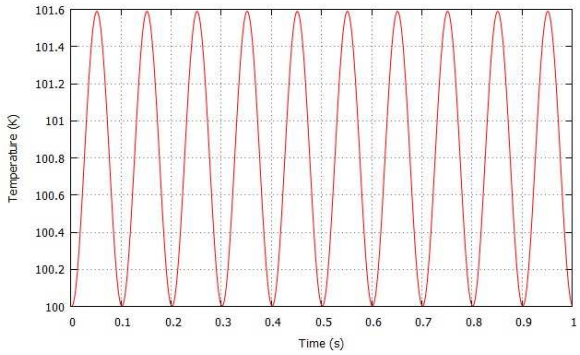

Figure 6.1: Temperature response at the opposite surface from the one that we adapted the heat source, versus time.

As we see from figure 6.1, when the diffusion time τ_p is smaller than the period T of the heat source, then the heat propagates ballistically.

case ii:

The heat source we adapt is the same in all cases. The only thing that we change is the diffusion time of the phonons in respect to the heat source period, and we see the results. Lets suppose that out diffusion time τ_p is equal to the heat source's period.

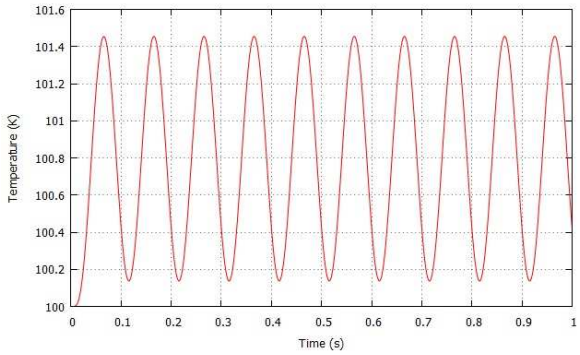

Figure 6.2: Temperature response at the opposite surface from the one that we adapted the heat source, versus time.

In this case, where $\tau_p = T$ we notice that the propagation is mostly ballistic, with a small diffusive character.

case iii:
In this case we suppose that the diffusion time τ_p is bigger than the period T, and more specifically we choose $\tau_p = 1s$.

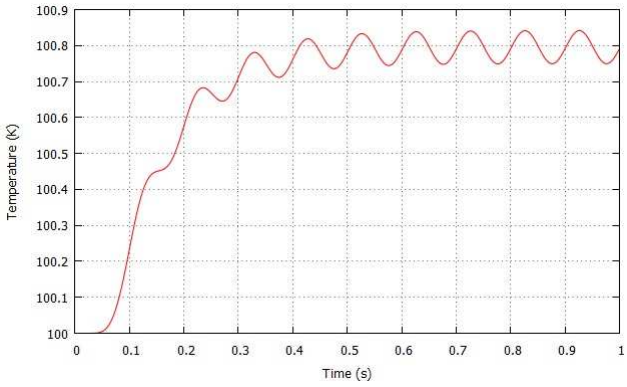

Figure 6.3: Temperature response at the opposite surface from the one that we adapted the heat source, versus time.

We observe that in this case, the heat propagates diffusivily in our material.

Concluding, in the case that we have one material with only phonons as heat carrier, we observe that when $\tau_p < T$ the heat propagates ballistically, but when $\tau_p \geq T$ the diffusive character is becoming more and more intense as the diffusion time τ_p becomes bigger than the period of the heat source.

6.1.2 Two heat carriers

Now we suppose that we still have one material but we have two heat carriers (phonons and magnons) in comparison with before that we had only phonons. So the new parameter that joins the study is the coupling/thermalization time τ_{mp}. Additional, we have to point out that the heat source transfers the heat into the phonon system, not the magnon one (but still can transferred to the magnon system via the phonon-magnon coupling). So, we consider that our heat source has the form of Equation 6.1,the thermalization time equals to $\tau_{mp} = 0.01s$ and now we ll study 3 different cases where we ll change the heat source period T in respect to τ_{mp}.

case i:

In the first case, we suppose that the period of the heat source is $T = 0.001s < \tau_{mp}$.

At first we set the diffusion times of phonons and magnons equal to $\tau_p = 0.0001s$ and $\tau_m = 0.1s$ respectively.

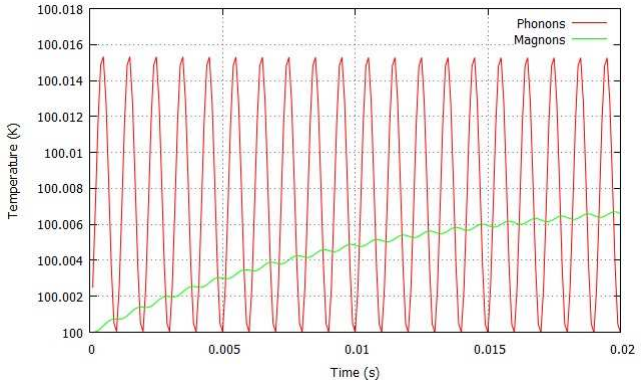

Figure 6.4: Phonons' (Red) and Magnons' (Green) temperature response at the opposite surface from the one that we adapted the heat source, versus time.

As we observe, the heat that is in the phonon system propagates ballistically when the heat that is in the magnon system diffusivily. This is a result that we were waiting since $\tau_p < T$ and $\tau_m > T$, and as we showed in the previous subsection, when the diffusion time is smaller than the period of the heat source we have ballistic transport, on the other hand when it is equal or bigger than the period we have diffusive transport.

Lets change the diffusion time of magnons to check what changes will occur and if magnons' diffusion time affects the way of how heat is propagated in the phonon system. We assume that $\tau_m = 0.0001s$ and after our numerical calculations, the figure that we get is exact the same as the figure 6.4 . So this results shows us that the magnon system has nothing to do with how heat propagates in the phonon system, and despite the value of τ_m the heat in the magnon system will propagate diffusively.

At this point, we have to point out that if we set the τ_p to be bigger than the period T, the heat will propagate diffusively in the phonon system, as we showed in the previous subsection where we had only phonons as heat carrier. This means, that at least for the case that we have only one material, tau_{mp} doesn't affect the way that heat propagates in the phonon system, only τ_p and T do.

case ii:

We now set $T = \tau_{mp} = 0.01s$ and the diffusion times of phonons and magnons are $tau_p = 0.001s$ and $\tau_m = 0.001s$ respectively.

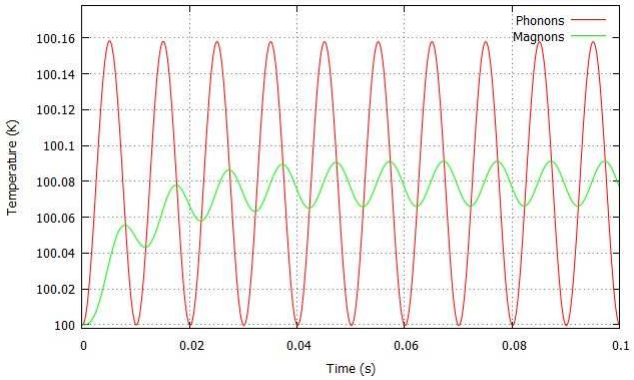

Figure 6.5: Phonons' (Red) and Magnons' (Green) temperature response at the opposite surface from the one that we adapted the heat source, versus time.

When $T = \tau_{mp}$, the heat in the phonon system will still propagate, as it is shown in the figure 6.5, ballistically (if $\tau_p < T$, otherwise if $\tau_p \geq T$ will propagate diffusively), and as for the magnon system the heat will propagate diffusively, as in the previous case (despite the value ot τ_m).

So the crucial result that we get from case *i* and *ii*, is that the heat in the phonon system will propagate ballistically if $\tau_p < T$ and doesn't get affected by the coupling with magnons, when at the same time the heat that is being transferred in the magnon system will propagate diffusively, no matter what the value of τ_m is, as long as $T \leq \tau_{mp}$.

case iii:

In the last case, we set the period of the heat source to be equal to $T = 0.1s$, so that $T > \tau_{mp}$. The phonons' and the magnons' diffusion times are $\tau_p = 0.01s = \tau_m$. We now notice that both phonons and magnons propagate ballistically. In this case

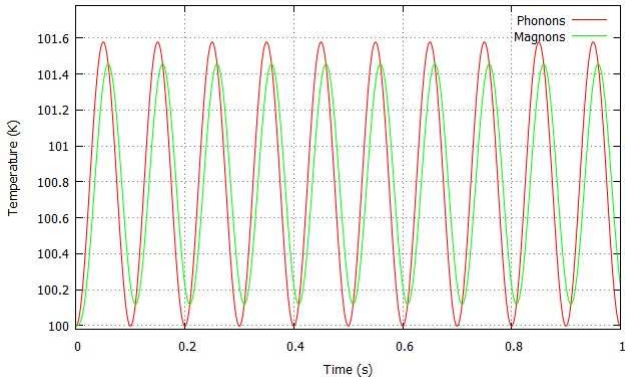

Figure 6.6: Phonons' (Red) and Magnons' (Green) temperature response at the opposite surface from the one that we adapted the heat source, versus time.

the magnons' diffusion time τ_m affects the way the heat propagates in the magnon system. If τ_m then the heat in the magnon system will propagate ballistically otherwise diffusively.

So, to conclude, in these three cases, where we have only 1 material, we get the following useful results:

- the way the phonons will propagate, depends only on the phonons' diffusion time and the period of the heat source T. If we have $\tau_p < T$ then heat will propagate ballistically, on the other hand if we have $\tau_p \geq T$, the heat ll propagate diffusively.
- magnons' diffusion time doesn't affect the way that heat propagates in the magnon system.
- thermalization time τ_{mp} doesn't affect the heat propagation in the phonon system, but only in the magnon system. If $\tau_{mp} \geq T$ then the heat in the magnon system will propagate diffusively, otherwise if $\tau_{mp} < T$ then the heat in the magnon system will propagate ballistically if $\tau_m \leq T$ and diffusively if $\tau_m > T$.

The last result can be explained by thinking that in the first two cases where $T \leq \tau_{mp}$, the period that the source is inserting/removing heat to/from our system is smaller than the coupling time, so a big part of the heat "doesn't make it in time"

to get transferred to magnon system, since the coupling is slower. That's why we observe a diffusive response in the magnon system. But in the third case where the coupling time is smaller than the period of the source, a big part of the heat is getting transferred in the magnon system via the phonon-magnon coupling, and is transferred out by the same mechanism, following the frequency of the heat source in the case where $tau_m < T$.

6.2 2 Materials

Let's suppose that we have two materials bounded together, the first one has two heat carriers (phonons and magnons that interact) and the second one has only phonons. We adapt a heat source (same heat source as Equation 6.1) at the left surface of the material and we measure the temperature response at the opposite surface, wanting to check in which cases the heat propagates ballistically and in which diffusively. We set the thermalization time $\tau_{mp} = 0.01s$ (which only exists in first material since in the second we have only phonons as heat carrier) and the parameters that we change are the diffusion times of phonons in both materials (τ_{p1} and tau_{p2}), the diffusion time of magnons (τ_m) that only exist in the first material and the period T of the heat source.

case i:

In our first case we set, the period of the heat source $T = 0.001s < \tau_{mp}$, the phonons' diffusion times equal to $\tau_{p1} = 0.01s$ and $\tau_{p2} = 0.0001s$, and the magnons' diffusion time in the first material equal to $\tau_m = 0.0001s$. As we notice, we chose the first's material phonon diffusion time bigger than the period of the heat source and the second's material phonon diffusion time smaller than period.

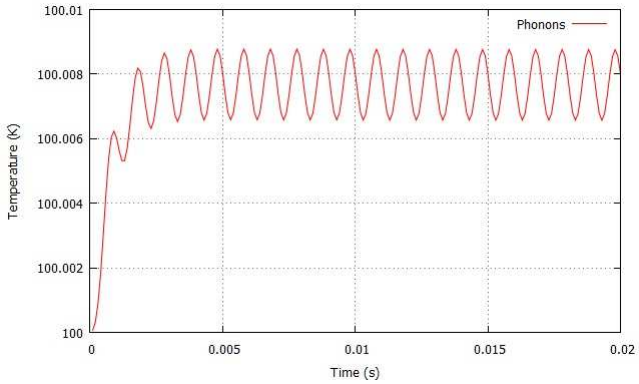

Figure 6.7: Phonons' temperature response at the opposite surface from the one that we adapted the heat source, versus time.

As we see from figure 6.7, if one's material phonon diffusion time is bigger than the period of the heat source, the heat propagation is mostly diffusive. If we change the magnons' diffusion time and set it $\tau_m = 1s$ we observer that this change doesn't affect the phonons' heat propagation. So, we can say that the way of heat's propagation depends only on the two diffusion times of the phonons.

Lets now set τ_{p1} to be equal to $\tau_{p1} = 0.1s$ and keep τ_{p2} as it was before.

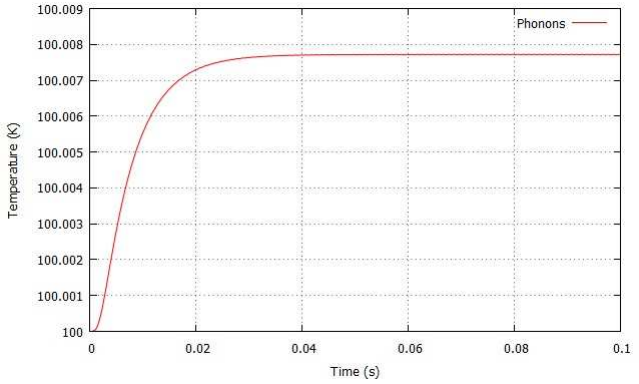

Figure 6.8: Phonons' temperature response at the opposite surface from the one that we adapted the heat source, versus time.

The interesting thing that we notice from figure 6.8 is that if one of the two phonons' diffusion time is more than one order of magnitude bigger than the heat period T, then the heat propagates full diffusively.

The next subcase we ll see, is when both phonons' diffusion times are smaller than the heat source's period T.

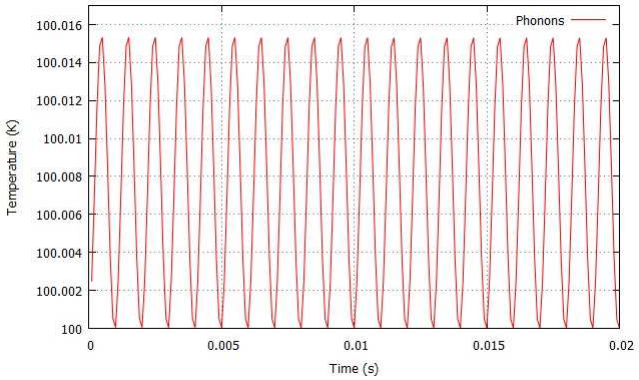

Figure 6.9: Phonons' temperature response at the opposite surface from the one that we adapted the heat source, versus time.

From figure 6.9, we observe what we expect, and that is that the heat, when $\tau_{p1} = \tau_{p2} < T$, propagates fully ballistically. This result comes to agree with the previous results that we extracted when we studied the 1 material case.

In the case now that the two phonons' diffusion times are $\tau_{p1} = \tau_{p2} = 0.01s$ (one order of magnitude bigger than T), then we get the following figure:

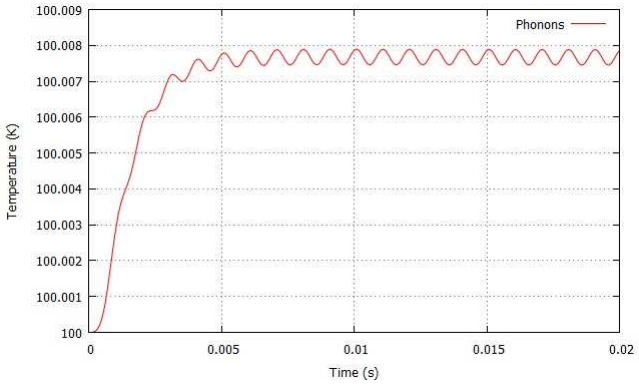

Figure 6.10: Phonons' temperature response at the opposite surface from the one that we adapted the heat source, versus time.

where as we see, the propagation is almost fully diffusive. So, if at least one τ_p is bigger than T then we see diffusive propagation.

The last 3 subcases of case 1 that we ll study are when $\tau_{p1} = T$ and $\tau_{p2} = 0.0001s$, T, $0.01s$ (in the first subcase the τ_{p2} is one order of magnitude smaller than T, in the second both τ_{p1} and τ_{p2} are equal to T, and in the third τ_{p2} is one order of magnitude bigger than T). We ll present the three figures altogether and then we ll discuss the

results.

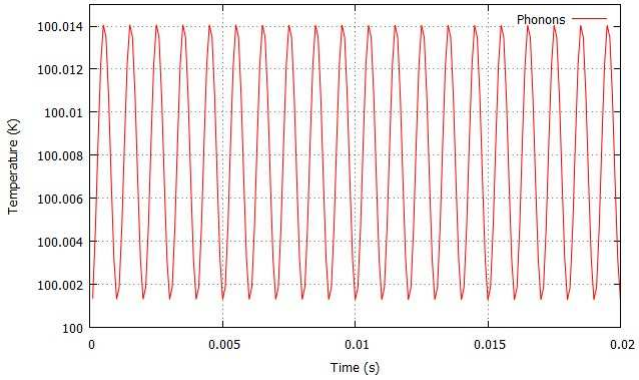

Figure 6.11: Phonons' temperature response at the opposite surface from the one that we adapted the heat source, versus time. In this subcase $\tau_{p1} = T$ and $\tau_{p2} = 0.0001s$.

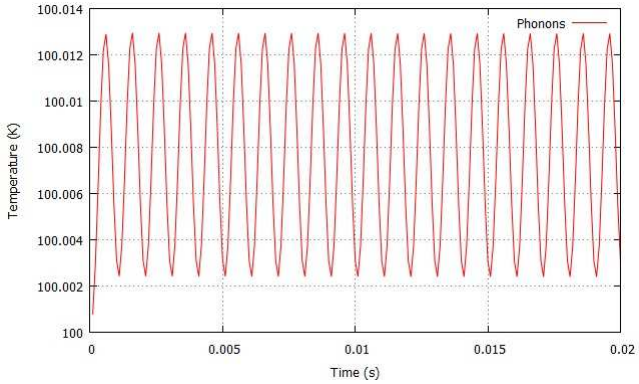

Figure 6.12: Phonons' temperature response at the opposite surface from the one that we adapted the heat source, versus time.In this subcase $\tau_{p1} = \tau_{p2} = T$.

From the above 3 figures (figures 6.9-6.11), we observe that in the case where $\tau_{p1} = T$ and τ_{p2} goes from one order of magnitude below T to one order of magnitude above T, the only subcase that we saw diffusive propagation was when $\tau_{p2} = 0.01s > T$. So, we can conclude to the result that if one of the two phonon diffusion time is equal to the period of the heat source, and the second one is equal or smaller to the period, then we observe ballistic transport. Otherwise, if the second one is bigger than the period, we observe diffusive transport. A useful notice that we should mention is that, as we see in figures 6.11 and 6.12, when phonons' diffusion times become smaller than T, the propagation tends to be purely ballistic, but when one or both of the τ_p have the same value with T, we observe mostly ballistic propagation and partly diffusive.

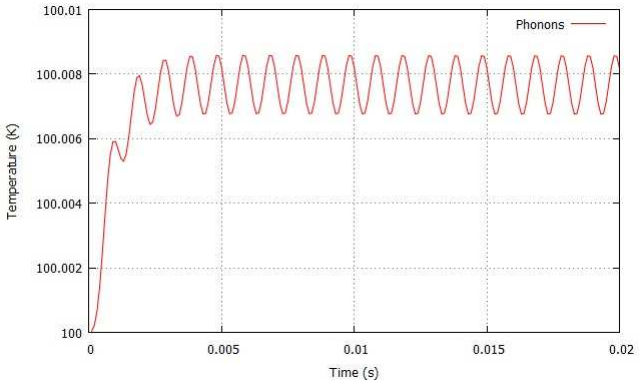

Figure 6.13: Phonons' temperature response at the opposite surface from the one that we adapted the heat source, versus time.In this subcase $\tau_{p1} = T$ and $\tau_{p2} = 0.01s$.

case ii: / case iii:

In the second case of the study of heat propagation in a material that is composed of two others that are bounded together, we set the heat source period T to be equal to the thermalization time τ_{mp} when in the third case we set period T to be one order of magnitude lower than τ_{mp}. By changing the two phonons' diffusion times we ll try to observe in which cases we see ballistic or diffusive heat propagation, as we did before.

In order to avoid posting the same figures as the previous case, we have to say that in both cases (*ii* and *iii*), we get the same results as case 1. More specifically, in order to see ballistic propagation, both phonons' diffusion times must be $\leq T$. In other cases we have diffusive propagation, as we had in case 1 too.

Concluding, in the case that we have two materials bounded together, where in the first one we have both phonons and magnons, when at the second we have only phonons, we observed the following:

- to observe ballistic propagation, the phonons' diffusion time in both materials must be $\leq T$. If both $\tau_p < T$ we observe fully ballistic transport, when if at least one is equal to T, then we observe mostly ballistic, and partly diffusive propagation
- if one τ_p is $\leq T$ and the other is $> T$, then we observe mostly diffusive and partly ballistic propagation (see figure 6.7)
- if both τ_p are $> T$ then we observe fully diffusive propagation
- lastly, we noticed that the magnons' diffusion time and the thermalization time in the first material, don't affect the way that the heat propagates.

7 Summary

Efficient heat removal is crucial to the performance of many electronic devices, since overheating often leads to a number of performance problems. If we take in mind that electronics are being miniturized more and more every year, then we conclude that we have to find a way to dissipate the heat in order to avoid system failures. The main goal of this thesis is to propose a possible device, a thermal diode, that allows the heat to flow in a forward direction while it can hardly flow in the opposite direction.

In this thesis, two types of one-dimensional quantum magnets are investigated, the spin chain system and the spin ladder system, in which the magnetic structure forms a chain and ladder, respectively. These are chosen because of their potential in applications in advanced thermal management. The spin ladder and spin chain materials are promising candidates for advanced cooling mechanisms, because of their advantageous properties. First of all, heat is conducted primarily along one crystal axis, hence the material can thermally insulate in one direction and carry away heat along another. Second, the thermal conductivity along the one-dimensional structure is $\kappa_{mag} \approx 100 W/m \cdot K$, i.e. comparable to a metal. The anisotropy in between different crystallographic directions is about 40. Third, these compounds are electrically insulating and can therefore be used to simultaneously electrically insulate electronic circuits and transport heat. Finally, heat is carried by localised spins which can be manipulated with magnetic fields or light. This opens the possibility of having a controllable thermal conductivity at room temperature. For example, doping with switchable magnetic

defects potentially makes tuning of the thermal conductivity achievable.

In chapter 2 the specific spin chain $SrCuO_2$, Sr_2CuO_3 and spin ladder systems $Ca_9La_5Cu_{24}O_{41}$ and $Sr_{10}La_4Cu_{24}O_{41}$, that are investigated in this thesis, are introduced. The temperature dependence of the steady state thermal conductivity for spin chains and ladders i, as is described in the chapter, shows a huge magnetic contribution along the ladder/chain that dwarfs the lattice contribution, leading to a large anisotropy between the ladder/chain direction and the other directions. After the introduction of the spin chain and ladder materials, we present a mathematical description of (anisotropic) heat diffusion. Along the one-dimensional spin system both magnetic and lattice excitations participate in the heat transport. During a thermal conductivity experiment, only the energy of the lattice excitations can be measured, therefore only the lattice excitations are contributing to the temperature measured. A standard macroscopic diffusion model can be used when the magnetic and lattice excitations reach thermal equilibrium at a time scale much faster than the time scale of the experiment. If this is not the case, both excitations have to be taken into account and a microscopic two-temperature diffusion model is needed to describe the problem. If in such case the macroscopic diffusion model is used, an effective thermal conductivity is obtained, of which the size depends on the degree of thermalization between the lattice and magnetic excitations.

In chapter 3, we introduce the concept of Thermal Rectification, that is a phenomenon in which thermal transport along a specific axis is dependent upon the sign of the temperature gradient or heat current. Furthermore, we examine under which circumstances we can achieve thermal rectification, in two independent cases, the static thermal rectification and the dynamic one. Our material consists of two other materials that are bounded together, each one having its own thermal conductivity. The main thing that we concluded is that, in order to observe thermal rectification phenomena, the thermal conductivities of these two materials must not be constants, but they must have temperature dependence. In chapter 4 and 5, we studied the cases of Static and Dynamic thermal rectification, respectively, for various combinations of bounded spin chain and ladders materials. The highest rectification factor for both cases is found in the Sr_2CuO_3 - $Ca_9La_5Cu_{24}O_{41}$ compound.

Lastly, in chapter 6, we study the case where we have a material and we adapt a time-dependent heat source at its left surface, measuring the temperature response at the opposite surface. The heat in this material, in most of the cases that we study, propagates via two heat carriers, the phonons and the magnons. So, in this chapter we want to conclude under which circumstances the heat propagates ballistically or

diffusively. The interesting thing that we pointed out is that if the phonons' diffusion time τ_p is equal or smaller than the heat source's period, then the heat propagates ballistically, otherwise diffusively.

In this work we showed that in a composite material with different temperature dependent thermal conductivities, thermal rectification is possible to occur. Thermal rectification exists at the macro and micro scales and a better understanding is being developed in both, which will eventually lead to efficient thermal rectifiers/diodes. Currently the many mechanisms that are known to exist in solid systems have shown only small levels of rectification and are not predictable, but theoretical and analytical models have predicted large rectification possible and are becoming more and more accurate. Experimental validation and realization of some of these mechanisms is crucial to the future application involving thermal rectifiers even if only a fraction of the predicted levels of rectification are achieved. Researchers are only now starting to think about what devices can be fabricated, what quantities can be measured and whether the theoretical systems can be realized in the lab. In fact, experimental study of thermal rectification is said to be ongoing in quite a few research labs.

Bibliography

[1] M. Otter, *Magnetic heat transport in low-dimensional quantum magnets*, PhD Thesis

[2] C. Hess. Heat conduction in low-dimensional quantum magnets. *Eur. Phys. J. Special Topics*, 151:73-83, 2007

[3] N. D. Mermin and H. Wagner. Absence of ferromagnetism or antiferromagnetism in one- or two- dimensional anisotropic heisenberg models. *Phys. Rev. Lett.*, 17(22):1133-1136, Nov 1966

[4] H. Fröhlich, W. Heitler, Proc. R. Soc. Lond. A 155, 640 (1936)

[5] X. Zotos, F. Naef, P. Prelovšek, *Phys. Rev. B* 55, 11029 (1997)

[6] X. Zotos, *Phys. Rev. Lett.* 82, 1764 (1999)

[7] K. Kudo, S. Ishikawa, T. Noji, T. Adachi, Y. Koike, K. Maki, S. Tsuji, K. Kumagai, *J. Low. Temp. Phys.* 117, 1689 (1999)

[8] A.V. Sologubenko, K. Giannò, H.R. Ott, U. Ammerahl, A. Revcolevschi, *Phys. Rev. Lett.* 84, 2714 (2000)

[9] C. Hess, C. Baumann, U. Ammerahl, B. Büchner, F. Heidrich-Meisner, W. Brenig, A. Revcolevschi, *Phys. Rev. B* 64, 184305 (2001)

[10] W. Kobayashi, Y. Teraoka and I. Terasaki, Appl. Phys. Lett. **95**, 171905 (2009)

[11] Jia Zhu, Kedar Hippalgaonkar, Sheng Shen, Kevin Wang, Junqiao Wu, Xiaobo Yin, Arun Majumdar, Xiang Zhang, Temperature Gated Thermal Rectifier, arXiv:1307.4069

[12] D. J. Sanders and D. Walton. Eect of magnon-phon thermal relaxation on heat transport by magnons. *Phys. Rev. B*, 15:1489, 1977